الجمهوريـــة الجزائريـــة الديمقراطيـــة الشعبـيـة
People's Democratic Republic of Algeria
وزارة التعليـــــــم العالـــــي والبـحـث العلمـــــــي
Ministry of Higher Education and Scientific Research
جامعـــــة غردايـــــة
University of Ghardaia
كليـــة العلـــوم والتـكنـولـوجيـا
Faculty of Science and Technology
قسـم التعليـم المشتـرك في العلـوم والتـكنـولـوجيـا
Department of Common Teaching in Sciences and Technology

MEMORY

For obtaining the Master's degree

Domain : Material Sciences

Field : Physics

Specialty : Energy Physics and Renewable Energies

Title

Numerical Analysis of Mixed Convection in a Trapezoidal Cavity Filled with a Hybrid Nanofluid

Presented by :

Amel Djemaa Ouled Hadj Youcef

In front of the jury composed of :

Pr. Djemoui LALMI	**Univ Ghardaia**	**President**
Dr. Reda TAHTAH	**Univ Ghardaia**	**Examiner**
Dr. Faris AISSAOUI	**Univ Ghardaia**	**Examiner**
Pr. Kamel BOUARAOUR	**Univ Ghardaia**	**Supervisor**

Academic year: 2024/2025

Dedication

To my teacher, my role model, and the first pillar of strength in my life,To the one who planted in my heart the love for knowledge my dear mother.

To my support and backbone my beloved father.

To my siblings my companions who shared my joys and sorrows.

To the companions of my journey and the balm in times of hardship my dear friends.

A special mention goes to my friend Khadidja, whose is true support and encouragement to me you have my deepest appreciation and gratitude.

To those who carry the noblest message in life,

To those who paved the way for us in the pursuit of knowledge our esteemed teachers

Acknowledgments

I thank Almighty Allah for His countless blessings. By His grace, this step in my academic journey has been achieved. All praise is due to Him, now and always.

I extend my deepest thanks and sincere gratitude to my supervisor, Professor Bouaraour Kamel, for his patience, dedication, and the valuable efforts he devoted to supervising this work. His insightful guidance, precise scientific observations, and rich knowledge had a great impact on enriching the subject of this study. He has my utmost respect and appreciation.

I also sincerely thank the esteemed members of the evaluation committee **Dr. Reda TAHTAH, Dr. Faris AISSAOUI** and **Pr. Djemoui LALMI** for accepting to review and assess this humble work.

Finally, I would like to thank everyone who contributed, directly or indirectly to the completion of this thesis

Abstract

In this thesis, a two-dimensional numerical simulation was conducted to investigate mixed convection heat transfer in a trapezoidal cavity filled with a hybrid nanofluid. The system is characterized by a hot lower wall, a colder moving upper lid, and thermally insulated vertical sidewalls. The results were analyzed using various parameters, with particular attention given to the relationship between the average Nusselt number and the Richardson number. The finite volume method was employed to solve the governing equations of the phenomenon, and the Nusselt number was calculated. The variation of the local Nusselt number along the bottom wall was evaluated under the influence of different volume fractions (φ) and Richardson number (Ri) values. Simulations were carried out for different Ri values (0.1, 1, 2, and 5) using Al_2O_3-Cu/water hybrid nanofluid at various volume fractions (φ = 0%, 2%, 4%, and 8%). The results demonstrated that the addition of nanoparticles to the base fluid enhances heat transfer, particularly with increasing nanoparticle concentration and Richardson number. The effect of nanoparticles was found to be more significant in natural convection-dominated regimes than in forced convection. The best thermal performance was observed at φ = 8% and Ri = 5, resulting in a 39.15% enhancement, representing the optimal case in this study. These findings suggest that nanofluids can be effectively used to reduce energy consumption.

Keywords: Mixed convection, trapezoidal cavity, nanofluid, finite volume method **FVM**

Résumé

Dans ce mémoire, une simulation numérique bidimensionnelle a été réalisée afin d'étudier le transfert de chaleur par convection mixte dans une cavité trapézoïdale remplie d'un nanofluide hybride. Le système est caractérisé par une paroi inférieure chaude, un couvercle supérieur mobile plus froid, et des parois latérales verticales isolées thermiquement. Les résultats ont été analysés en fonction de plusieurs paramètres, avec une attention particulière portée à la relation entre le nombre de Nusselt moyen et le nombre de Richardson. La méthode des volumes finis a été utilisée pour résoudre les équations gouvernantes du phénomène, et le nombre de Nusselt a été calculé. La variation du nombre de Nusselt local le long de la paroi inférieure a été évaluée sous l'effet de différentes fractions volumiques (φ) et de valeurs du nombre de Richardson (Ri). Les simulations ont été effectuées pour différentes valeurs de Ri (0,1 ; 1 ; 2 ; et 5) en utilisant un nanofluide hybride Al_2O_3-Cu/eau à diverses fractions volumiques (φ = 0 %, 2 %, 4 % et 8 %). Les résultats ont montré que l'ajout de nanoparticules au fluide de base améliore le transfert de chaleur, en particulier avec l'augmentation de la concentration en nanoparticules et du nombre de Richardson. L'effet des nanoparticules s'est révélé plus significatif dans les régimes dominés par la convection naturelle que dans ceux dominés par la convection forcée. La meilleure performance thermique a été observée pour φ = 8 % et Ri = 5, entraînant une amélioration de 39,15 %, représentant le cas optimal de cette étude. Ces résultats suggèrent que les nanofluides peuvent être utilisés efficacement pour réduire la consommation énergétique.

Mots-clés : Convection mixte, cavité trapézoïdale, nanofluide, méthode des volumes finis (**FVM**)

ملخص

في هذه الرسالة، أُجريت محاكاة عددية ثنائية الأبعاد لدراسة انتقال الحرارة بالحمل الحراري المختلط في تجويف شبه منحرف مملوء بسائل نانوي هجين. يتميز النظام بجدار سفلي ساخن، وغطاء علوي متحرك أكثر برودة، وجدران جانبية رأسية معزولة حرارياً. حُللت النتائج بناءً على عدة معايير، مع إيلاء اهتمام خاص للعلاقة بين متوسط رقم نوسلت ورقم ريتشاردسون. استُخدمت طريقة الحجم المحدود لحل المعادلات الحاكمة للظاهرة، وحُسب رقم نوسلت. قُيِّم تغير رقم نوسلت المحلي على طول الجدار السفلي تحت تأثير قيم مختلفة لكسور الحجم (φ) وقيم رقم ريتشاردسون (Ri). أُجريت عمليات محاكاة لقيم مختلفة لـ Ri (0,1 ; 1 ; 2 ; 5) باستخدام سائل نانوي هجين من Al_2O_3-Cu /ماء عند كسور حجم مختلفة (φ = 0%، 2%، 4%، و8%). أظهرت النتائج أن إضافة الجسيمات النانوية إلى السائل الأساسي تُحسّن انتقال الحرارة، خاصةً مع زيادة تركيز الجسيمات النانوية ورقم ريتشاردسون. كان تأثير الجسيمات النانوية أكثر وضوحًا في الأنظمة التي يهيمن عليها الحمل الحراري الطبيعي مقارنةً بالأنظمة التي يهيمن عليها الحمل الحراري القسري. لوحظ أفضل أداء حراري عند φ = 8% و Ri = 5، مما أدى إلى تحسن بنسبة 39.15%، وهو ما يمثل الحالة المثلى في هذه الدراسة. تشير هذه النتائج إلى إمكانية استخدام السوائل النانوية بفعالية لتقليل استهلاك الطاقة.

الكلمات المفتاحية: الحمل الحراري المختلط، التجويف شبه المنحرف، السائل النانوي، طريقة الحجم المحدود **FVM**

CHAPTER III

List of figures

CHAPTER I : Mixed Convection in a Trapezoidal Cavity

List of Table

CHAPTER XV : Results and Discussion

Nomenclature	Description	Unit
g	Gravitational acceleration	m/s^2
H	Cavity height	m
L	Cavity length	m
P	Pressure	$Pa(N/m^2)$
T	Temperature	K
h	Convective heat transfer coefficient	$W/(m^2 \cdot K)$
Cp	Specific heat at constant pressure	$J/(kg \cdot K)$
K_f	Thermal conductivity of the base fluid	$W/(m \cdot K)$
K_{hnf}	Thermal conductivity of the hybrid nanofluid	$W/(m \cdot K)$
u ; v	Dimension velocities in the x- and y-directions	—
X ; Y	Dimensionless coordinates	—
U ; V	Dimensionless velocity components	—
$\overline{u_i' u_j'}$	Reynolds stress tensor	—
u_i	The velocity component	m/s
$\overline{u_i}$	Mean velocity component	m/s
u_i'	A fluctuating component of velocity	m/s
μ_t	The vortex viscosity coefficient	$Pa \cdot s$ $(kg/(m \cdot s))$
σ_k	turbulent Prandtl number for k.	—
P_k	the production of turbulent kinetic energy	m^2/s^3
E_{ij}	The mean strain rate tensor	1/s
ε	The dissipation rate of turbulent kinetic energy	m^2/s^3
k	The turbulent kinetic energy.	m^2/s^2
C_μ ; $C_{1\varepsilon}$; $C_{2\varepsilon}$	Model constants in the k–ε turbulence model	—
Re	Reynolds number	—
Gr	Grashof number	—
Pr	Prandtl number	—
Ri	Richardson number	—
Ra	Rayleigh number	—

Nu	Local Nusselt number	—
Nu_{ave}	Average Nusselt number	—

Greeks

ρ_f	Density of the base fluid	kg/m³
ρ_{hnf}	Density of the hybrid nanofluid	kg/m³
μ	Dynamic viscosity of the fluid	Pa·s (kg/m·s)
μ_{hnf}	Dynamic viscosity of the hybrid nanofluid	Pa·s (kg/m·s)
ν	Kinematic viscosity	m²/s
ψ	Stream function	—
β	Thermal expansion coefficient	1/K
h	Convective heat transfer coefficient	W/(m²·K)
α_{hnf}	Thermal diffusivity of the hybrid nanofluid	m²/s
θ	Dimensionless temperature	—
φ	Nanoparticle volume fraction	—

Subscripts

hnf	refers to the hybrid nanofluid
RANS	Reynolds-Averaged Navier-Stokes
PDE	Partial differential equation
FDM	Finite Difference Methods
FEM	Finite Element Methods
SM	Spectral Methods
FVM	Finite Volume Methods

General
INTRODUCTION

General Introduction

Amid the rapid and ongoing advancements in technology and industry, heat transfer has become increasingly significant from both scientific and practical perspectives. Despite its various mechanisms conduction, convection, and radiation convection has emerged as the most extensively studied due to its diverse forms: natural, forced, and mixed. It plays a critical role in numerous practical applications such as air conditioning and residential heating, cooling in thermal instrumentation, mechanical and electronic systems, and fluid heating processes including those in solar collectors and heat exchangers. This mode of heat transfer is inherently associated with fluids, whether liquid or gaseous.

•Forced Convection: occurs when fluid motion is driven by external forces (e.g, pumps or fans), leading to relatively high flow velocities. Consequently, the rate of heat transfer is directly influenced by the nature of the fluid's flow. [2]

•Natural Convection: arises from fluid movement induced by density variations between heated and cooled regions within a body force field such as gravity. The strength of this mode depends on the intrinsic properties of the fluid and is typically examined in gravitational fields devoid of other body forces.

•Mixed Convection: Represents a superposition of forced and natural convection effects, where both contribute comparably to fluid motion. This results in a relatively complex heat transfer behavior requiring careful analysis.

Mixed convection and fluid flow within enclosures remain key areas of investigation due to their relevance in various engineering applications and natural systems, including thermal power stations, petrochemical industries, aerospace engineering, and the construction sector, So that research in this area consistently emphasizes the central role of the Richardson Number in characterizing mixed convection behavior. At low Richardson numbers, forced convection predominates, while natural convection becomes increasingly influential as the number rises.

Heat transfer processes underpin many industrial operations that intersect with everyday life. Enhancing these processes and boosting their efficiency has become a priority across industries, regulatory authorities, and society at large, which is becoming more conscious of diminishing energy

resources and the need for sustainable energy solutions, improving heat transfer through convection has thus become a focal point in academic and industrial research. To this end, a vast array of theoretical, numerical, and experimental studies have been undertaken to analyze the governing phenomena of convection. These efforts are of great industrial importance due to their wide applicability, in many industries such as automotive and electronics enhancing heat exchanger performance requires optimizing convective heat transfer. While passive enhancement techniques applied to surface geometry have been extensively investigated, they have largely reached their performance limits. This has spurred interest in alternative methods, including the use of advanced heat transfer fluids like nanofluids, so that nanofluids are a notable breakthrough in thermal science. Characterized by their unique physical and chemical properties especially their high thermal conductivity they outperform conventional fluids such as water, oil, and ethylene glycol in terms of heat transfer efficiency. Despite variations in findings, most studies have demonstrated promising results, positioning nanofluids as an innovative and effective solution for enhancing heat exchanger performance, in addition nanofluids hold vast potential across several strategic sectors, including electronic cooling, HVAC systems, aerospace, and more. Under the right conditions, they may offer transformative solutions in these domain.[2]

This study investigates mixed convection flow and heat transfer in a trapezoidal cavity filled with a hybrid nanofluid. The objective is to evaluate how the volume fraction of nanoparticles affects the convection mechanism, focusing on the influences of the Richardson number and solid volume fraction on the distribution of different variables such as velocity, stream fuction, temperature and some important quantities such as local and average Nusselt number, which quantifies heat transfer.

This Master's thesis is organized as follows, in addition to a general introduction and concluding remarks:

•The first chapter provides a literature review and an overview about nanofluid properties.

•For the second chapter, we will present the mathematical modeling derived from established theoretical studies.

•The third chapter details the numerical methodology using Gambit (v2.4.6) for drawing and meshing geometry and Fluent (v6.3.26) for simulation and solution procedures.

•The fourth chapter is dedicated to the analysis and interpretation of the simulation results.

The work concludes with a general summary highlighting the key outcomes of the results.

CHAPTER I:

Mixed Convection in a Trapezoidal Cavity

I.1. Introduction

The central issue of heat transfer by convection whether natural, forced, or mixed within enclosures has received significant attention from researchers due to its prevalence in numerous engineering applications, such as electronic component cooling, drying processes, and heat transfer in solar ponds, among others. The ongoing need to improve heat transfer efficiency has led to the emergence of a new class of fluids known as nanofluids. These are solutions consisting of nanoscale particles suspended in a base fluid and are utilized for their enhanced thermal performance characteristics.

This chapter presents a review of key previous studies that have investigated convective heat transfer within enclosures filled with various fluids and subjected to different boundary conditions. It will also cover the different types of nanofluids and the preparation techniques commonly used in both research and engineering applications.

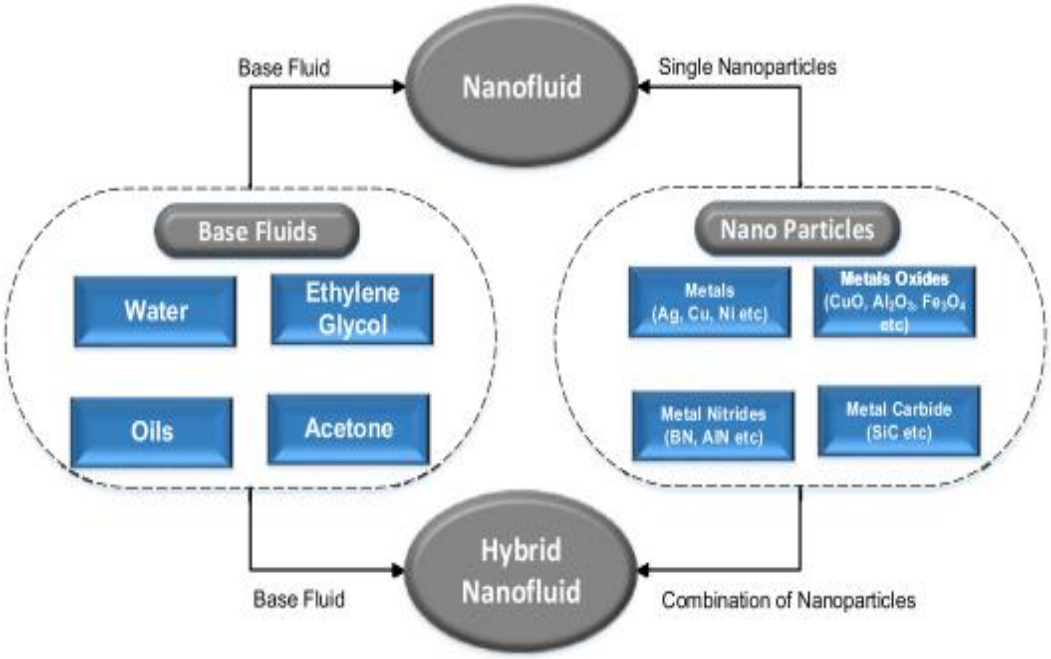

Figure I.1: Manufacturing Scheme of Nanofluids and Hybrid Nanofluid [1]

I.2 General Information of Nanofluids

In recent years, the industrial sector has witnessed the development of various energy systems that generate extremely high heat fluxes, rendering conventional cooling fluids such as water, ethylene glycol, and oil ineffective. To enhance the thermophysical properties of these fluids, researchers have introduced solid nanoparticles with excellent thermal characteristics into base fluids. This innovation gave rise to a new class of fluids known as nanofluids. The term "nanofluid" was first coined by Choi at Argonne National Laboratory in the United States in 1995 and has since been widely used to describe these colloidal suspensions. Nanofluids are essentially stable mixtures of nanoparticles ranging in size from 1 to 100 nanometers dispersed in a base liquid.

A wide variety of nanoparticles can be used in nanofluid formulations, including:

- **Metal oxide nanoparticles**: such as aluminum oxide (Al_2O_3), copper oxide (CuO), silicon dioxide (SiO_2), and titanium dioxide (TiO_2).
- **Metallic nanoparticles**: such as aluminum (Al), copper (Cu), silver (Ag), gold (Au), and silicon (Si).
- **Non-metallic nanoparticles**: such as carbon nanotubes (CNT) and diamond particles and (C).

The choice of base liquid plays a crucial role in the stability of the nanofluid, as it helps prevent particle agglomeration over time. The base liquid is selected based on the nature and compatibility of the nanoparticles used. [2]

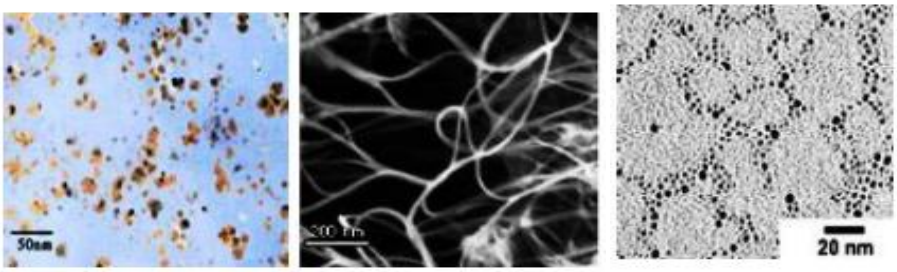

Figure I.2: Nanofluids Viewed Under an Electron Microscope: ethylene glycol + copper at 0.5%; water + alumina; water + gold at 20 nm [2] [3]

I.3 Methods of Producing Nanofluids

Nanoparticles can be produced through various manufacturing processes, which are broadly categorized into two types:

- Physical processes: such as mechanical grinding.
- Chemical processes: including techniques like laser pyrolysis or chemical precipitation.

There are two primary methods for producing nanofluids: [4]

I.3.1. The Two-Step Method: This approach involves synthesizing nanoparticles first and then dispersing them into the base fluid. Effective dispersion requires intense stirring, often using a rotary stirrer or ultrasonic waves, to break up any agglomerates.

I.3.2. The One-Step Method: This method involves producing nanoparticles directly within the base fluid. However, it is only suitable for specific types of nanofluids. An example of this process includes condensing metal vapor in a reactor onto a low-vapor-pressure liquid film, resulting in the formation of nanoparticles. [2]

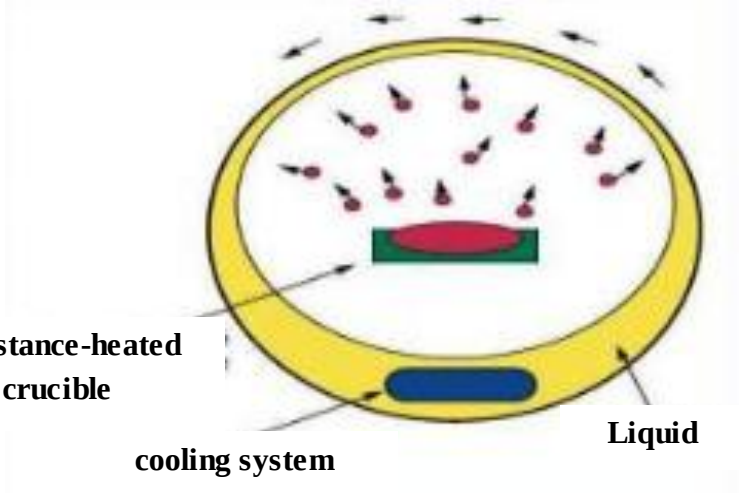

Figure I.3: Single-step Nanofluid Synthesis Process [2]

I.4 Bibliographic Synthesis

Due to the growing interest in nanofluids, numerous studies have been carried out to evaluate their thermal behavior and physical properties such as the heat transfer coefficient and dynamic viscosity. These investigations have consistently shown that nanofluids significantly outperform conventional base fluids, offering superior heat transfer and thermophysical properties. In pioneering research, Choi (1995) demonstrated that introducing a small volume fraction (1% to 5%) of $Al_2 O_3$ nanoparticles could result in a 20% increase in thermal conductivity, particularly when using carbon nanotubes. [2]

Al-Sarkhi et al. (2003) conducted a numerical investigation on the effects of mixed convection in a vertically oriented shrouded fin. The Nusselt number (Nu) and the product of the friction factor and Reynolds number (fr.Re) were analyzed as functions of buoyancy forces, which are strongly influenced by the geometry of the shrouded fin. Both Nu and fr.Re exhibited a nonlinear increase with the rise in clearance space above the fin tip. The outcomes of this study provide valuable insight for evaluating the thermal and hydrodynamic performance characteristics of shrouded fin configurations. [5]

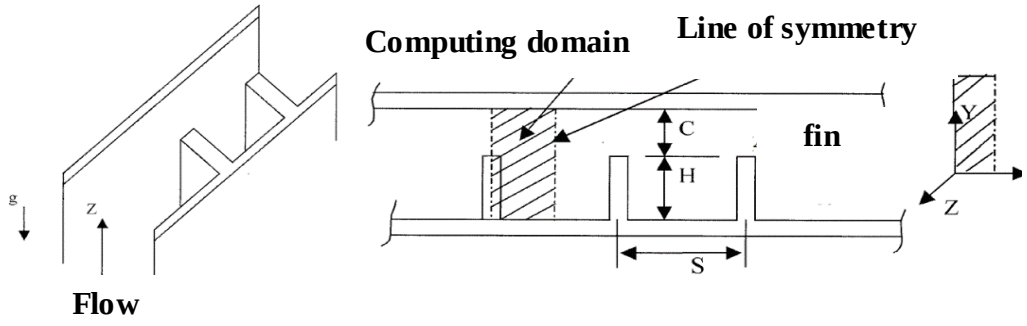

Figure I.4: Schematic Diagram of a Fin Array [5] [6]

In his study, **Oztop et al. (2004)** investigates numerically steady two-dimensional mixed convection in a vertical two-sided lid-driven square cavity with differentially heated vertical walls and adiabatic horizontal boundaries. The analysis considers three wall motion configurations, Richardson number in the range ($0.01 < Ri < 100$) and a fixed Prandtl number $Pr = 0.7$ is considered. Results demonstrate that both the Richardson number and lid movement direction significantly influence the flow and thermal fields. At low Ri, wall motion dominates and yields symmetric heat transfer for opposite wall motions. At high Ri, natural convection prevails, with enhanced heat transfer due to the

emergence of secondary vortices and a central counter-rotating cell, especially under opposing buoyancy and shear effects. [4]

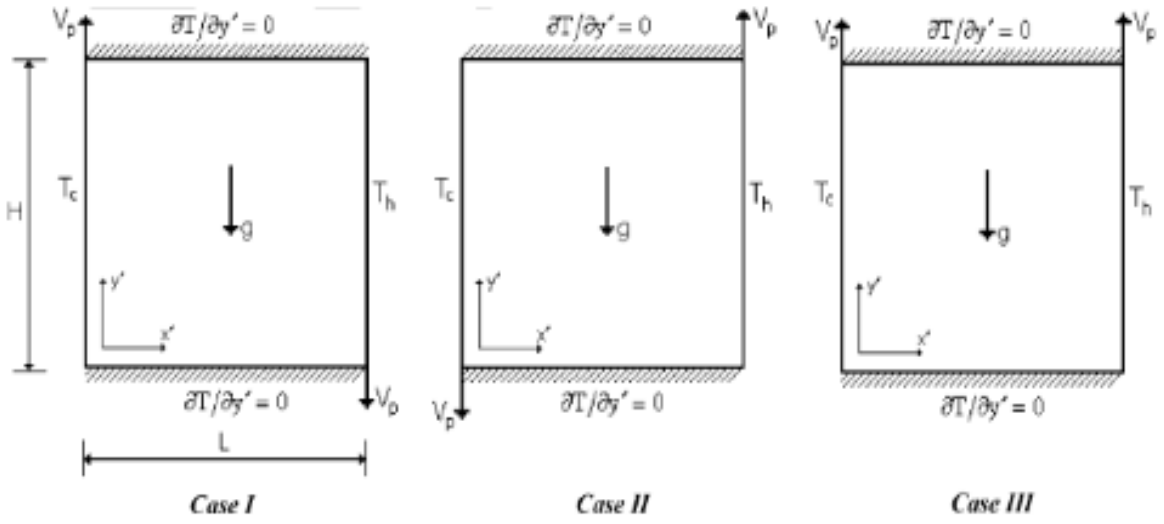

Figure I.5: Physical Model for Three Cases and the Coordinate System [6] [7]

Maiga et al. (2005) conducted a numerical investigation of laminar forced convection within a radially configured channel, uniformly heated by a system of parallel, coaxial heated discs. Their findings, based on the use of an Al_2O_3 water nanofluid, demonstrated a significant enhancement in heat transfer due to the presence of nanoparticles. This improvement became increasingly pronounced as the volume concentration of nanoparticles was increased, highlighting the positive impact of nanoparticle addition on thermal performance compared to the base fluid. [8]

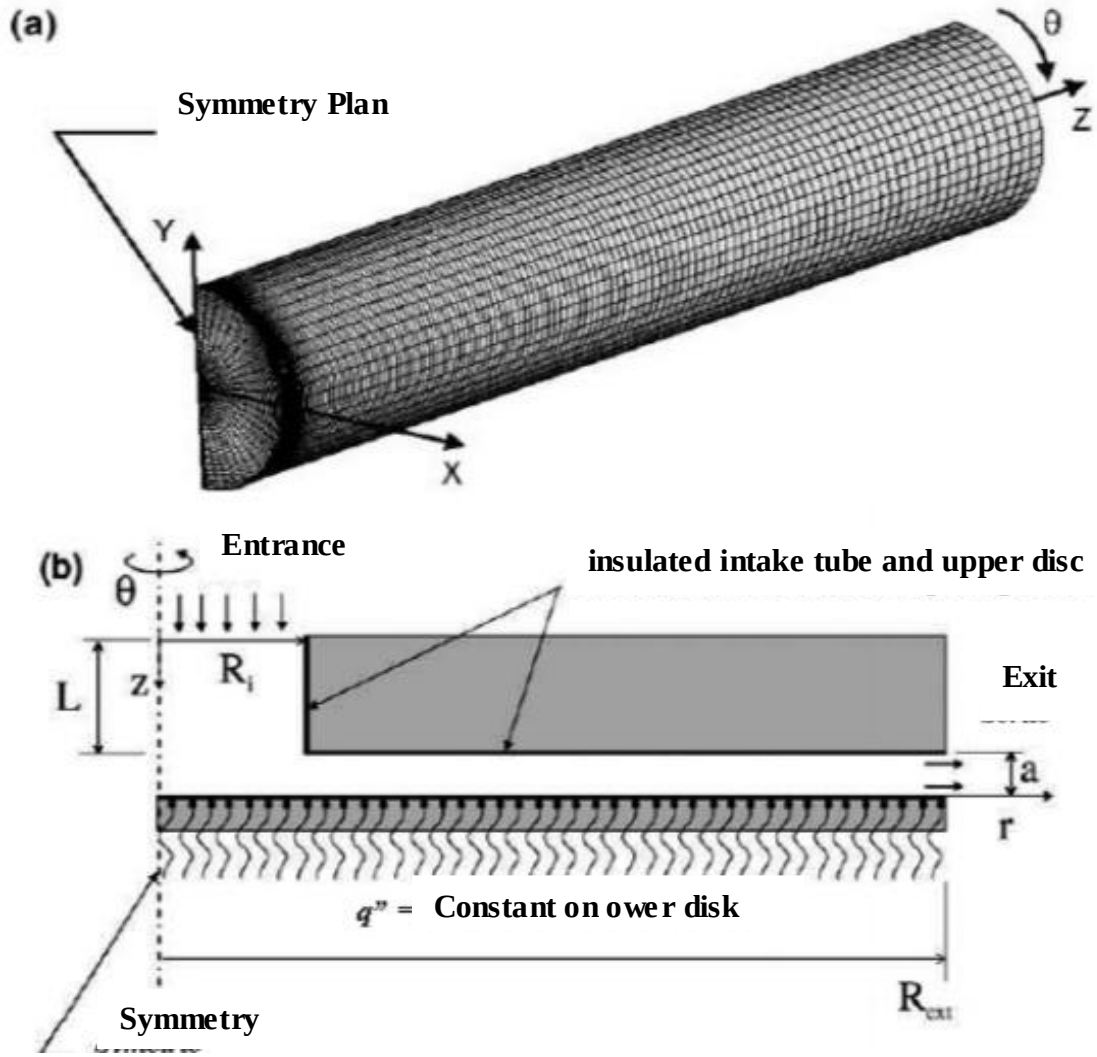

Figure I.6: Geometrical configuration : (a) Mesh of Configuration and (b) a Radial Chanal Between Heated Discs [2]

A numerical investigation is conducted by **Hakan et al. (2006).** The aim was to analyzed combined convective heat transfer and fluid flow within a partially heated, porous, lid-driven enclosure. The upper wall of the enclosure translates horizontally from left to right at a constant velocity and temperature. A finite-length heater is embedded on one of the stationary walls, with its central position varied along the vertical boundaries. The simulation employs a finite volume approach based on the finite difference method. Key dimensionless parameters influencing the flow and thermal behavior include the Richardson number, Darcy number, heater length, and the heater's vertical

position. The results indicate that optimal heat transfer occurs when the heater is positioned on the left vertical wall. [9]

Akbari et al. (2008) investigated numerically the fully developed laminar mixed convection of a water– Al_2O_3 nanofluid in horizontal and inclined tubes. Using three-dimensional steady governing equations, the effects of Grashof and Reynolds numbers are analyzed. Results align well with previous experimental and numerical findings. The study shows that nanoparticle concentration has little effect on flow behavior but enhances heat transfer by up to 15% at 4% volume fraction of Al_2O_3. Skin friction increases with tube inclination, while the heat transfer coefficient peaks at a 45° angle. [10]

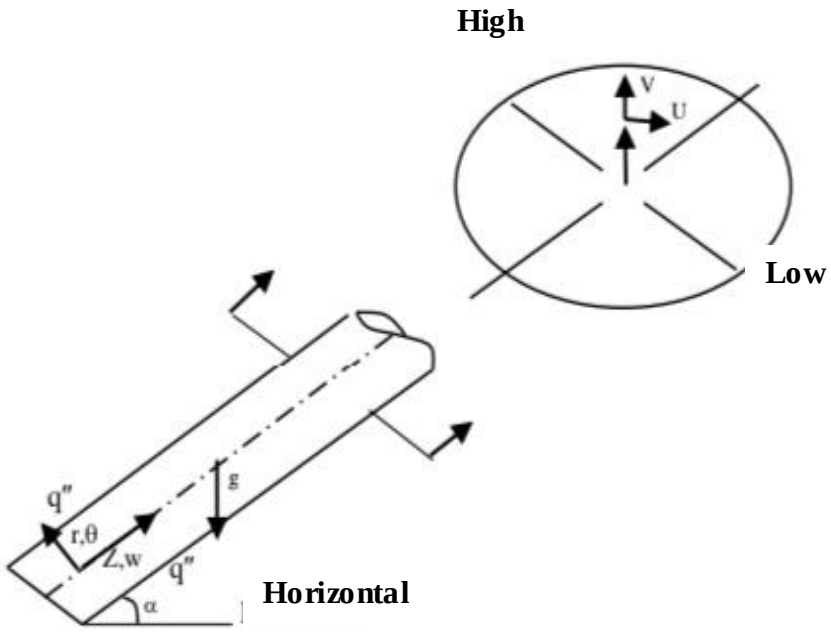

Figure I.7: Diagram of the Inclined Tube [9, 10]

Abu Nada and Chamkha (2010) analyzed numerically the steady laminar mixed convection in an inclined lid-driven square cavity filled with water– Al_2O_3 nanofluid. Results show that nanoparticle addition and cavity inclination enhance heat transfer, especially at higher Richardson numbers. [11]

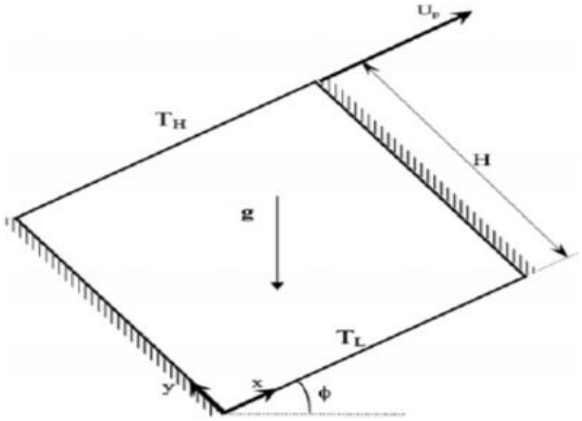

Figure I.8: Schematic View of the Enclosure [12]

A numerical study is performed by A **Karimipour et al. (2011)** to examined periodic mixed convection of a water–copper nanofluid within a rectangular cavity of aspect ratio 3, subjected to a sinusoidally oscillating top lid and a heated bottom wall. The effects of Richardson number Ri and nanoparticle volume fraction φ on flow and thermal fields are analyzed. Results indicate enhanced heat transfer for Ri < 100, with reduced oscillation amplitude of the mean Nusselt number at higher Ri. Moreover, increasing volume fraction leads to improve thermal performance. [12]

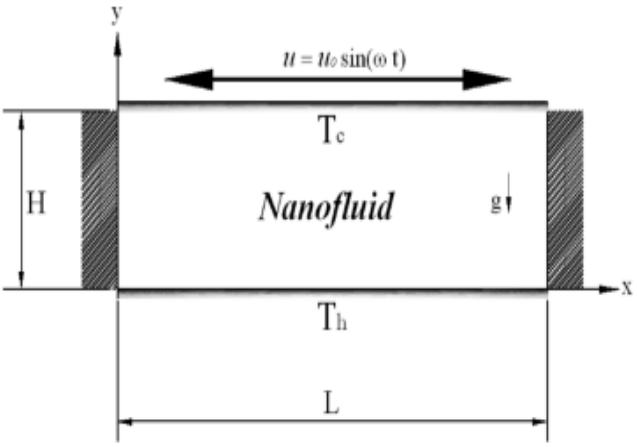

Figure I.9: Cavity With Top Lid Sinusoidal Motion [13]

The numerical study of **Arani et al. (2012),** examined mixed convection of Cu–water nanofluid in a lid-driven square cavity with adiabatic horizontal walls and sinusoidally heated vertical walls. The

analysis focuses on the influence of Richardson number, phase deviation of thermal boundary conditions, and nanoparticle volume fraction on flow structure and heat transfer. Results indicate that at fixed Grashof number, a single clockwise vortex dominates, and heat transfer increases with decreasing Richardson number and increasing nanoparticle concentration. For constant Reynolds number, a transition to multicellular flow is observed at high Richardson numbers (Ri ≥ 10), accompanied by enhanced thermal performance. [14]

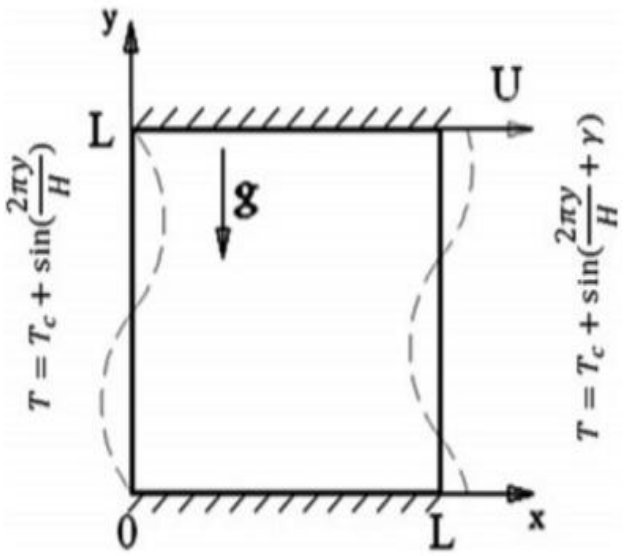

Figure I.10: Schematic Representation of the Square Cavity Along with the Applied Boundary Conditions Within the Computational Domain. [14]

Nasrin et al. (2012) examined the steady laminar combined convection in a vertical triangular wavy enclosure filled with water–CuO nanofluid. The vertical walls are wavy, and the horizontal walls move at equal speeds in opposite directions while maintained at lower temperatures. Using the Brinkman model and the Pak and Cho correlation, the non-dimensional governing equations are solved via the Galerkin finite element method. Results are validated against published data, show that heat transfer is significantly enhanced by nanoparticles and moderately influenced by decreasing Richardson number, and increasing Reynolds number and nanoparticle concentration. [15]

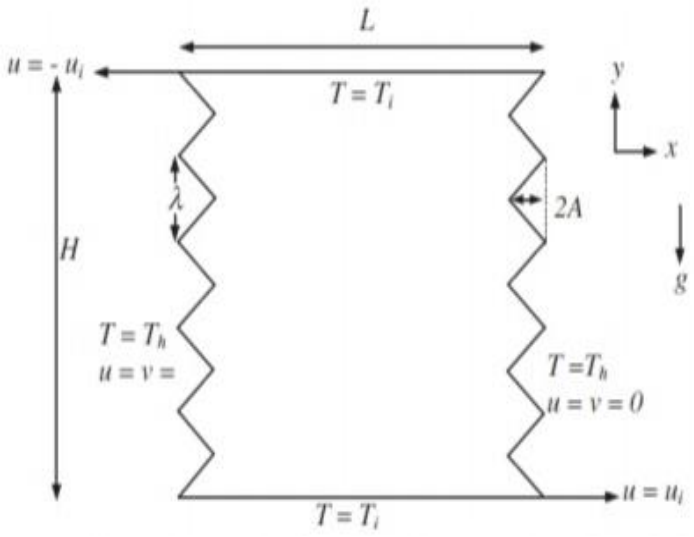

Figure I.11: Schematic Representation of a Triangular Cavity With Wavy Boundaries [15]

A numerical study of heat transfer and fluid flow in a square cavity with partially heated vertical walls filled with nanofluid was conducted by **Jmai et al. (2013)** using the finite volume method with a multigrid solver. Two constant heat flux sources are embedded in the sidewalls, while the top and bottom walls are cooled. The effects of Rayleigh number, nanoparticle type, solid volume fraction, and heat source location were analyzed. Results show that increasing Rayleigh number and nanoparticle concentration enhances heat transfer, with maximum performance depending on specific configurations. Empirical correlations were proposed linking Nusselt number to Rayleigh number and volume fraction. [16]

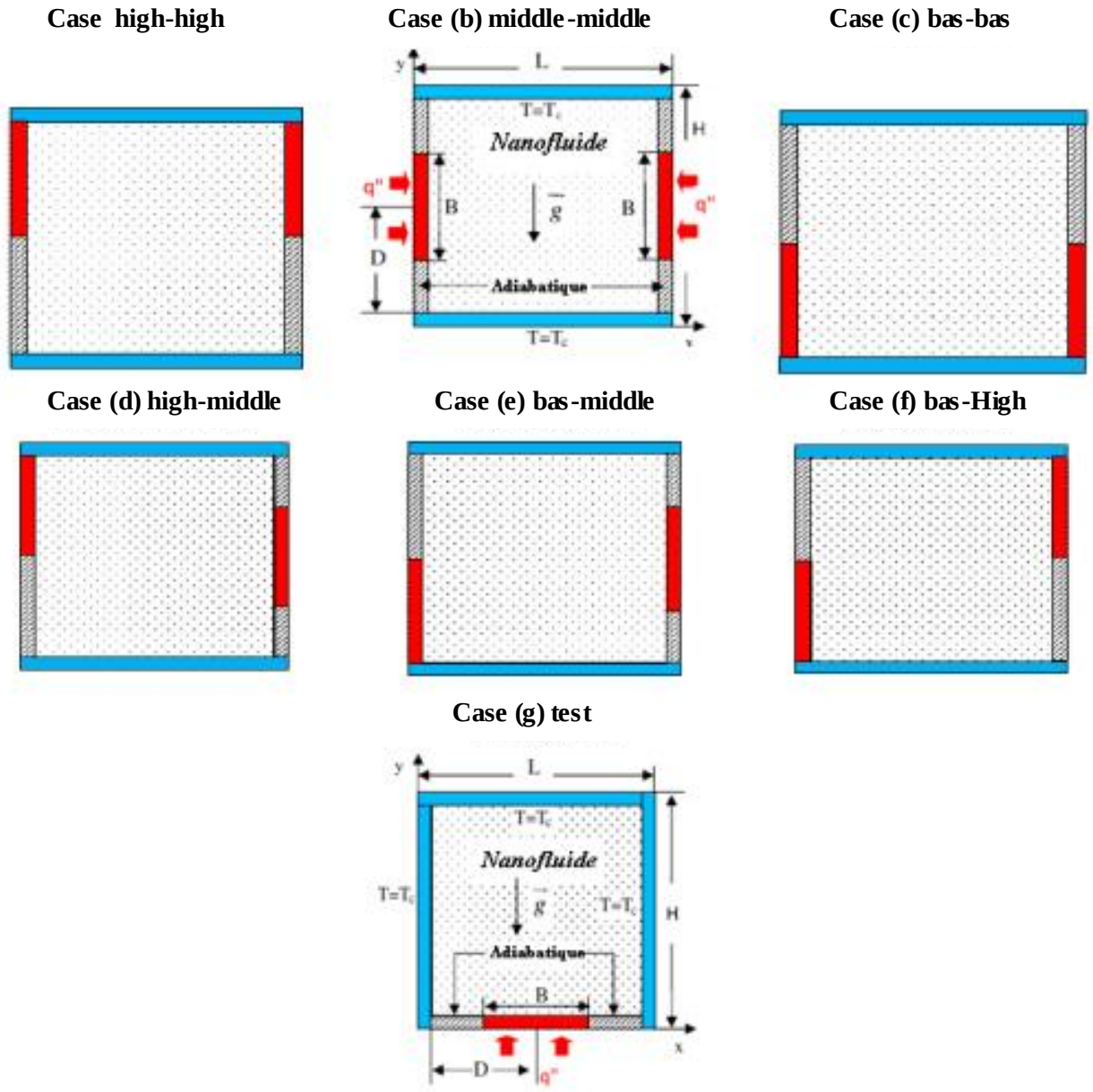

Figure I.12: Physical Model and Boundary Conditions for a Square Cavity With Thermally Active Sidewalls as Investigated in Various Studied Cases [16]

Billah and Rahman (2013) presented a numerical analysis of nanofluid flow and heat transfer in a lid-driven triangular enclosure with a partially heated bottom wall. The influence of heater length on convective behavior is investigated using the Galerkin finite element method to solve the continuity, momentum, and energy equations. Model validation shows excellent agreement with existing literature.

Simulations are conducted for various Richardson numbers and heater lengths using a copper–water nanofluid (Pr = 6.2). Results include streamlines, isotherms, average Nusselt number on the heated surface, and mean fluid temperature [17]

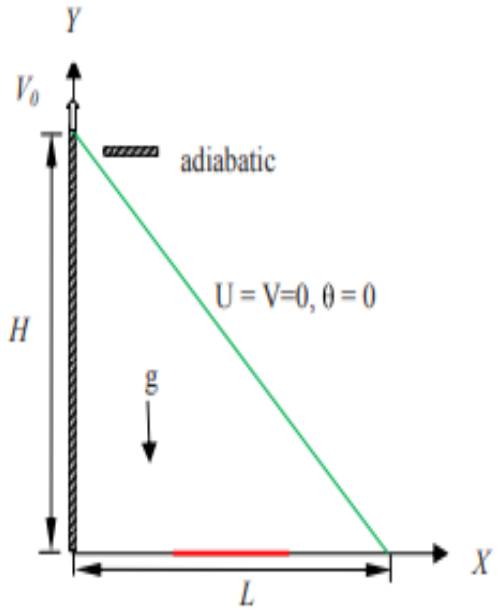

Figure I.13: Schematic Representation of the Physical Model Illustrating the Computational Domain Along with the Associated Boundary Conditions. [17]

A numerical investigation of natural and mixed convection in a laterally-heated square cavity was performed by **Garoosi et al . (2014**). The cavity is filled with Al_2O_3 -water nanofluid using the finite volume method. The effects of Rayleigh number, Richardson number, Grashof number, nanoparticle volume fraction, and particle size on heat transfer and nanoparticle distribution were analyzed. Results show the existence of an optimal volume fraction maximizing heat transfer for each Ra and Ri. Additionally, nanoparticle distribution is non-uniform at low Ra and high Ri, while it becomes nearly uniform at high Ra and low Ri in natural and mixed convection cases, respectively. [18]

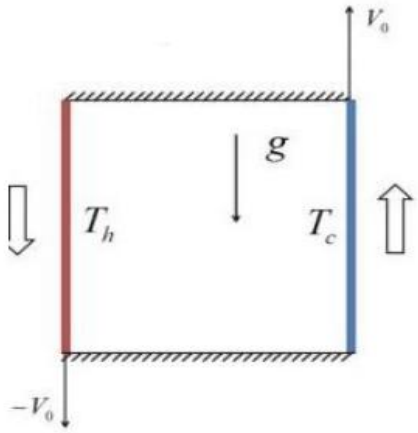

Figure I.14: Mixed Convection in a Horizontally Heated Square Cavity Filled with Al_2O_3 Water Nanofluids [18] [19]

The numerical study of **Mehrez et al. (2015)** analyzed the entropy generation and mixed convection heat transfer in Cu water nanofluid flow within an inclined open cavity uniformly heated from the vertical wall. The finite volume method is employed to solve the continuity, momentum, and energy equations. Results reveal a strong dependence of flow structure, thermal behavior, heat transfer characteristics, and entropy generation on the inclination angle, Reynolds number, and nanoparticle concentration. [20]

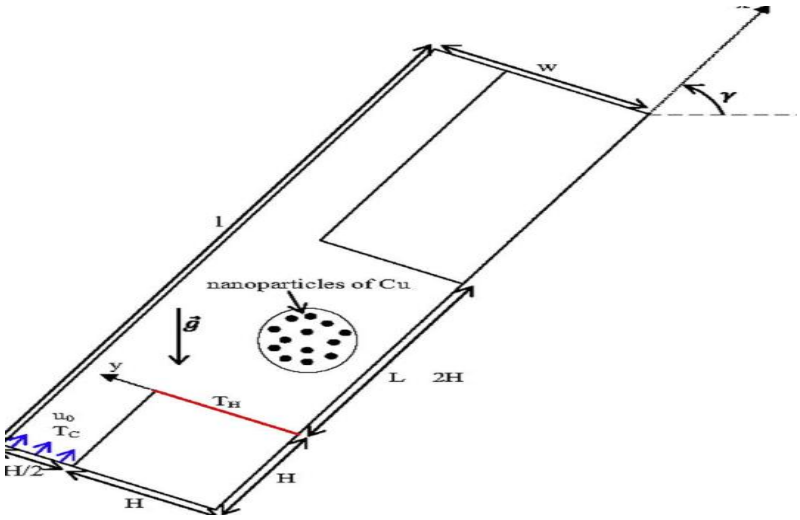

Figure I.15: Cu–Water Nanofluid FlowWithin an Inclined Open Cavity Uniformly Heated from the Vertical Wall [20]

The numerical investigation of **Hasib et al. (2015**) performed an analysis of the influence of inclination on mixed convection heat transfer in two lid-driven trapezoidal enclosures. One with the heated wall located on the shorter base and the other on the longer base. The top lid is modeled as an isothermal cold surface translating at constant velocity, while the bottom wall is subjected to a uniform high temperature. The working fluid is a water Al_2O_3 nanofluid. The dimensionless form of the governing Navier–Stokes and energy equations is solved using the Galerkin finite element method. Flow and thermal characteristics are examined using streamline and isotherm contours. The effects of inclination angle on the average Nusselt number at the heated wall and the mean fluid temperature within the cavity are analyzed to assess the thermal performance under varying geometric and flow conditions. [21]

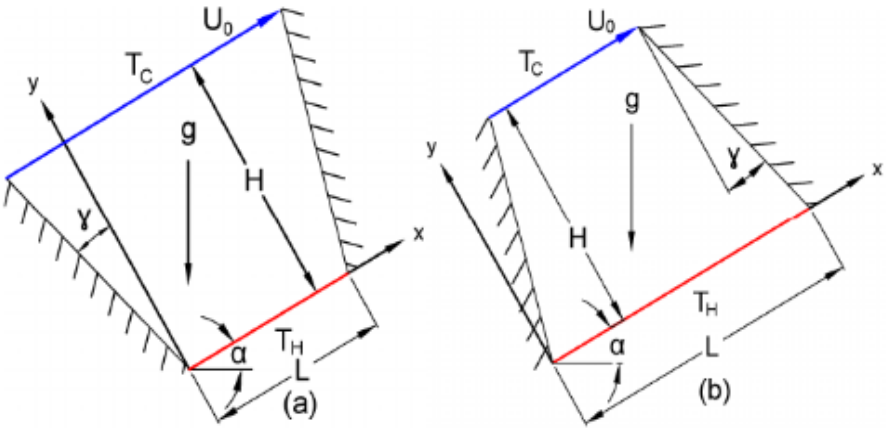

Figure I.16: Schematic Representation of Trapezoids Having Heated Wall on: Short Base (a) and long base (b) [21] [22]

The numerical study of **Aghaei et al. (2016**) studied the effect of a transverse magnetic field on mixed convection, heat transfer, and entropy generation of Cu–water nanofluid in a trapezoidal cavity with a heated bottom wall, insulated inclined sidewalls, and a cold moving top lid. The study is conducted for varying Reynolds numbers, Hartmann numbers, and nanoparticle volume fractions. The results show that increasing the magnetic field weakens convective flow, shifting the heat transfer mechanism from forced convection to conduction, which decreases the average Nusselt number. Increasing nanoparticle volume fraction reduces flow intensity, and entropy generation is primarily due to thermal irreversibility. The direction of lid motion significantly affects heat transfer and entropy generation at low Reynolds numbers but has little effect at high Reynolds numbers. [23]

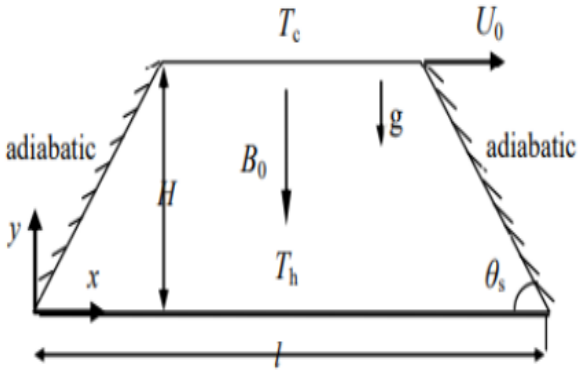

Figure I.17: Geometrical Configuration of the Trapezoidal Cavity [23] [24]

Zeghbid et al. (2017) analysed numerically the two-dimensional laminar mixed convection in a lid-driven square cavity filled with a nanofluid, heated by two vertical heat sources. The effects of Rayleigh number, Reynolds number, nanoparticle volume fraction, heat source position, and nanofluid type (Cu, Ag, Al_2O_3, TiO_2) on heat transfer are examined. Results show that the average Nusselt number increases with Rayleigh number and nanoparticle volume fraction, with Cu-water nanofluid enhancing heat transfer. The heat source position also affects flow and thermal fields, influencing local and average Nusselt numbers. [2]

Raizah et al. (2018) investigated the steady laminar magnetohydrodynamic mixed-convection flow in trapezoidal enclosures filled with water-based micropolar nanofluids. Key parameters such as Hartmann number, Richardson number, nanofluid type, magnetic field orientation, heat source location, and solid volume fraction are examined. Results show that the average Nusselt number increases with decreasing Richardson number and increasing solid volume fraction, but decreases as heat source length increases. The Hartmann number, heat source location, and viscosity significantly influence the heat transfer rate. The results align well with previous studies. [25]

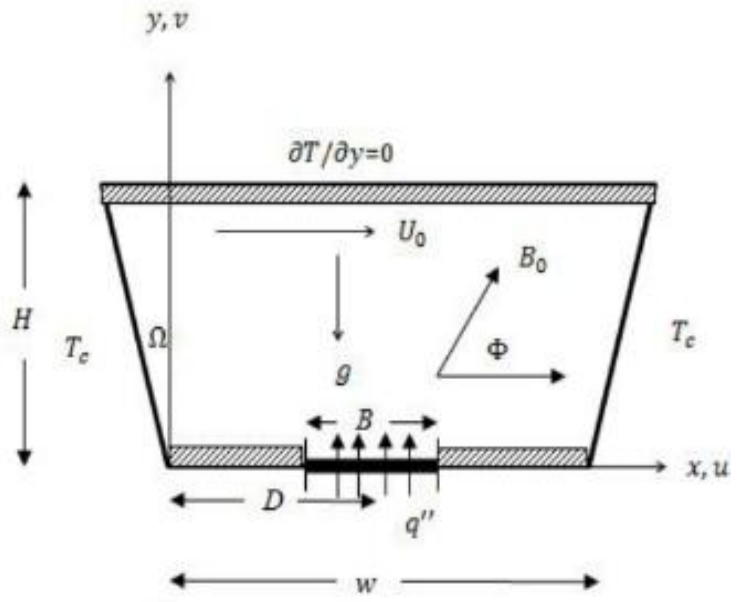

Figure I.18: Physical Model and the Coordinates System [25] [22]

In the study of **Abdullah et al. (2019)** the flow and heat transfer of a water–copper nanofluid in a trapezoidal enclosure with porous media were examined. Simulations are performed for different sidewall angles, Reynolds numbers, Darcy numbers, and nanoparticle volume fractions. Results show that the average Nusselt number increases with nanoparticle volume fraction and Reynolds number. A higher Darcy number enhances heat transfer, while a lower Darcy number reduces convection and heat transfer. [26]

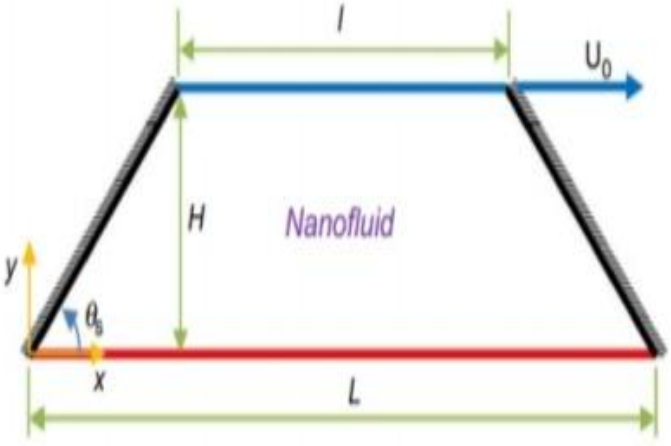

Figure I.19: Trapezoidal Enclosure with Porous Media [26]

Muhammad et al. (2020) investigated the mixed convective flow of Ag-ethylene glycol nanofluid within a cavity containing a heated central region. The cavity's side walls are maintained at a constant low temperature, while a constant heat source is applied to the bottom wall, with the remaining sections of the top and bottom walls being thermally insulated. The Cattaneo–Christov heat flux model is employed for heat transfer analysis. The results indicate that Fourier's law of heat conduction yields higher heat transfer rates compared to the Cattaneo–Christov model, as the latter introduces a more complex implicit formulation. Numerical simulations are carried out using the projection method, with results presented in terms of isothermal contours, streamline patterns, velocity profiles, and average Nusselt numbers. [27]

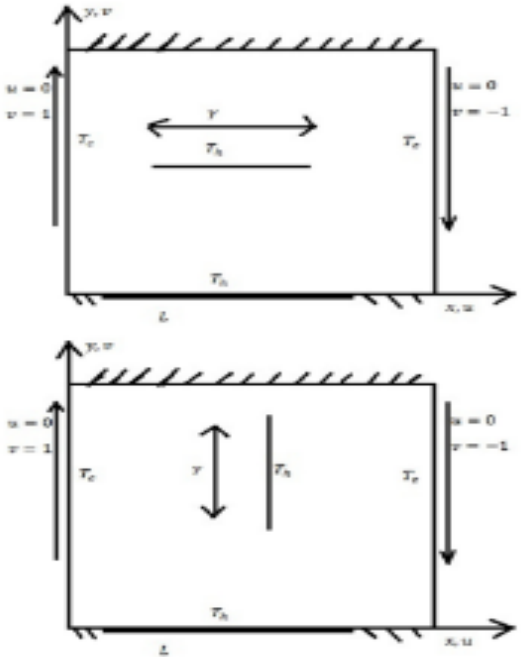

Figure I.20: Geometrical Configuration and Boundary Conditions of the Cavity with a Heated Central Region [27]

Ardalan et al. (2021) explored numerically the unsteady laminar mixed convection in a lid-driven enclosure filled with Cu–water nanofluid using the lattice Boltzmann method. The top wall moves with either constant or sinusoidal velocity, while the other walls are stationary. The top and bottom walls are held at cold and hot temperatures, respectively, and vertical walls are adiabatic. The effects of Richardson number and nanoparticle volume fraction on flow and heat transfer are analyzed. The study uniquely considers the mechanical power needed to drive the top wall, showing that nanofluids require

more power than pure fluids. However, applying a sinusoidal wall motion reduces power demand while maintaining heat transfer. Heat transfer improves with lower Richardson numbers, higher nanoparticle volume fractions, and lower oscillation frequencies, offering new insights into unsteady mixed convection in oscillating-wall enclosures. [28]

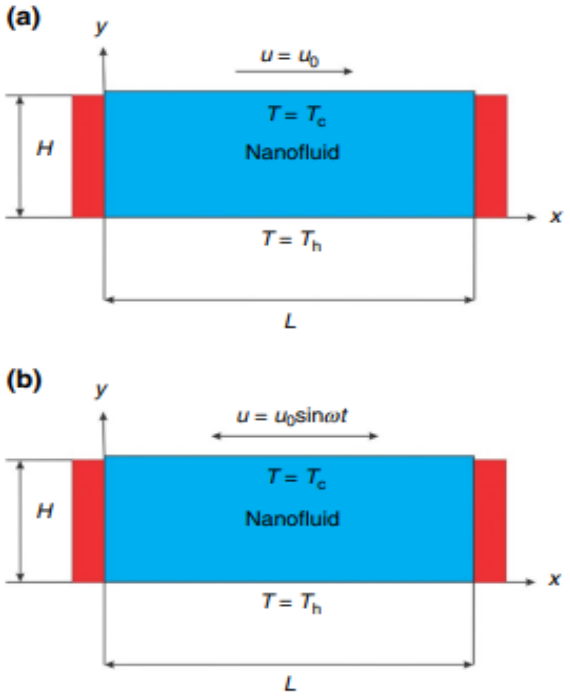

Figure I.21: The Schematic Representation of the Present Configuration with: (a) Sinusoidal and (b) Constant Velocity of the Top Moving Wall [28]

The numerical study of **Abbou et al. (2022)** inspested the effect of aspect ratio and non-uniform sinusoidal heating on mixed convection in an enclosure with moving, isothermal sidewalls and an adiabatic top wall. two counter-rotating vortices form, the vortices elongate and shift toward the heated wall. Numerical results show that heat transfer is highest at the center of the sinusoidally heated bottom wall and lowest at the edges. [12]

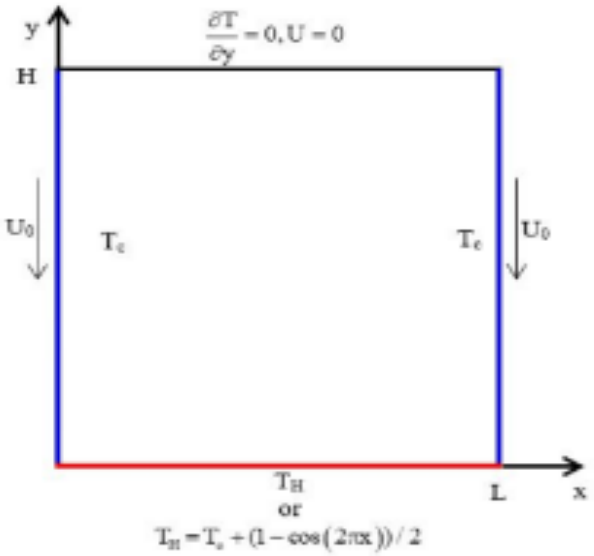

Figure I.22: An Enclosure Featuring Isothermal Sidewalls in Motion and a Adiabatic Top Wall [12]

Shinwari et al. (2024) presented a numerical investigation of magnetohydrodynamic (MHD) flow and entropy generation in a trihybrid nanofluid composed of ethylene glycol containing 2% each of Fe_2O_3, Ag, and Cu nanoparticles. Results demonstrate that the trihybrid nanofluid exhibits enhanced thermal conductivity compared to conventional fluids, nanofluids, and hybrid nanofluids. The presence of a magnetic field reduces the velocity field while increasing the temperature distribution. Key thermophysical parameters such as skin friction coefficient, Bejan number, entropy generation rate, and heat transfer rate are evaluated. It is observed that the Bejan number increases with the radiation parameter, and the numerical results show strong agreement with existing literature for curved surfaces at high thermal conductivity limits. [29]

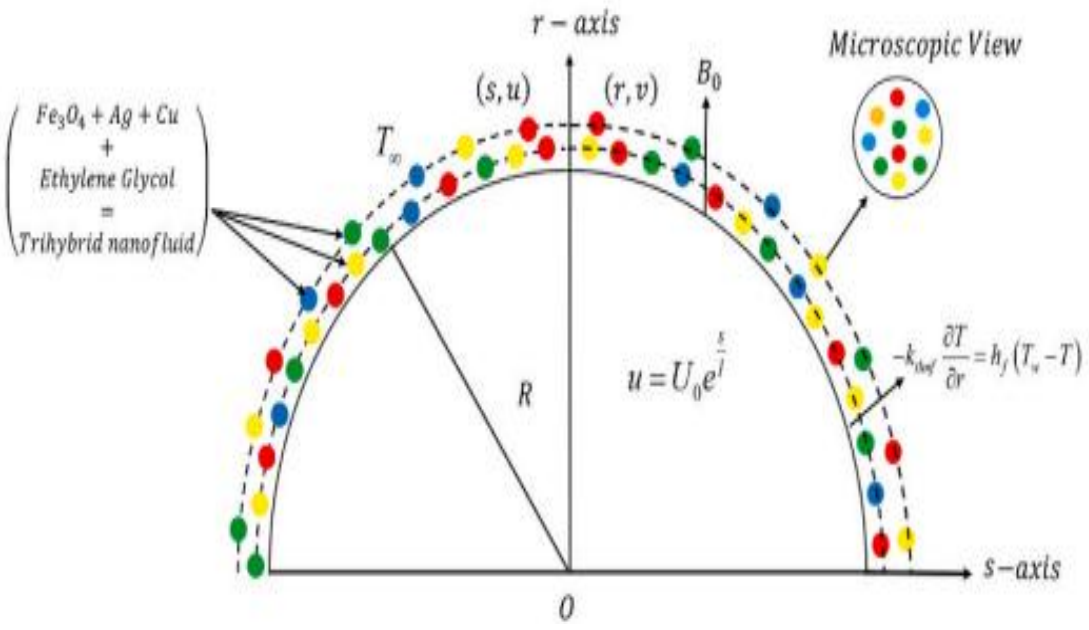

Figure I.23: Flow Diagram [29]

Al-kaby et al. (2025) studied the mixed convection heat transfer in a two-lid-driven enclosure with corrugated sidewalls, filled with a porous nanofluid, under an angled magnetic field. Using SWCNT-water and MWCNT-water nanofluids, the study analyzes the effects of parameters like Richardson number, Darcy number, Reynolds number, Hartmann number, and nanoparticle volume fraction. The results show that heat transfer increases with Darcy, Reynolds, and Richardson numbers, while Hartmann number and wave amplitude reduce heat transfer. MWCNT nanofluids lead to a 3% temperature rise compared to the base fluid. The findings are validated with existing literature. [30]

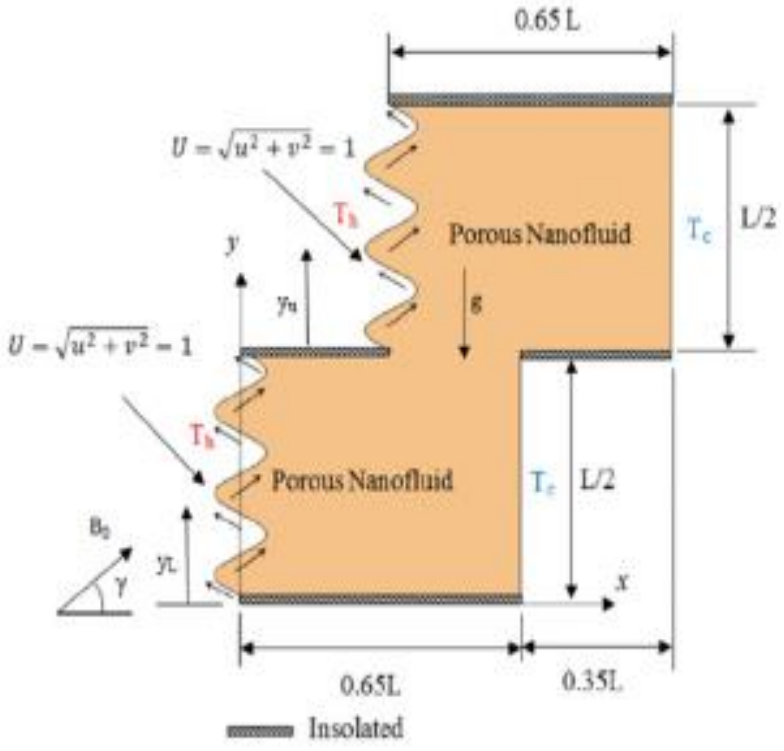

Figure I.24: Schematic View and Boundary Conditions of the Studied Configuration in Reference [30]

I.5 Conclusion

In the first chapter, we presented a general overview of nanofluids, followed by a literature review covering various studies. Researchers conducted analytical, numerical, and experimental studies, and specialists in the field focused on these works to better understand flow characteristics, heat transfer and cooling issues using mixed convection.

CHAPTER II:

Mathematical Modeling

II.1. Introduction

Heat transfer and fluid flow within a trapezoidal cavity are governed by the continuity equation, momentum equations, and energy equations. The mathematical convection model is based on equations that integrate several properties, such as pressure, temperature, and velocity. This chapter aims to evaluate the behavior of turbulent flow. It focuses on modeling and formulating the governing equations (continuity, momentum, and energy) and formulating them according to appropriate boundary conditions. It also highlights the relevant dimensionless numbers and thermophysical properties of the base fluids and nanoparticles used in numerical simulation.

II.2 Simplifying Assumptions

It is now necessary to make a number of assumptions in order to establish a simple mathematical model that describes the physics of this problem. Therefore, the following assumptions are adopted:

- The flow is steady and two-dimensional.
- The fluid is assumed to be incompressible.
- The generated flow is turbulence.
- Heat transfer by radiation is negligible.
- The physical properties of the fluid are constant except for the density, which obeys to the Boussinesq approximation in the buoyancy term.
- The flow is Homogene.
- The dissipated power density is negligible.

II.3 Dimensionalization of The Equations

II.3.1 Continuity Equation

The principle of conservation of the mass, during a flow, is expressed mathematically and represented as follows:

$$\frac{\partial}{\partial x_i}(\rho u_i) = 0 \qquad \text{II.1}$$

II.3.2 Momentum Equations

The principle of conservation of the quantity of movement makes it possible to establish the relations between the characteristics of the fluid and its movement and the cause, which produces it. The rate of change of momentum delimited in the volume may be equivalent to the total of all outside forces acting on it. For an incompressible Newtonian fluid, the Navier-Stokesequations for mixed convection in 2D are written in the following form

$$\frac{\partial}{\partial x_i}\left(\rho u_j u_j\right) = \frac{\partial P}{\partial x_i} + \frac{\partial}{\partial x_j}\left[\mu\left(\frac{\partial u_i}{\partial x_j} + \frac{\partial u_j}{\partial x_i}\right)\right] + \frac{\partial}{\partial x_j}\left(\rho\overline{u_i' u_j'}\right) \qquad \text{II.2}$$

II.3.3 Equation of Energy Conservation

It is a local expression of the first law of thermodynamics, which translates that the variation with respect to time of the total energy per unit volume. This principle connects different terms:

$$\frac{\partial}{\partial x_i}\left(\rho u_j T\right) = \frac{\partial}{\partial x_j}\left((\Gamma + \Gamma_t)\frac{\partial T}{\partial x_j}\right) \qquad \text{II.3}$$

$$\Gamma = \frac{\mu}{Pr} \qquad \text{II.4}$$

$$\Gamma_t = \frac{\mu_t}{Pr_t} \qquad \text{II.5}$$

The density, the specific heat and the thermal expansion coefficient are respectively presented by the following relations [31]:

$$\rho_{hnf} = (1-\varphi)\rho_f + \varphi_1\rho_1 + \varphi_2\rho_2 \qquad \text{II.6}$$

$$(\rho C_p)_{hnf} = (1-\varphi)(\rho C_p)_{hnf} + \varphi_1(\rho C_p)_1 + \varphi_2(\rho C_p)_2 \qquad \text{II.7}$$

$$(\rho\beta)_{hnf} = (1-\varphi)(\rho\beta)_{hnf} + \varphi_1(\rho\beta)_1 + \varphi_2(\rho\beta)_2 \qquad \text{II.8}$$

The Dynamic viscosity of the hybrid nanofluid is related to the volume fraction and the dynamic viscosity of the base fluid by the following relation [32]:

$$\mu_{hnf} = \frac{\mu_f}{(1-\varphi)^{2.5}} \qquad \text{II.9}$$

Thermal Conductivity is expressed by [33]:

$$K_{hnf} = K_f \left[\frac{\left(\frac{\rho_1 K_1 + \rho_2 K_2}{\varphi}\right) + 2K_f + 2(\rho_1 K_1 + \rho_2 K_2) - 2\varphi K_f}{\left(\left(\frac{\rho_1 K_1 + \rho_2 K_2}{\varphi}\right)\right) + 2K_f - (\rho_1 K_1 + \rho_2 K_2) + \varphi K_f} \right] \quad \text{II.10}$$

$$\alpha_{hnf} = \frac{K_{hnf}}{(\rho C_p)_{hnf}} \quad \text{II.11}$$

II.4 Boundary Condition

➢ *Temperature :*

- Bottom :T_c
- Top : T_f = 298 k
- Right and Left : $\frac{\partial T}{\partial x} = 0$

➢ *Velocity :*

- Bottom : U=V= 0
- Top: $U = U_0 \quad ; \quad V = 0$

Left and right walls: U=V= 0

II.5 Non-dimensionalization of the equations

The non-dimensional form is used to find general solutions to physical problems regardless of the unit systems, and to reduce the number of parameters in our study. It also allows for the simplification of solving systems of equations. To highlight the control parameters of the studied problem, it is necessary to introduce reference quantities.

Characteristic Quantities

The characteristic quantities are defined as follows:

- H is the characteristic length
- U_0 is the reference velocity
- ΔT is the characteristic temperature difference

$$X = \frac{x}{H} \quad , \quad T = \frac{T - T_c}{T_h - T_c}$$

$$Y = \frac{y}{H} , \quad , \quad P = \frac{p}{U_0{}^2 \rho_{hnf}}$$

$$U = \frac{u}{U_0} \quad , \quad V = \frac{v}{U_0}$$

After substituting the dimensionless variables into the equations of the mathematical model and into the boundary conditions, the following system of dimensionless equations is obtained

II.5.1 Equation of continuity

$$\frac{\partial U}{\partial X} + \frac{\partial V}{\partial Y} = 0 \qquad \text{II.12}$$

II.5.2 Momentum equations

- ✓ **Momentum equation along the axis (x)**

$$U\frac{\partial U}{\partial X} + V\frac{\partial U}{\partial Y} = -\frac{\partial P}{\partial X} + \frac{1}{Re}\left(\frac{\partial^2 U}{\partial X^2} + \frac{\partial^2 U}{\partial Y^2}\right) - \frac{\overline{\partial U'U'}}{\partial X} - \frac{\overline{\partial U'V'}}{\partial Y} \qquad \text{II.13}$$

- ✓ **Momentum equation along the axis (y)**

$$U\frac{\partial V}{\partial X} + V\frac{\partial V}{\partial Y} = -\frac{\partial P}{\partial X} + \frac{1}{Re}\left(\frac{\partial^2 U}{\partial X^2} + \frac{\partial^2 U}{\partial Y^2}\right) - \frac{\overline{\partial V'U'}}{\partial X} - \frac{\overline{\partial V'V'}}{\partial Y} + Ri.T \qquad \text{II.14}$$

II.5.3 Equation of energy conservation

$$U\frac{\partial T}{\partial X} + V\frac{\partial T}{\partial Y} = \frac{1}{\mathrm{Re\,Pr}}\left[\frac{\partial}{\partial X}\left(1 + \frac{\alpha_t}{\alpha}\right)\frac{\partial T}{\partial X}\right) + \frac{\partial}{\partial Y}\left(1 + \frac{\alpha_t}{\alpha}\right)\frac{\partial T}{\partial Y}\right)\Big] \qquad \text{II.15}$$

The geometrical configuration and its boundary conditions is presented in Figure II.1.

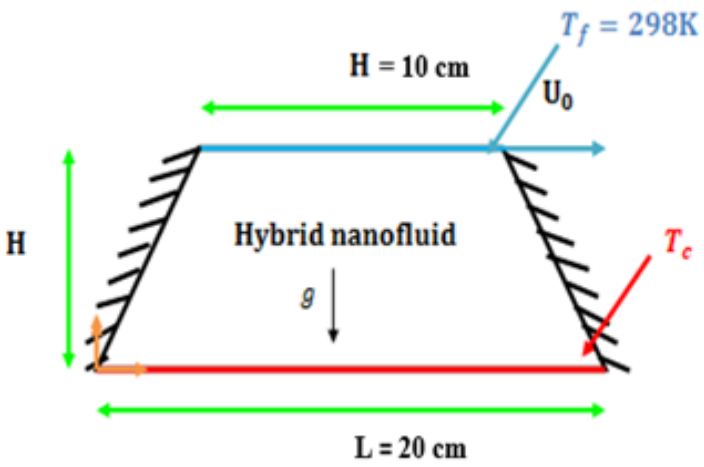

Figure II.1: Geometrical Configuration

II.6 Dimensionless Numbers [34]

In equations the last equations the dimensionless numbers (Pr, Re, Ri) are defined as follows:

- Prandtl number : $Pr = \frac{\upsilon_f}{\alpha_f}$
- Reynolds number: $Re = \frac{\rho v D}{\mu} = \frac{U_0\, H}{\upsilon_f}$
- Grashofnumber: $Gr = \frac{g\beta L^3 (T_h - T_0)}{\upsilon^2}$
- Richardson number: $Ri = \frac{Gr}{Re^2} = \frac{g\beta L (T_h - T_0)}{{U_0}^2}$
- Rayleigh number: $Ra = Pr.Gr = \frac{g\beta L^3 (T_h - T_0)}{\alpha_f \upsilon_f}$
- Nusselt Number : $Nu = \frac{h\, L}{\mathrm{K}}$

For Y = 1 ; $0.5 < X < 1.5$; $U = 1$; V = 0 ; T = 0

For Y = 0 ; $0 < X < 2$; : U = 0 ; $V = 0$; T = 1

Right and Left wall : U = 0 ; $V = 0$; $\frac{\partial \mathrm{T}}{\partial \mathrm{x}} = 0$

II.7 Reynolds-Averaged Navier-Stokes (RANS) Equations

For incompressible flow, the RANS equations decompose the velocity component u_i into a mean component $\overline{u_i}$ and a fluctuating component u_i', as indicated in [35] and [36]:

$$\frac{\partial \overline{u_i}}{\partial t} + \overline{u_j}\frac{\partial \overline{u_i}}{\partial x_j} = -\frac{1}{\rho}\frac{\partial \overline{P}}{\partial x_i} + \vartheta\frac{\partial^2 \overline{u_i}}{\partial {x_j}^2} - \frac{\partial \overline{u_i' u_j'}}{\partial x_j} \qquad \text{II.16}$$

II.8 k–ε Model Equations

The standard k-ε model introduces two transport equations to close the RANS system:

II.8 .1 Turbulent Kinetic Energy Equation (k-equation)

The turbulent kinetic energy K represents the energy contained in turbulent velocity fluctuations and is defined as:

$$K = \frac{1}{2}\overline{u_i' u_i'} \qquad \text{II.17}$$

$$\frac{\partial(\rho K)}{\partial t} + \frac{\partial(\rho K \overline{u_i})}{\partial x_i} = \frac{\partial}{\partial x_j}\left[(\mu + \frac{\mu_t}{\sigma_k})\frac{\partial K}{\partial x_j}\right] + P_k - \rho_\varepsilon \qquad \text{II.18}$$

where:

- σ_k is the turbulent Prandtl number for k.
- P_k is the production of turbulent kinetic energy due to the mean velocity gradient,

$$P_k = 2\mu_t E_{ij} E_{ij} \qquad \text{II.19}$$

- E_{ij} is the mean strain rate tensor.

$$E_{ij} = \frac{1}{2}\left(\frac{\partial \overline{u_i}}{\partial x_j} + \frac{\partial \overline{u_j}}{\partial x_i}\right) \qquad \text{II.20}$$

II.8.2 Dissipation Rate (ε) Equation

The dissipation rate (ε) characterizes the rate at which turbulent kinetic energy is converted into thermal energy by viscous effects [36, 37] . It is governed by the following transport equation:

$$\frac{\partial(\rho\varepsilon)}{\partial t}+\frac{\partial(\rho\varepsilon\overline{u_i})}{\partial x_j}=\frac{\partial}{\partial x_j}\left[(\mu+\frac{\mu_t}{\sigma_\epsilon})\frac{\partial\varepsilon}{\partial x_j}\right]+C_{1\varepsilon}\frac{\varepsilon}{K}P_k-C_{2\varepsilon}\rho\frac{\varepsilon^2}{K} \qquad \text{II.21}$$

where:

- σ_ϵ is the turbulent Prandtl number for ε.
- k is the turbulent kinetic energy.
- ε is the dissipation rate of turbulent kinetic energy.
- μ_t is the eddy (turbulent) viscosity coefficient.

$$\mu_t=\rho C_\mu\frac{K^2}{\varepsilon} \qquad \text{II.22}$$

$$C_\mu=0.09\ ;\ C_{1\varepsilon}=1.44\ ;\ C_{2\varepsilon}=1.92\ ;\ \sigma_\epsilon=1.3\ ;\ \sigma_\mu=1$$

II.9 Conclusion

In this chapter, we presented the assumptions considered in our work. The aim was also to present the problem geometry and its formulation, beginning with a detailed description of the methods used to create and generate the mesh of the physical domain. The continuity, momentum, and energy equations with the boundary conditions were used for describing the flow and heat transfer inside the cavity. We also presented the reference dimensionless parameters and the dimensionless numbers. This information can be used to simulate the flow and study the effects of various parameters. On the other hand, a clear approach was provided for the methods to be followed in solving the equations governing this phenomenon.

CHAPTER III:

Numerical Study

III .1.Introduction

Heat transfer prediction and the analysis of phenomena occurring during fluid flow can be approached through three main methods: experimentation, theoretical calculation, and numerical calculation. In this chapter, we will focus on numerical calculations and outline the steps involved in solving a fluid flow problem numerically.

III.2 Numerical Modeling and Simulation

Numerical computation involves the transformation of a mathematical model, typically formulated as a partial differential equation (PDE), into a system of algebraic equations.

III.2 .1 Principle of Numerical Calcul

The most commonly used discretization methods are:

– Finite Difference Methods (FDM) .
– Finite Element Methods (FEM) .
– Spectral Methods (SM).
– Finite Volume Methods (FVM).

The numerical solution algorithm involves time integration and decoupling methods, such as the ¨SIMPLE¨, ¨SIMPLER¨, ¨SIMPLEC¨, and ¨PISO¨ algorithms.

III.2 .1 .1 Advantages Numerical Computation

- Enables the calculation of numerical solutions for nearly all practical problems that can be modeled mathematically.
- Is cost-effective, with a tendency for decreasing costs.
- Offers speed and flexibility (e.g., easy modification of geometry, boundary conditions, etc.).
- Provides complete information about all fields, at every point and at any time.
- Has the ability to simulate exceptional real-world conditions.
- Allows the simulation of idealized conditions.

III.2 .1 .2 Disadvantages of Numerical Computation

- Entirely dependent on the initial mathematical model.
- Difficulty in selecting the "correct" solution in the case of multiple mathematical solutions.
- Sometimes more expensive than experimental approaches.

For the present study, the finite volume method (FVM) was chosen due to its significant advantages. It is simple to implement , It ensures the conservation of mass and momentum in each control volume and across the entire computational domain, it is applicable to complex geometries.

III.2 .2 Overview of the Finite Volume Method (FVM)

The method was first described in 1971 by Patankar and Spalding, and later published in 1980 by Patankar in Numerical Heat Transfer and Fluid Flow. It is a discretization technique that transforms conservation equations in partial differential form into algebraic equations solvable numerically. The control volume approach consists of integrating the partial differential equations over each control volume to obtain discretized equations that preserve all physical quantities over a control volume (CV).

III.2 .2 .1 Advantages of the Finite Volume Method

- Preserves the conservative nature of equations on each control volume (continuity of fluxes at interfaces), regardless of mesh resolution;
- Relatively easy to implement;
- Applicable to complex geometries;
- Offers reasonable computation time and memory requirements (banded matrix structure).

III.2 .2 .2 Disadvantages

Generally less accurate than spectral methods.

III.2 .3 Steps of the Numerical Algorithm

1. Discretization of the computational domain into finite volumes (mesh generation).
2. Formal integration of the governing equations over all control volumes.

3. Discretization, which involves replacing the integrated terms with approximations (usually finite differences) representing various flow phenomena such as convection, diffusion, and source terms. The result is a system of algebraic equations.
4. Solving the system of algebraic equations using an appropriate numerical method. [37]

III.2 .4 The Different Phases of the Numerical Approach

The main phases of the numerical approach can be summarized as follows:

- **Geometry generation and domain discretization**: These two operations are carried out using Gambit software. A fine mesh, especially near the walls, is required to accurately capture the high velocity and pressure gradients in these regions.
- **Application of boundary conditions**: This step is also performed in *Gambit*, where the appropriate hydrodynamic and thermal conditions are imposed on the domain boundaries.
- **Numerical simulation using the FLUENT solver**: The problem is solved using FLUENT software, which integrates the governing conservation equations through suitable numerical methods. [37]

III.3 Introduction to the GAMBIT Software

GAMBIT (Geometry And Mesh Building Intelligent Toolkit) is a 2D/3D meshing software and pre-processor designed for discretizing the geometric domains of Computational Fluid Dynamics (CFD) problems. It facilitates the generation of both structured and unstructured meshes in Cartesian, polar, cylindrical, or axisymmetric coordinate systems. GAMBIT supports the creation of complex meshes in two or three dimensions using either rectangular or triangular elements. Its mesh generation options offer considerable flexibility.

The geometric domain can be subdivided into multiple subregions to facilitate structured meshing. Alternatively, GAMBIT can automatically generate an unstructured mesh that conforms to the specific characteristics of the constructed geometry. The integrated mesh verification tools enable efficient identification of meshing defects.

GAMBIT can be employed to construct geometry directly and generate its corresponding mesh. Additionally, geometry created using other CAD software can be imported into this pre-processor. The software exports mesh files in the *.msh format compatible with Fluent. [38]

III.3.1 Launching GAMBIT

The executable path for launching GAMBIT is: **`/Fluent.Inc/ntbin/ntx86/Gambit.exe`.** It is recommended to create a shortcut on the taskbar for ease of access. In case of execution issues, delete all ***.lok** files located in the **`/Fluent.Inc/ntbin/ntx86` directory** and restart **Gambit.exe.**(Initiation aux logiciels Gambit et Fluent)

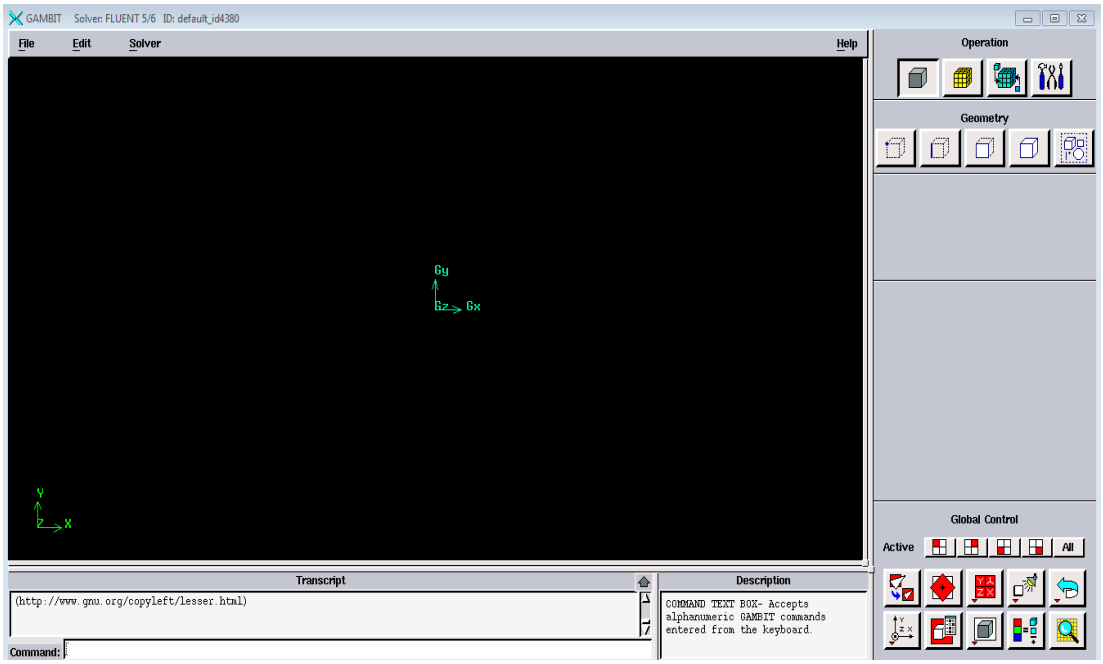

Figure III.1: Gambit Launch.

III.3.2 Gambit Functions

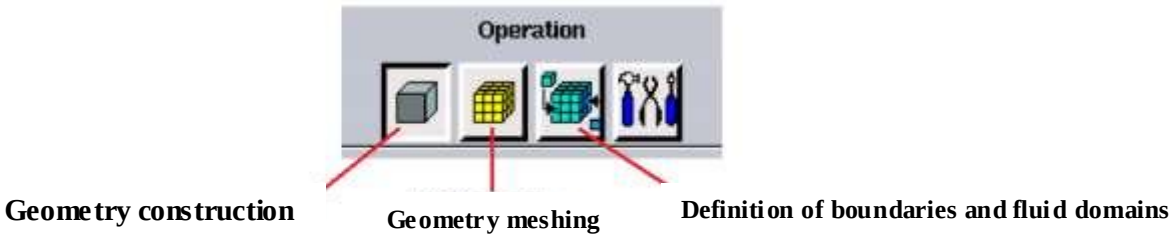

Figure III.2: Main functions of the Gambit General Menu [38]

Click on the menu function to generate a second menu that corresponds to the screen immediately

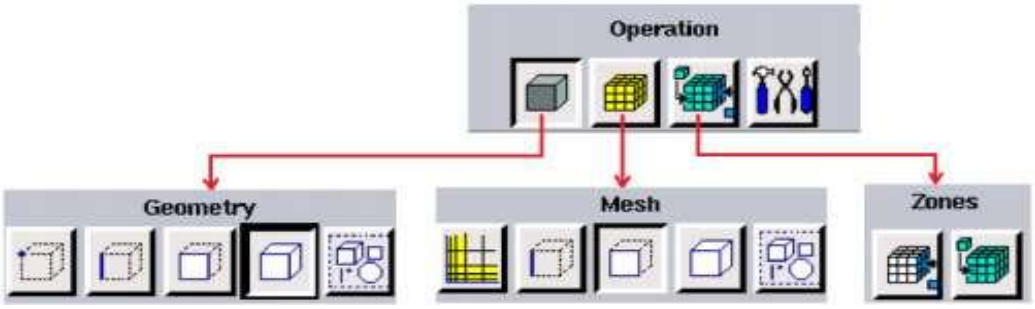

Figure III.3: Gambit Secondary Menus [38]

III.3.2 .1 Description of the Geometry Menu

The final construction of the geometry is to determine the calculus domains that serve faces in a 2D problem and volumes in a 3D problem.

Commande	Point	Segment	Face	Volume	Groupe
Symbole					

Figure III.4: Description of the Geometry Menu Commands [38]

Step 1: Create the Initial Vertices

Generate vertices that represent the structure of the geometric model

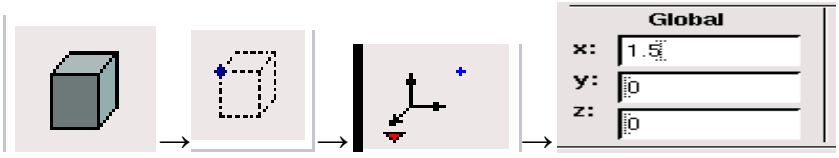

Figure III.5: Create the Initial Vertices

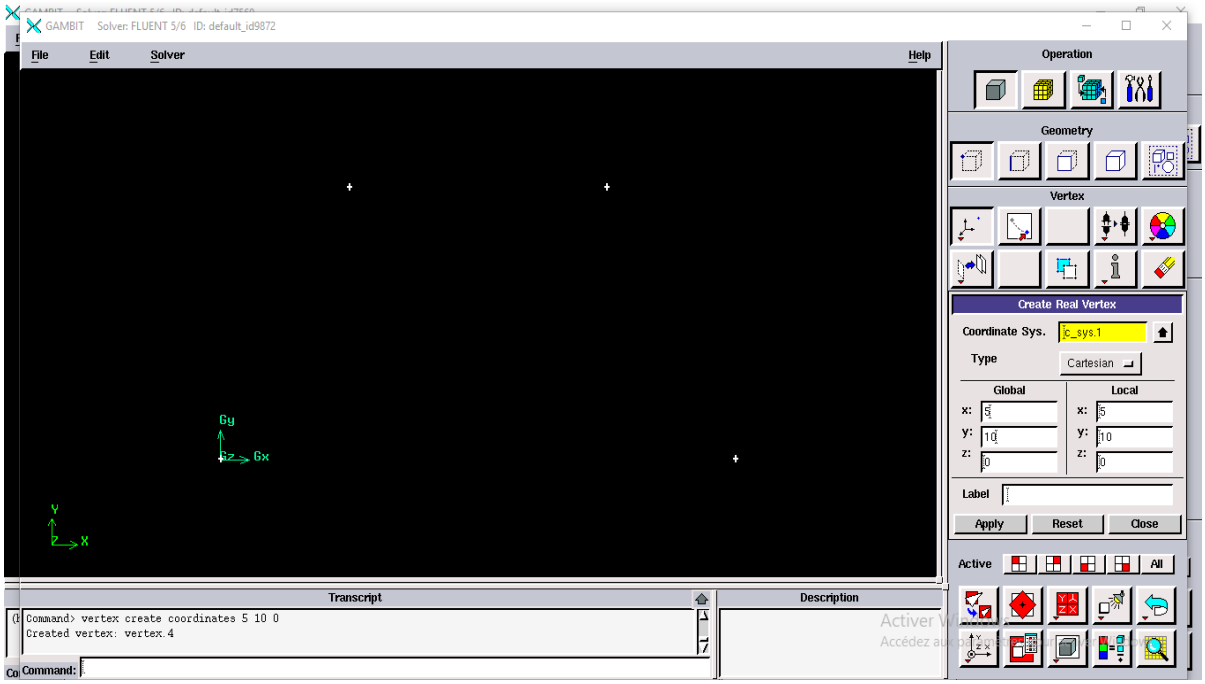

Figure III.6: Vertices

Step 2: Connect the vertices with straight edges

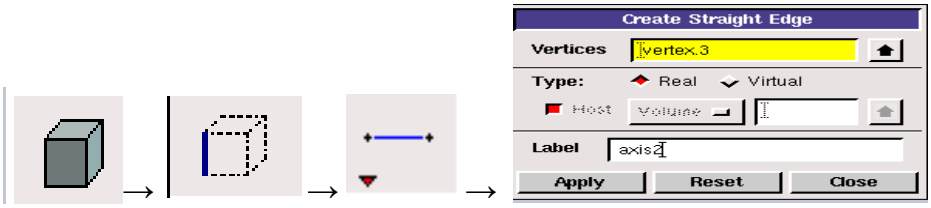

Figure III.7: Connect the Vertices with Straight Edges

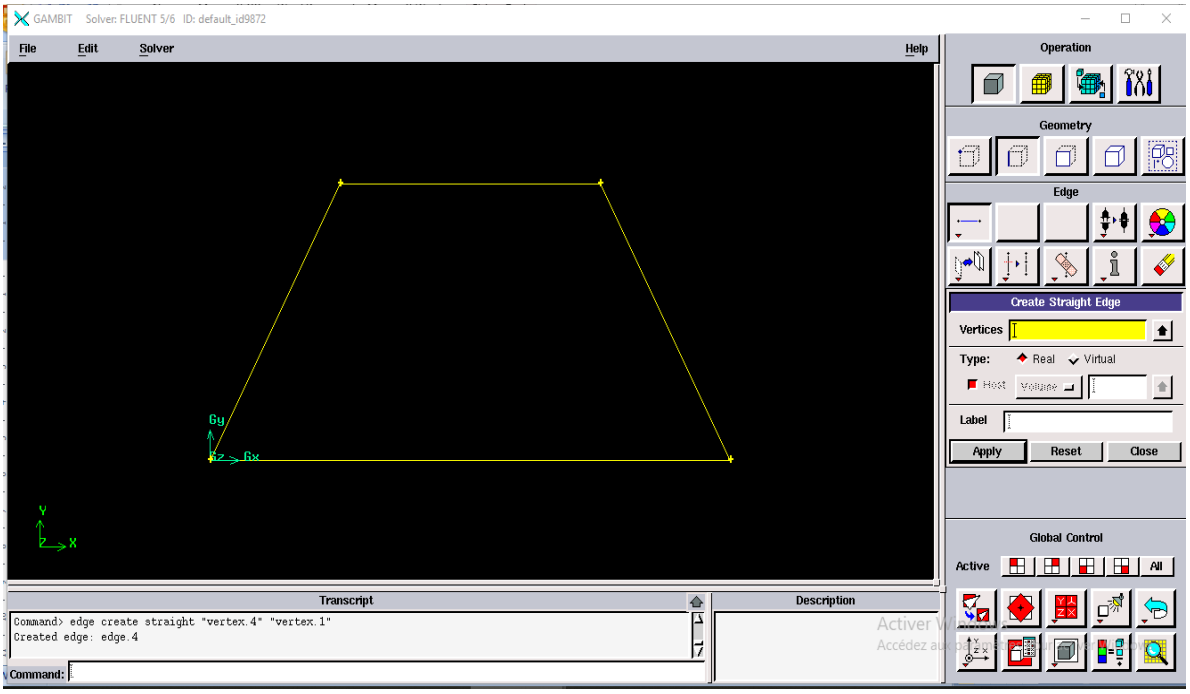

Figure III.8: A Face

Step 3: Construct a face from the selected edges

Mesh generation can be performed as either a two-dimensional surface mesh applicable in the present study or as a three-dimensional volumetric mesh. Prior to the construction of the geometric model, meticulous planning of the topological decomposition of the physical domain is imperative. The choice of mesh type plays a pivotal role in determining the accuracy and computational efficiency of the numerical simulation and must be appropriately aligned with the characteristics of the problem being addressed. [2]

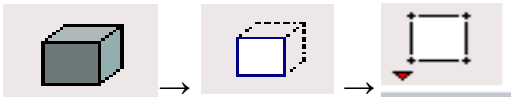

Figure III.9: Construct a Face from the Selected Edges

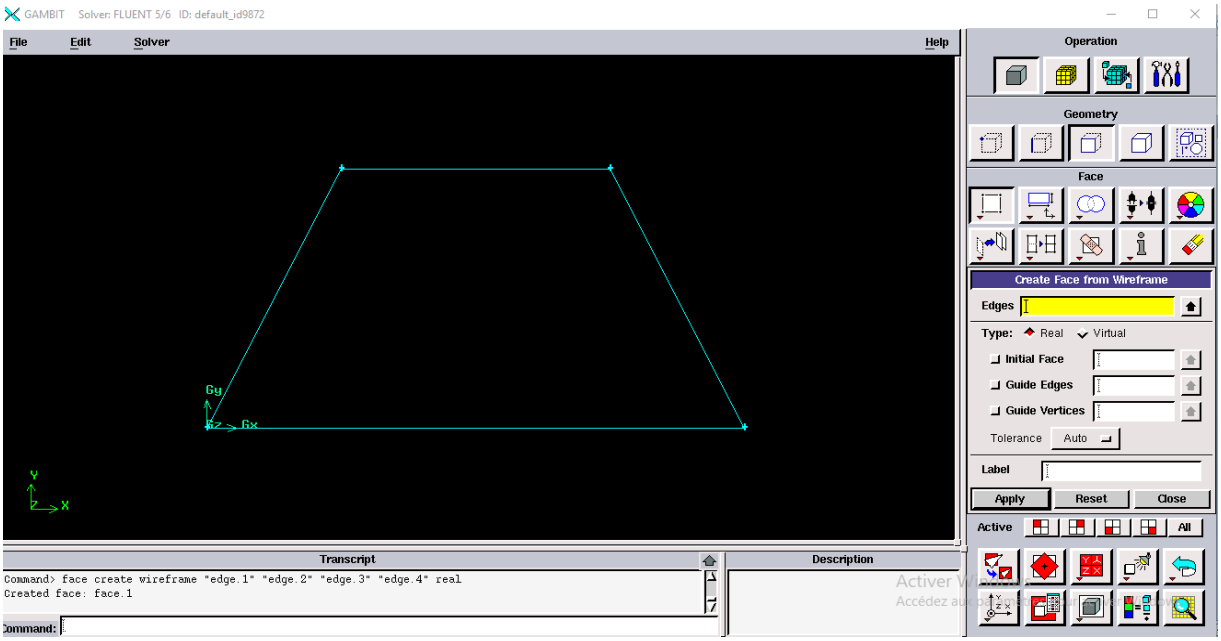

Figure III.10: Creation of Geometry

III.3.2 .2 Description of the Mesh Menu

The Mesh menu contains five buttons, as outlined in the table below

Commande	Couches limites	Segment	Faces	Volume	Groupe
Symbole					

Figure III.11: Description of the Mesh Menu Commands [38]

Step 1: Create structured or non structured meshes on the edges

Figure III.12: Create Structured/Non Structured Meshes on the edges

We have chosen the non structured mesh to capt the important gradient of variables near to the upper and lower walls, in these regions

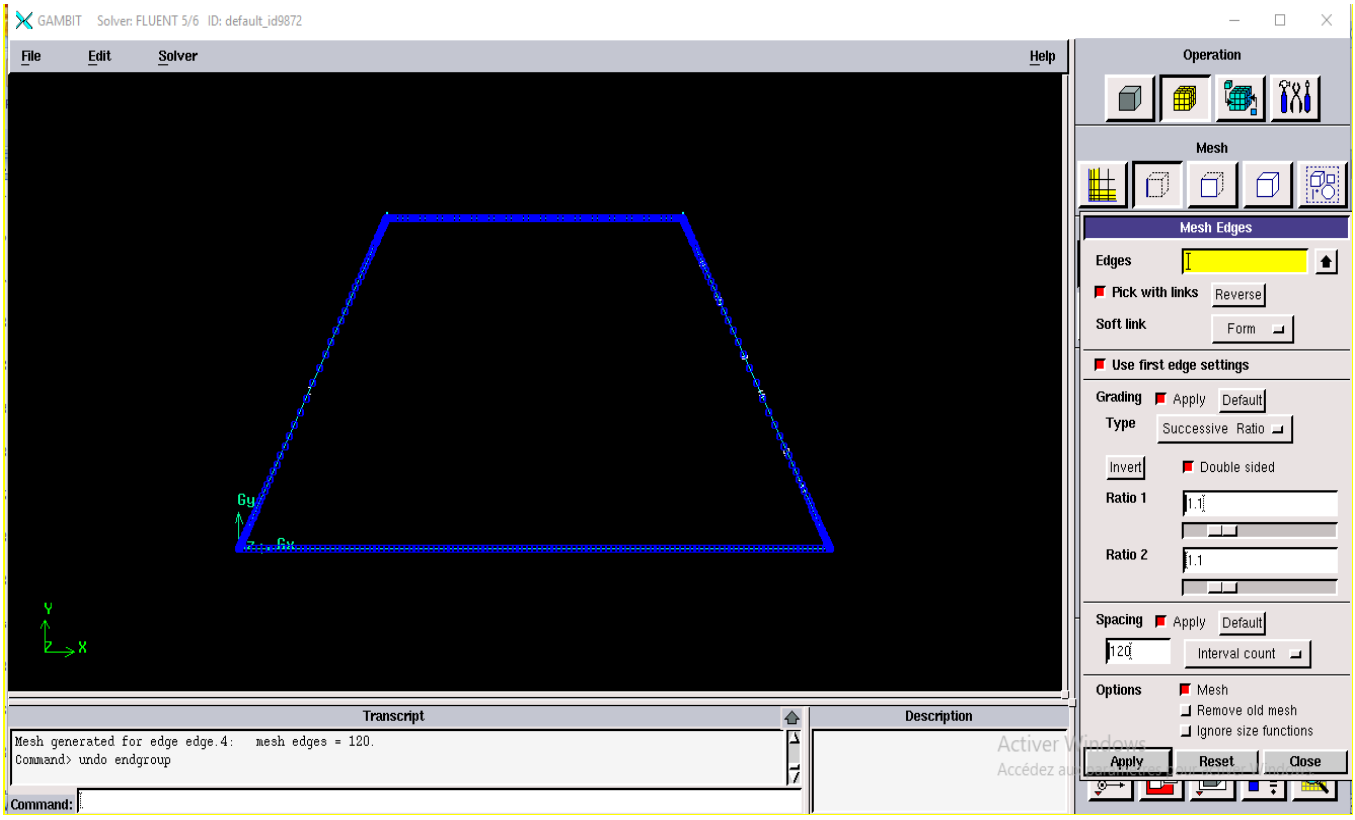

Figure III.13: Non Structured Meshes

Step 2: Create structured meshes on the faces

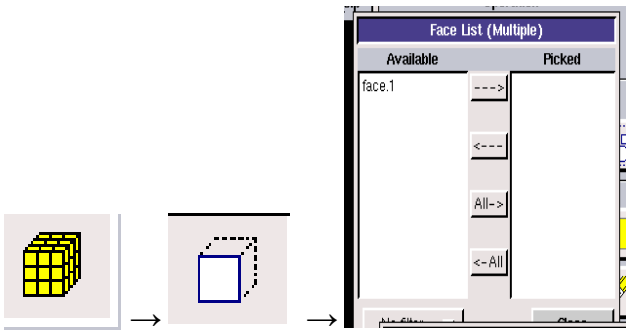

Figure III.14: Create Structured Meshes on the Faces

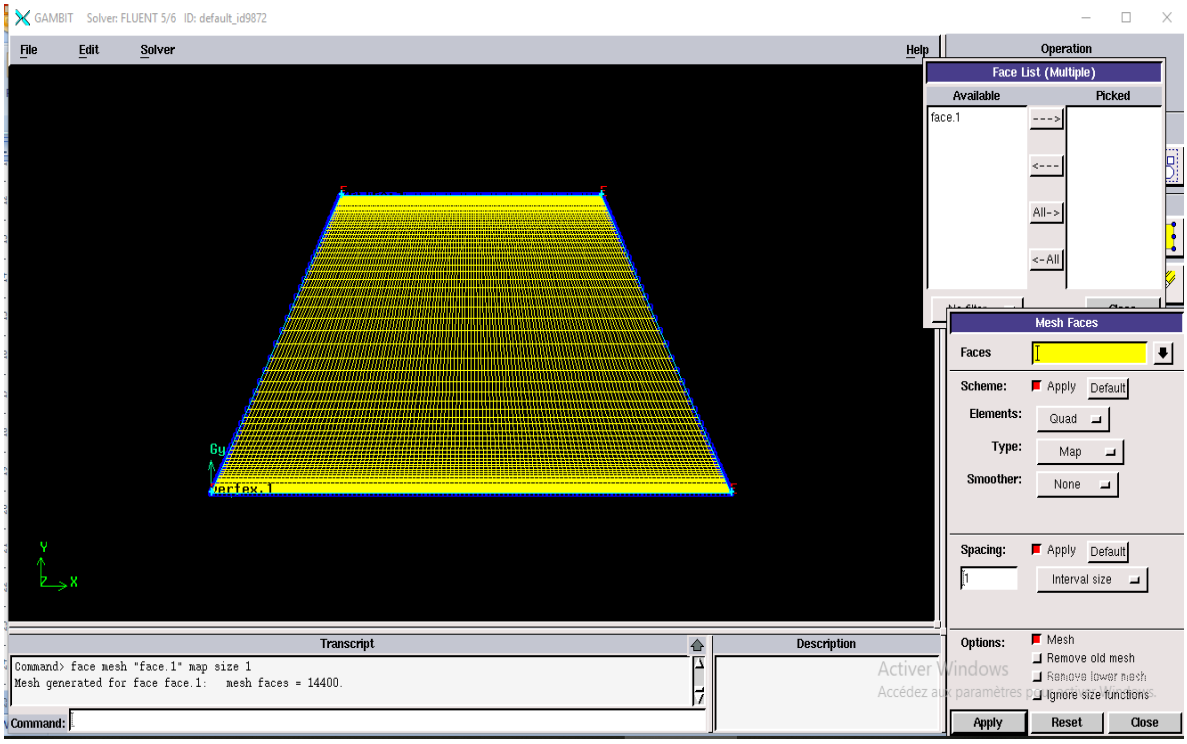

Figure III.15: Surface Mesh

III.3.3 Conditions and Limits and Domain Definitions

When we finish meshing the domain, we set the boundary conditions

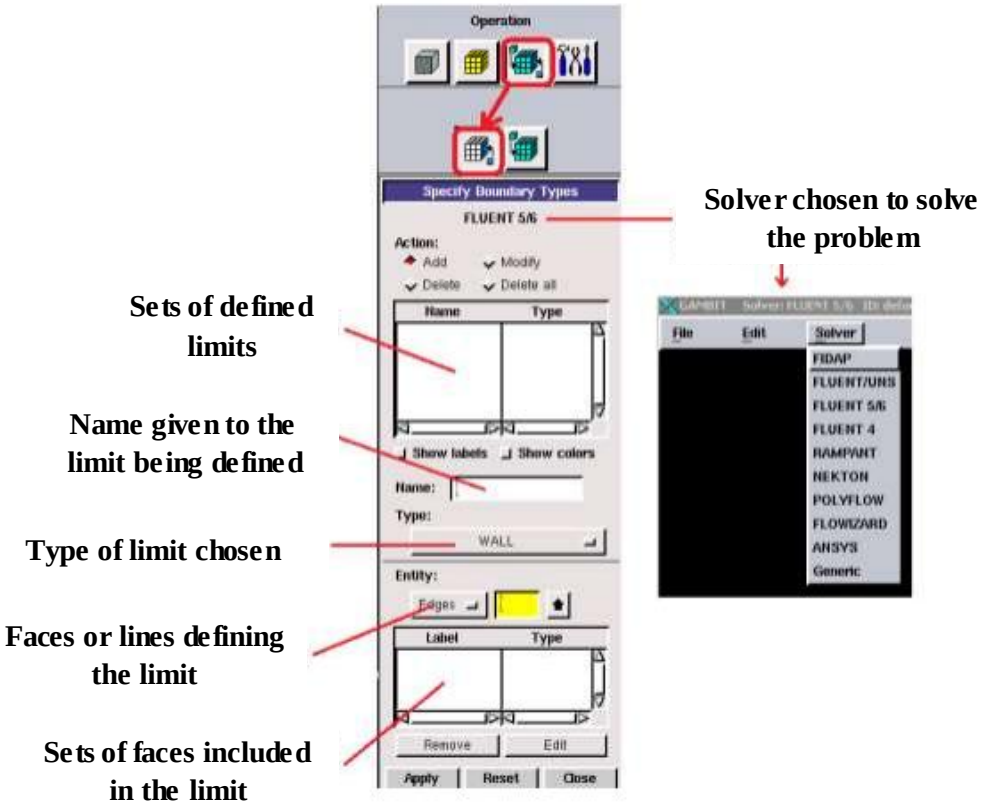

Figure III.16: Main Menus for Boundary Conditions [38]

Step 1: Defining boundaries

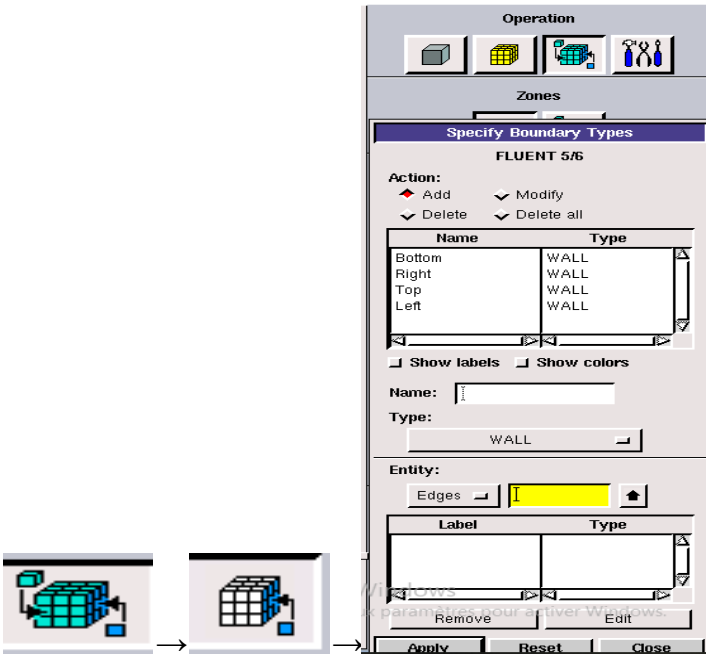

Figure III.17: Main Menus for Boundary Conditions.

Step 2: Defining the fluid domains

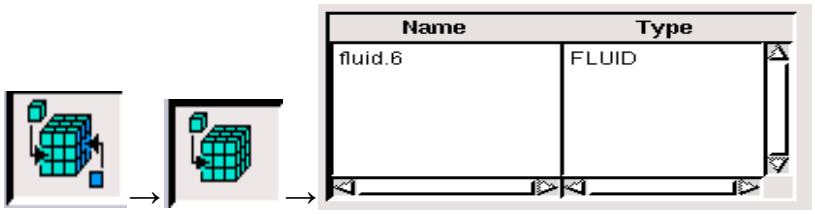

Figure III.18: The Fluid Domains

III.3.4 Exporting the Mesh from Gambit

After creating the geometry and defining the boundary conditions, the mesh needs to be exported so it can be read and used by Fluent. Once the export is complete, you can save your session and close Gambit before launching Fluent [2]

Figure III.19: Exporting Mesh

III.4. Fluent Software

Fluent is a widely used commercial CFD (Computational Fluid Dynamics) and using so much in the industry. It is designed to solve problems involving fluid flow and heat transfer across various applications. For example, it can calculate the lift of an aircraft wing, the drag on a car, or the cooling of electronic circuits using ventilated air, among others.

When launching Fluent, the user must first select the computational domain dimensions (2D or 3D) and specify the desired calculation precision either single or double precision. [2]

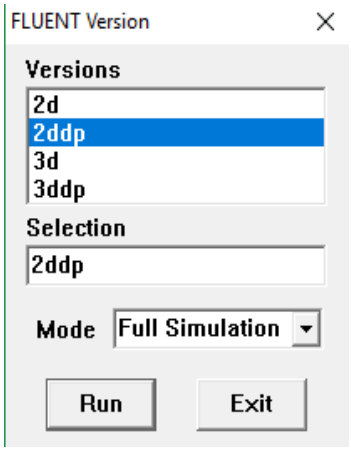

Figure III.20: Resolution Type

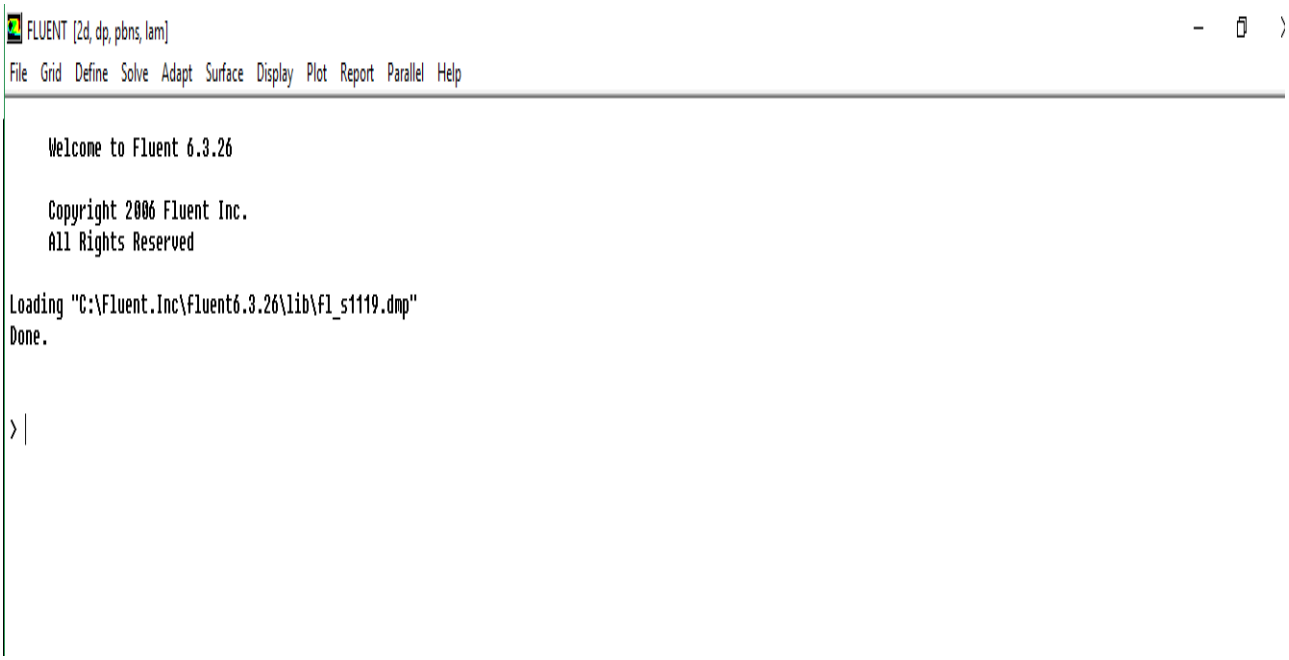

Figure III.21: Fluent Overview

III.4.1 Importing Geometry (*.msh)

To initiate the simulation, the mesh file (*.msh) generated in Gambit must be imported into Fluent.

File →Read →Case...

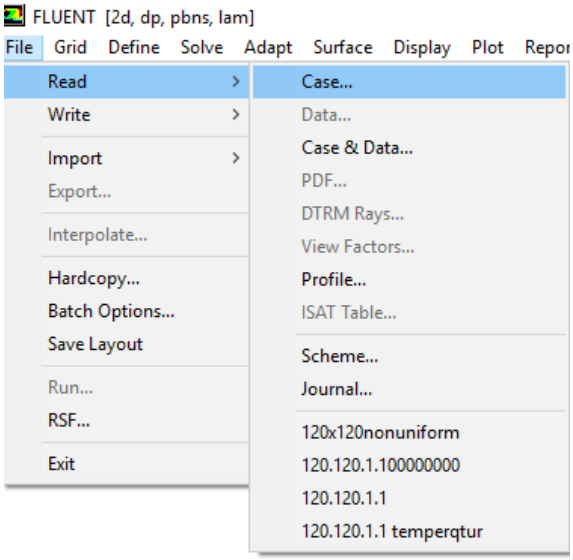

Figure III.22: Reading the Grid

III.4.2 Checking the Imported Mesh

This step checks whether the imported mesh contains any errors or negative volumes.

Grid →Check

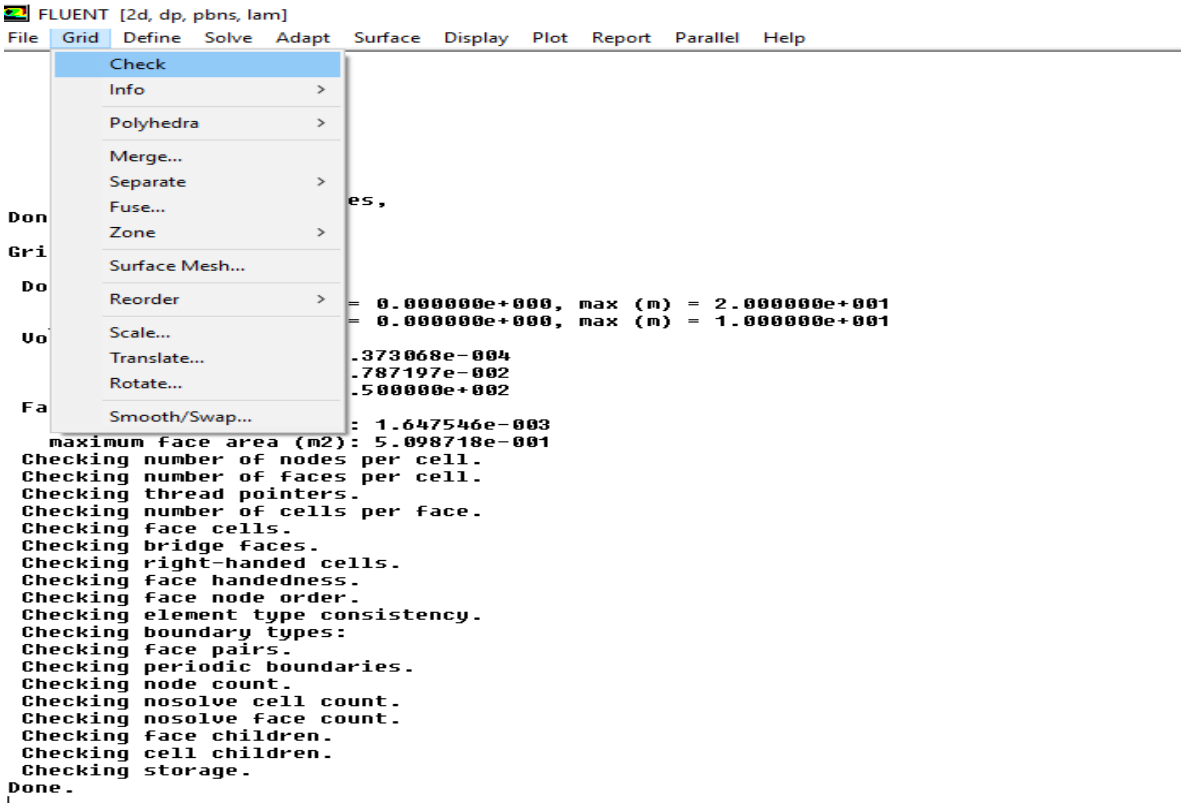

Figure III.23: Mesh Verification in Fluent

III.4.3 Verifying the Scale

It is essential to verify that the displayed geometric dimensions accurately correspond to the physical dimensions defined in the problem specification.

Grid →Scale

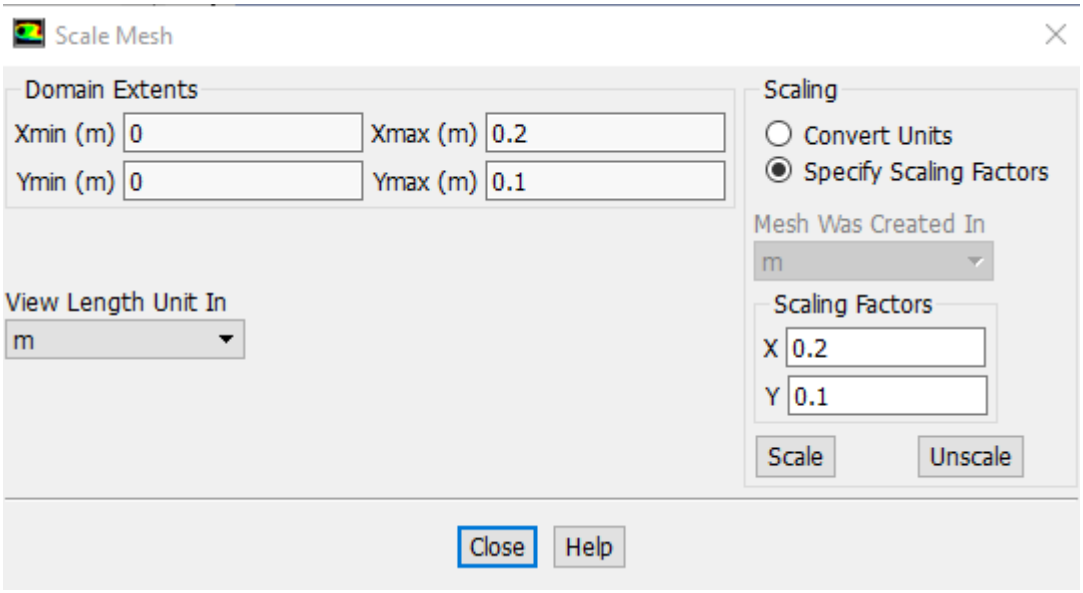

Figure.III.24: Scale Verification.

III.4.4 Solver Selection

To select one of the solution formulas, we use the solver panel :

Define →Models →Solver...

In our problem, the flow is steady, so we choose the steady case and 2D. Click OK

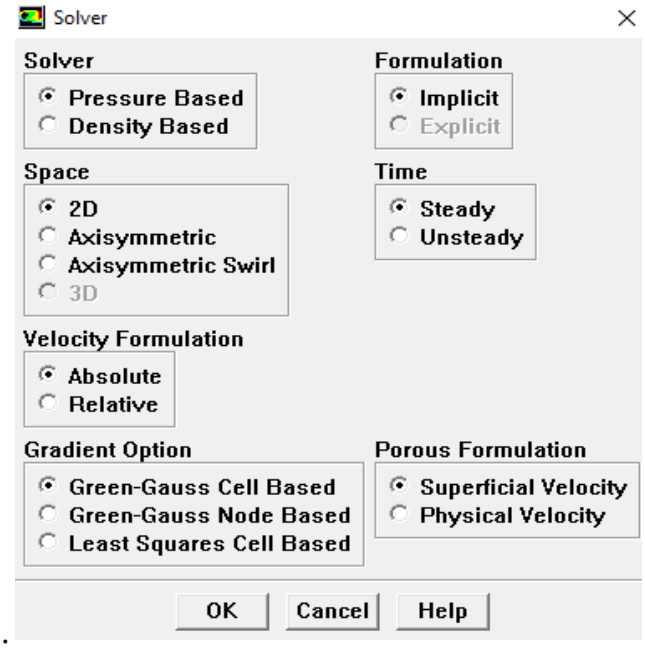

Figure.III.25: Choice of Solver

III.4.5 Model Selection

First, we introduce the energy equation into the system of equations to be solved.

Define → Models → Energy

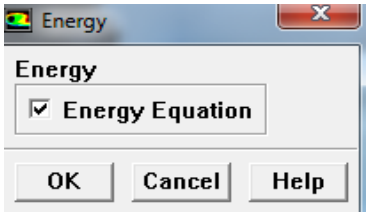

Figure.III.26: Energy Equation

III.4.6 Choice of Flow Model

If the flow is turbulent, we select one of the turbulent models. We select on:

Define → Models → Viscous

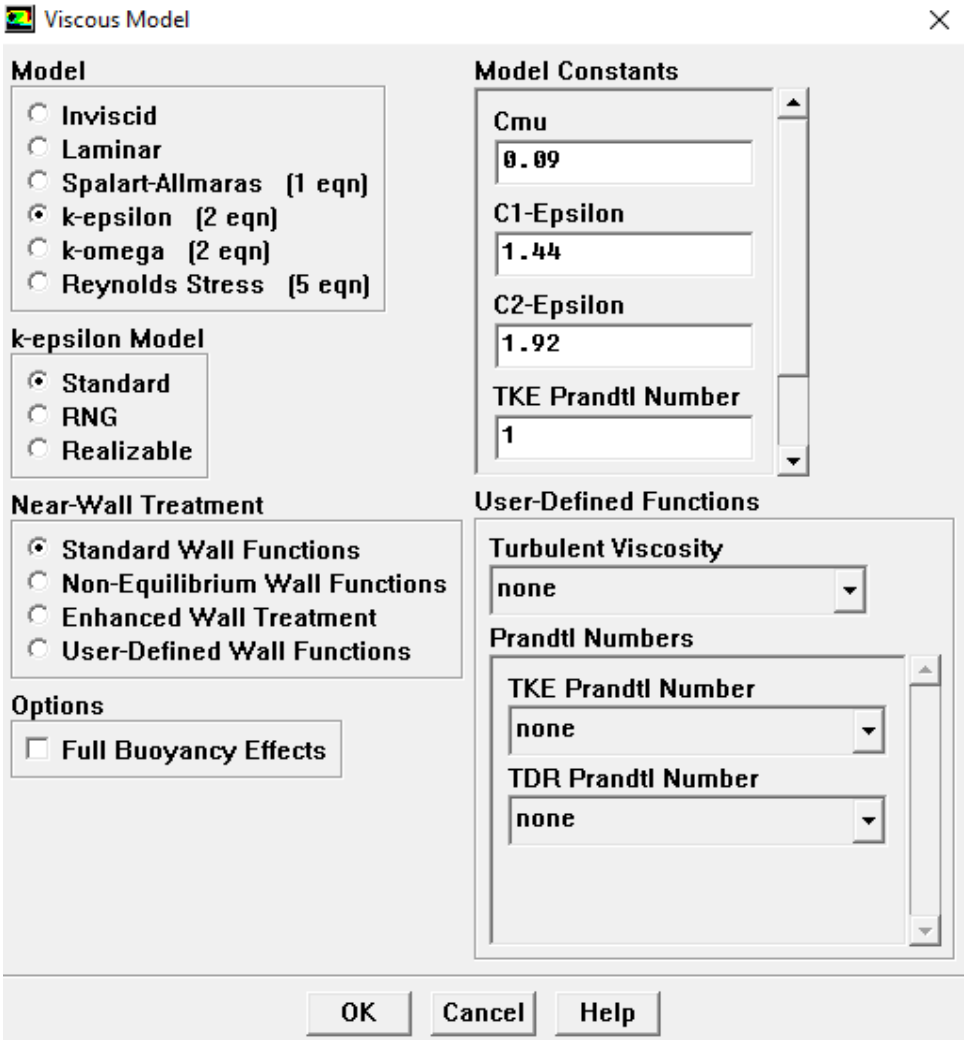

Figure III.27: Choice of Flow Type

III.4.7 Defining Fluid Properties

The characteristics of the fluid are assigned by selecting the appropriate fluid from Fluent's built-in material database.

Define →Materials

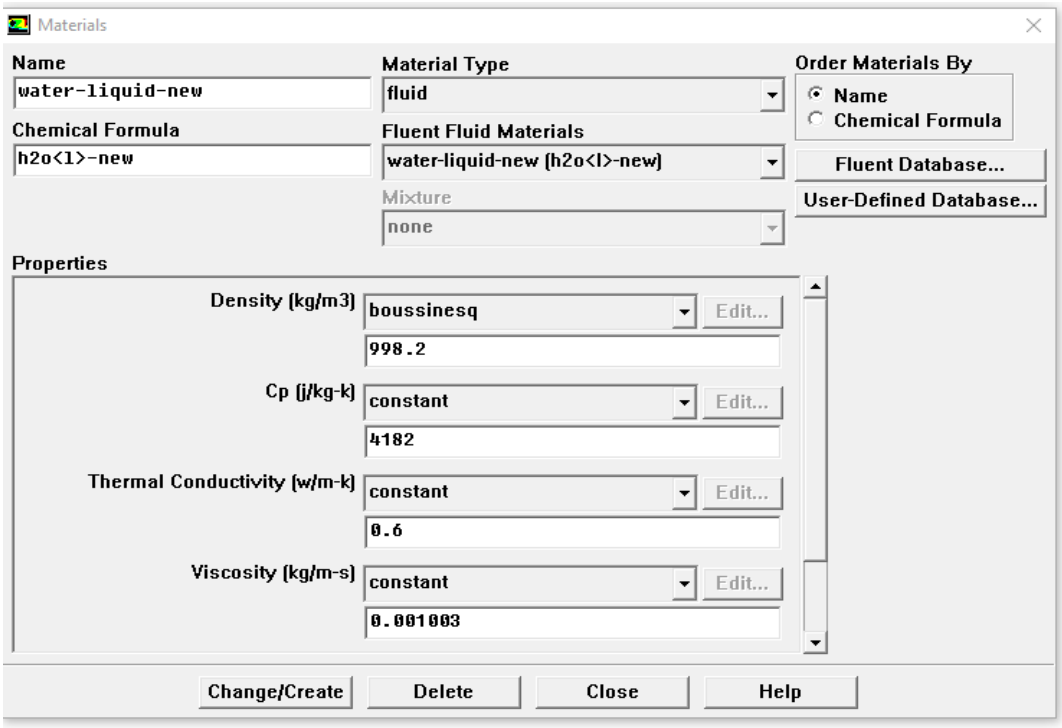

Figure.III.28: Choice of Materials Model

III.4.8 Operating Conditions

Fluent defines gravity along the Y axis.

Define → Operating condition

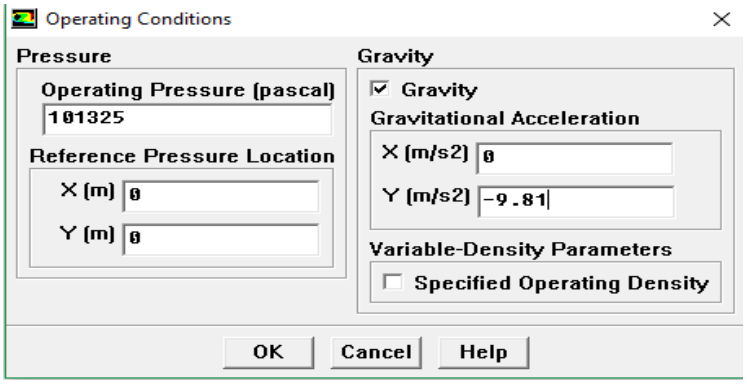

Figure.III.29: Choice of Reference Gravity

III.4.9 Boundary Conditions

Then, the values of the boundary conditions must be fixed.

Define →Boundary Conditions

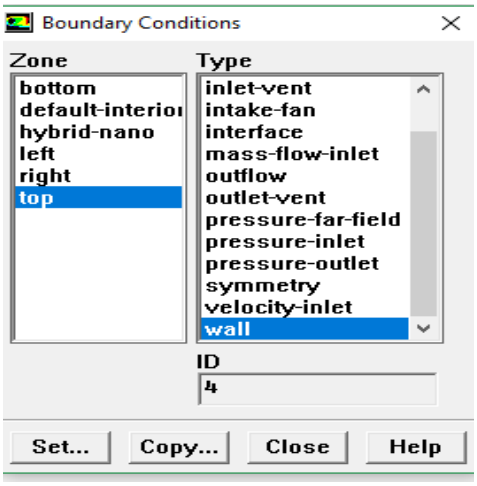

Figure III.30: Values of Boundary Conditions

III.4.10 Controls Solution

Solve→Controls→ Solution

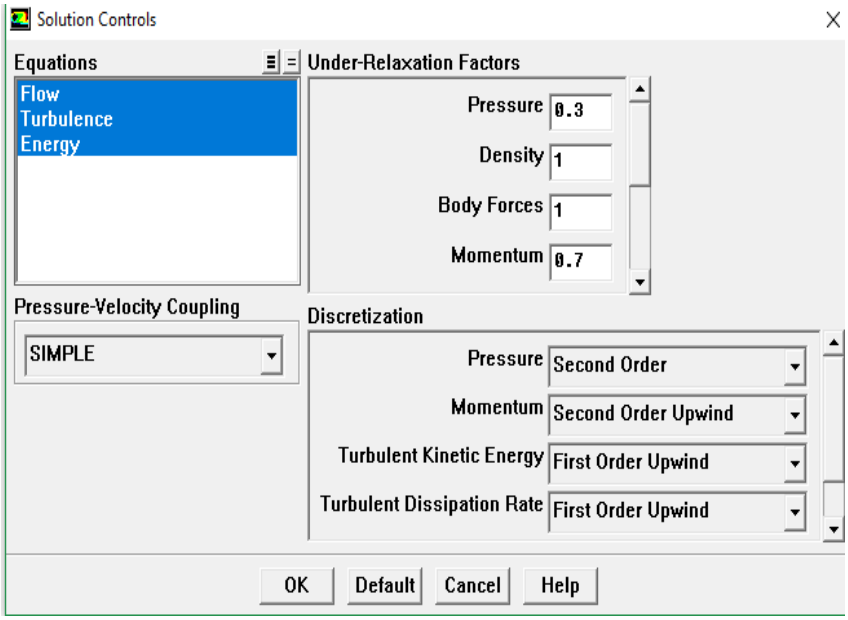

Figure III.31: Choice of Controls Solution

III.4.11 Initialize Calculation

Initialize the flow field for the inlet value

Solve→Initialize→Initialize

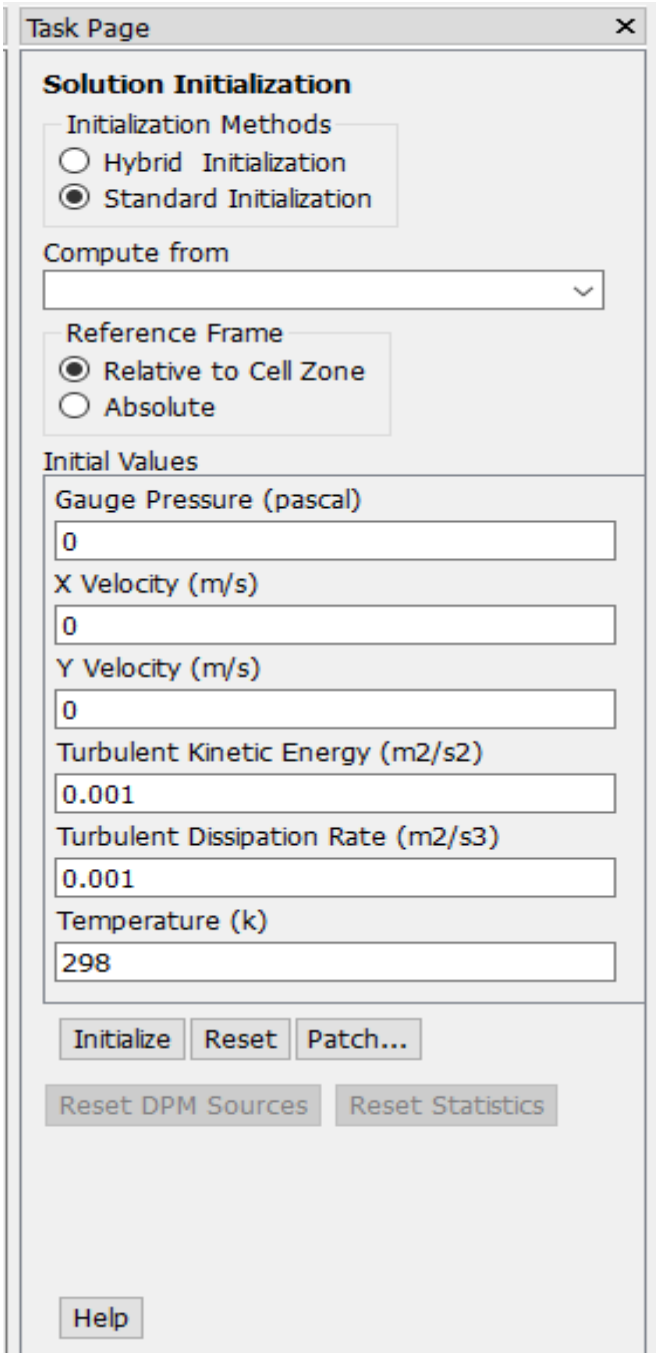

Figure III.32: Initialization Solution

III.4.12 Choice of Convergence Criteria

This involves choosing the criteria that must be verified for the simulation calculations to stop.

Solve →Monitors →Residual

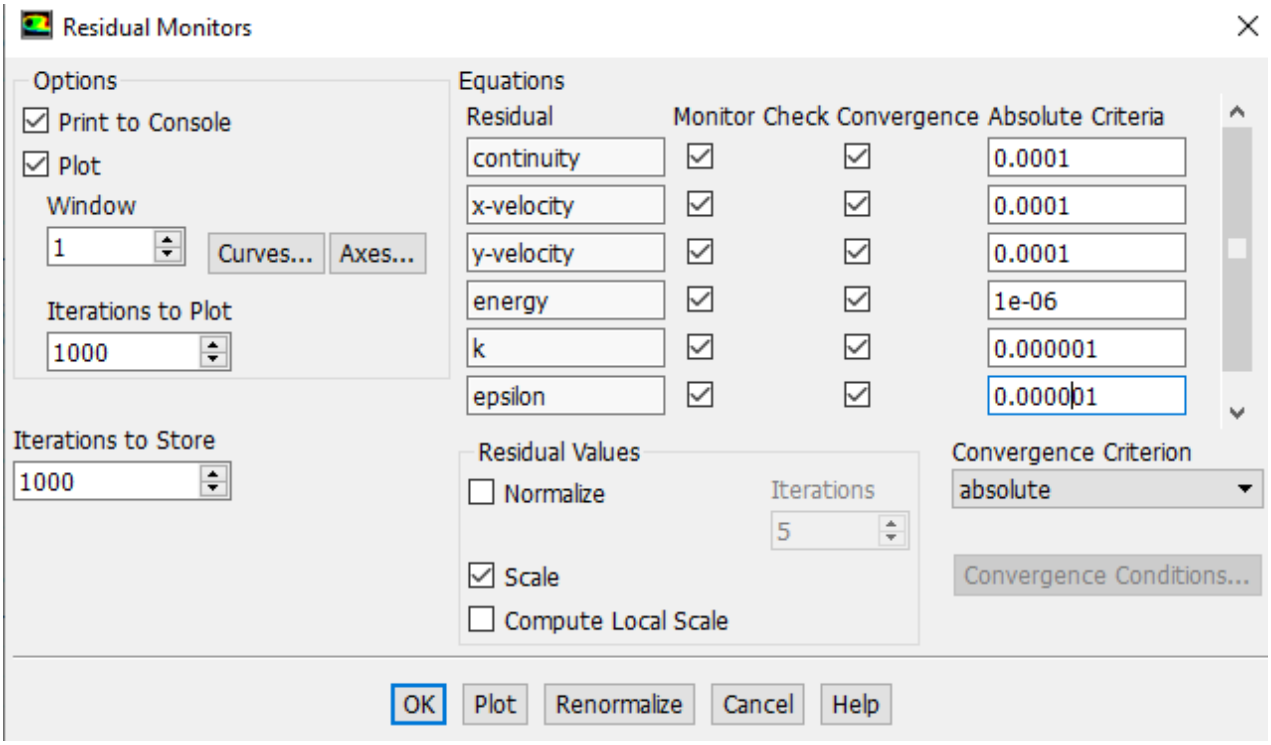

Figure III.33: Choice of Residuals

III.4.13 Begining of Iterations

An iteration limit is specified, and the simulation is initiated by clicking the "Iterate" button.

Solve→Iterate

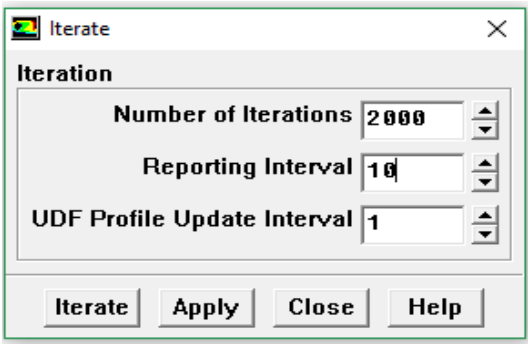

Figure III.34: Choice of the Number of Iterations

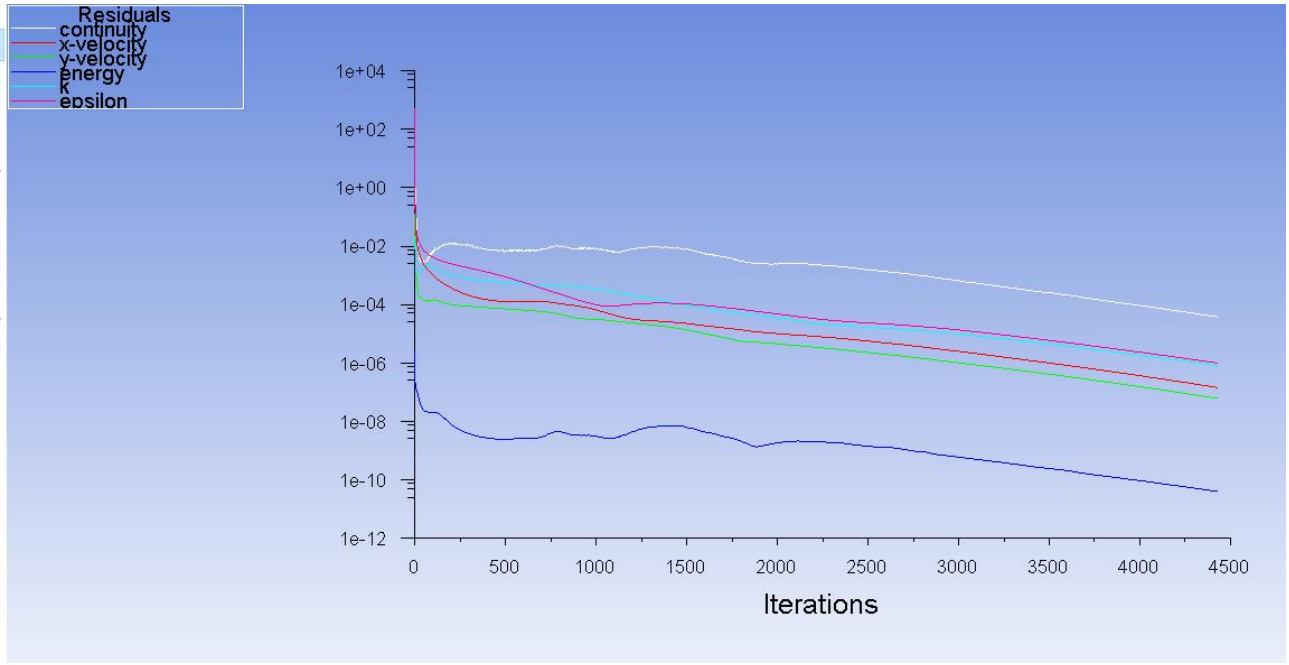

Figure III.35: Residuals

III.4.14 File Backup

The obtained numerical results is then saved:

File → Write → Case & Data

III.5 Conclusion

In this chapter, we presented the simulation steps and an overview of the Gambit software, along with the computational code (Fluent) used to solve the problem numerically. The final step consists of extracting the various results in the form of curves using the graphical tools available in Fluent and Origin, enabling us to process the information derived from the computational fluid dynamics solution and easily present our results.

CHAPTER VI:
Results and Discussion

IV.1 Introduction

This chapter aims to present the numerical simulation results for a two-dimensional model. Hence, the main objective is to show the ability of the CFD computer code "Fluent" to model and explore the mixed convection flow in a cavity filled with several fluids.

IV.2 Code validation

The mathematical model and numerical method were validated by comparing them to the results of Hirpho and Ibrahim [39] for a steady mixed convection in a partially heated trapezoidal enclosure. The cavity is filled with Al_2O_3-Cu/water hybrid nanofluid, presumed to be in a laminar and incompressible state. The top wall of the enclosure is insulated and moves at a constant speed U_{lid}. The side walls of the enclosure are kept at a uniform temperature T_c. The middle portion of the bottom wall is heated and maintained at uniform temperature T_h. The remaining parts of the bottom wall are maintained insulated. A schematic view of the configuration is shown in Figure IV.1.

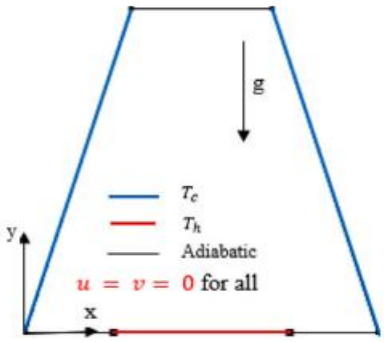

Figure IV.1: Trapezoidal cavity of Hirpho and Ibrahim [39]

For a constant Reynolds number of 100, various Richardson numbers of 0.1, 1 and 10 were examined, together with varying volume fractions ($0 \leq \varphi \leq 0.02$). The mean Nusselt number obtained from our numerical analysis closely matched the values reported by Hirpho and Ibrahim as demonstrated in Table 2.

Table IV.1: The validation of the mean Nusselt numbers for Re= 100 and $\varphi = 0.01$

Ri	Nu_{ave} (Hirpho and Ibrahim)	Nu_{ave} (This study)
0.1	4.3960	4.3325
1	9.7698	9.8891
10	17.569	17.4886

IV.3 Grid Independence

To select the adequate number of nodes, a grid independent treatment is used where three non-uniform meshes of different number of elements are used (80x80, 120x120 and 150x150). Reynolds number based on the upper wall velocity U_0 and the length of the upper wall H was taken Re = 3160.

Table IV.2: Effect of the Mesh Size on the Mean Nusselt Number.

Number of elements	Mean Nusselt number	Deviation %
80x80	43.77	-
120x120	35.66532	22.72 %
150x150	35.3228	0.96 %

For φ= 0%, the average deviation was less than 1% between the two last meshes for the mean Nusselt number of the heated wall located at the bottom of the cavity as indicated in Table 3. This is why the mesh 150x150 was adopted.

IV.4 Results and Discussion

For the present study, numerical simulations are reported for a fixed Reynolds number Re=3160, and for Richardson numbers: Ri=0.1, 1, 2 and 5. Many volume fractions were tested: φ = 0%, 2%, 4% and 8%.

IV.4.1 The Thermophysical Properties

The characteristics of hybrid nanofluid used in our study are presented in the next table .

Table IV.3: Thermophysical Properties of the Base Fluid, Water, and Nanoparticles Cu and Al_2O_3

	$\rho(\mathrm{Kg.m^{-3}})$	$Cp(J.Kg^{-1}.K^{-1})$	$\beta\ (K^{-1})$	$K(W.m^{-1}.K^{-1})$	$\mu(m^2.s^{-1})$
Water	998.2	4179	25.9×10^{-5}	0.613	0.001003
Cu	8933	385	1.67×10^{-5}	401	/
Al_2O_3	3970	765	0.85×10^{-5}	40	/

Table IV.4: Thermophysical Properties Nanofluid at Different Concentrations

	$\rho(Kg.m^{-3})$	$Cp(J.Kg^{-1}.K^{-1})$	$\beta\ (K^{-1})$	$K(W.m^{-1}.K^{-1})$	$\mu(m^2.s^{-1})$
φ (0%)	998.2	4179	0.000259	0.613	0.001003
φ (2%)	1107,266	3753,17947	0,00023047	0,63643041	0,00105496
φ (4%)	1216,332	3736,26664	0,00020706	0,67436591	0,00111077
φ (8%)	1434,464	3702,44099	0,00017091	0,7551414	0,00123547

In order to study mixed convection within a trapezoidal enclosure filled with a hybrid nanofluid (composed of copper Cu and aluminum oxide Al_2O_3), where the bottom wall is maintained at a higher temperature than the top lid, the top wall is moving and the side walls are adiabatic, a series of numerical simulations were conducted. The Richardson number (Ri) was considered a key governing parameter. Simulations were performed for different values of Richardson number (Ri = 0.1, 1, 2, 5) for both a pure fluid (water) and a hybrid nanofluid with varying concentrations, in order to investigate the impact of Ri on the flow structure and heat transfer. The numerical results are described and analyzed throw horizontal and vertical velocity contours and also throw the temperature contours. The relationship between the average Nusselt number and the Richardson number, which indicates relative importance between natural and forced convection is also examined. The variation of the local Nusselt number along the bottom wall of the cavity under the influence of the volume fraction φ is demonstrated for different Richardson number.

IV.4.2 Horizontal Velocity Contours

Figures (III.2-3-4-5) show contour plots of horizontal velocity inside the trapezoidal cavity for different Ri values and nanofluid concentrations.

- For φ = 0 %

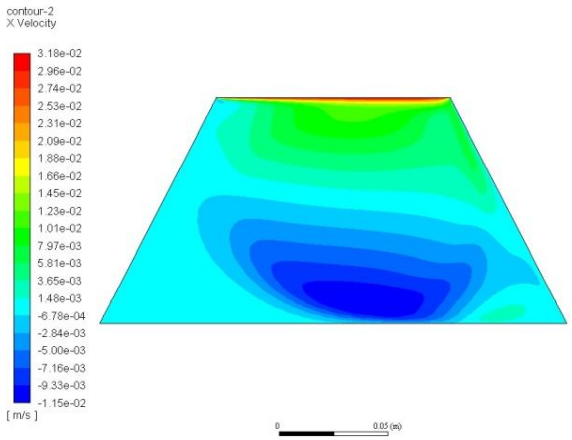

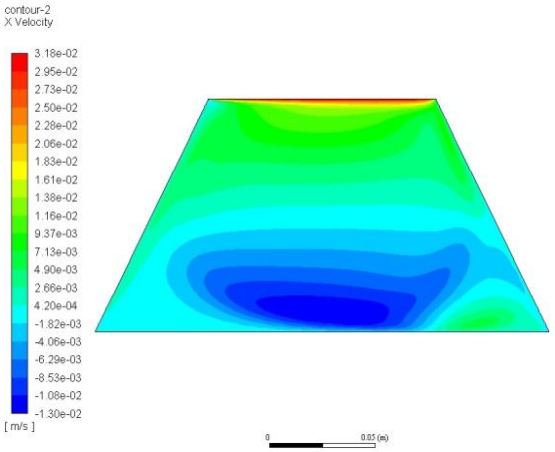

Ri= 0.1 Ri= 1

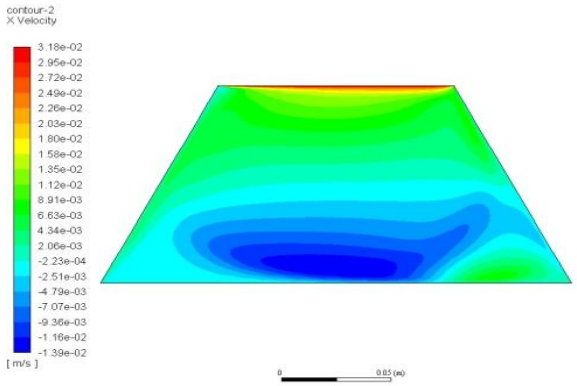

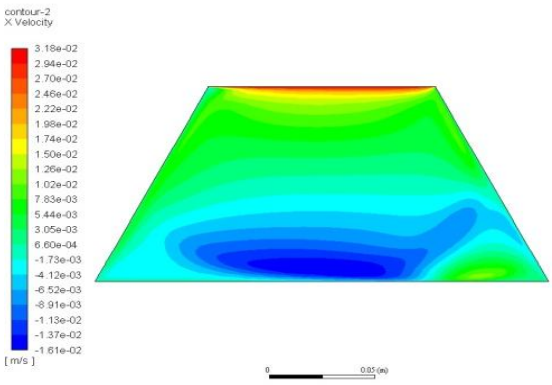

Ri= 2 Ri= 5

Figure IV.2: Horizontal Velocity Contours For φ = 0 %

- For φ = 2 %

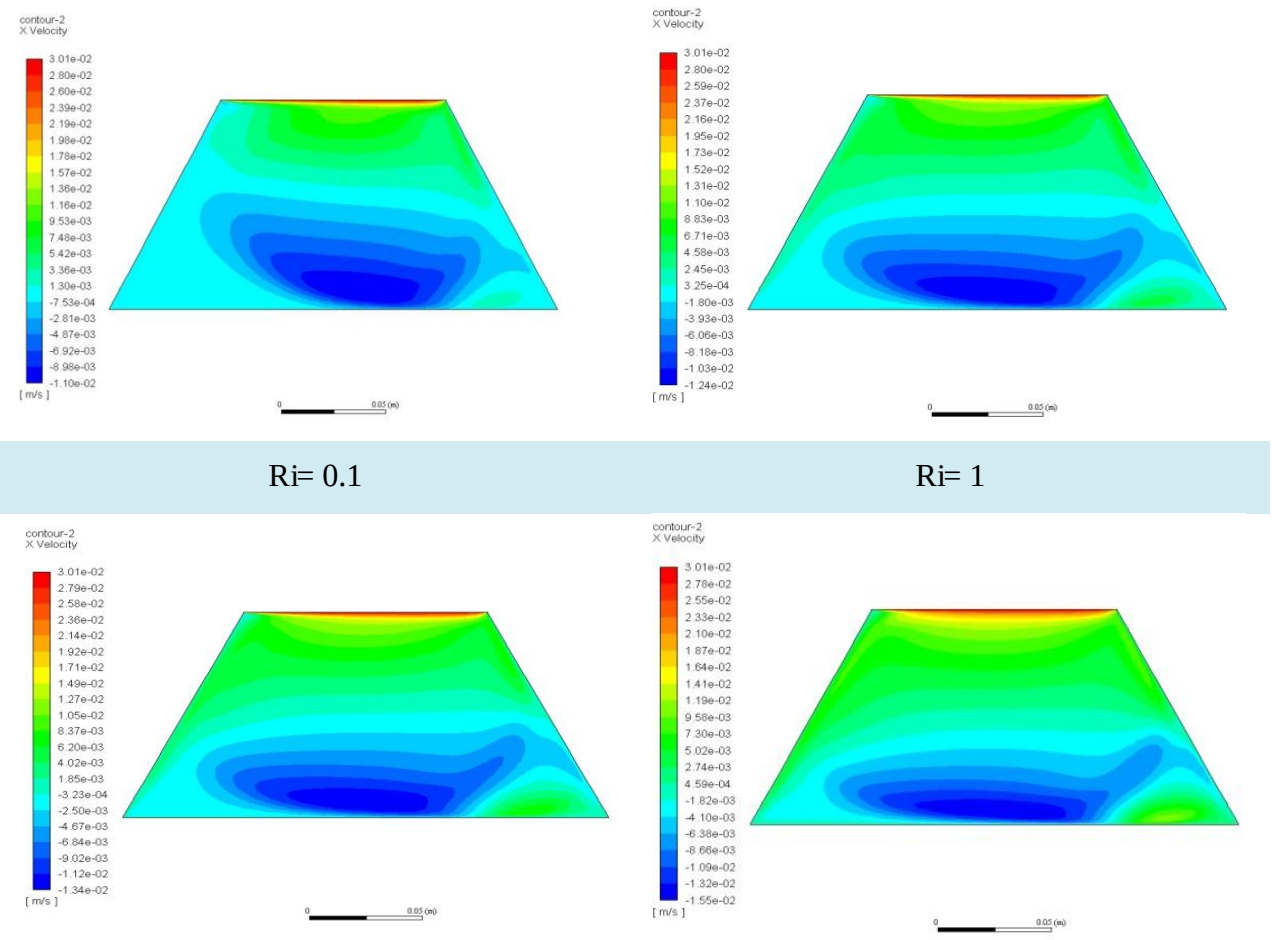

Figure IV.3: Horizontal Velocity Contours For φ = 2 %

- For φ = 4 %

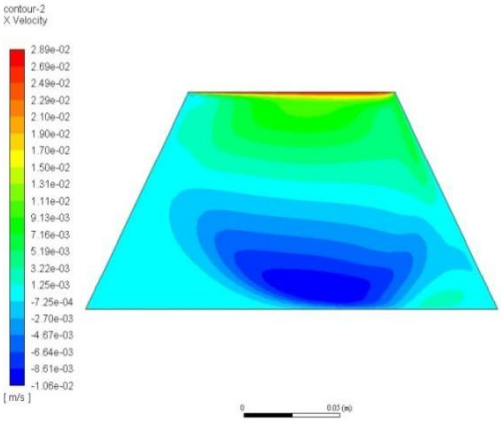

Ri=0.1

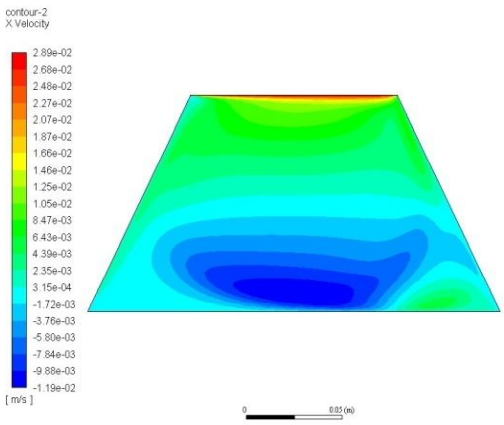

Ri=1

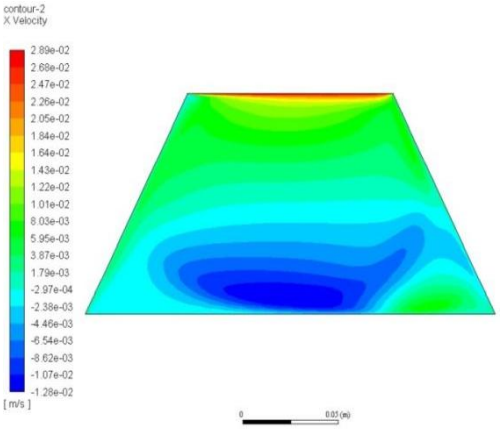

Ri=2

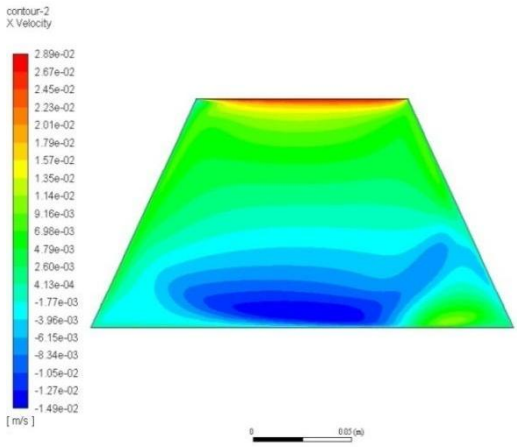

Ri=5

Figure IV.4: Horizontal Velocity Contours for φ = 4 %

For φ = 8 %

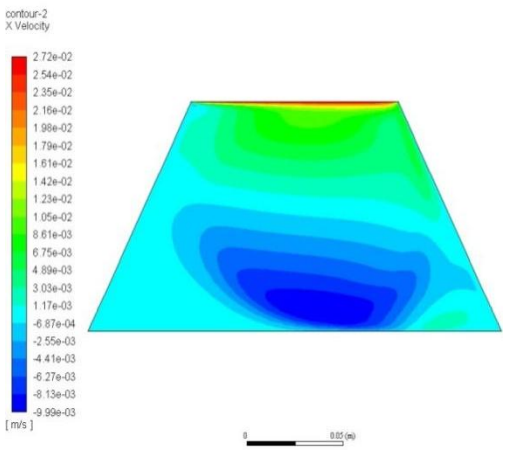

Ri=0.1

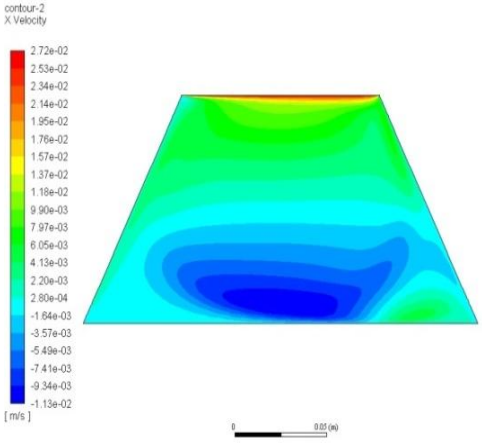

Ri=1

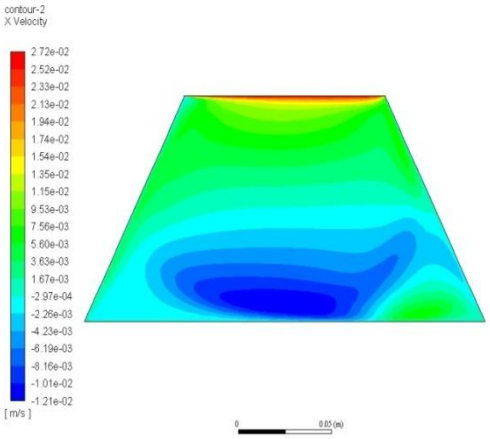

Ri= 2

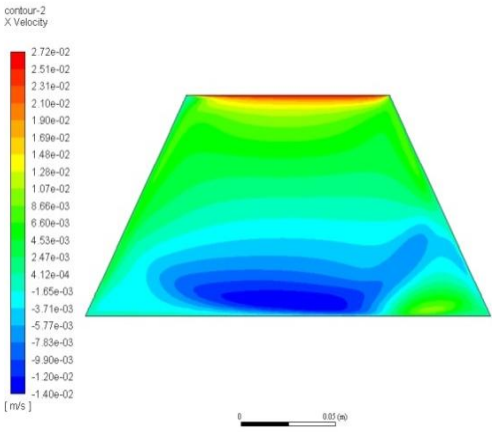

Ri= 5

Figure IV.5: Horizontal Velocity Contours for φ = 8 %

•For Ri = 0.1, a large central region with negative horizontal velocity appears near the bottom, indicating strong forced convection.

• For Ri = 1, the low-velocity zone becomes smaller, while high-velocity regions expand, indicating a greater balance between forced and natural convection.

• For Ri = 2, high-velocity regions spread in the upper cavity, while low-velocity regions dominate the bottom, suggesting increasing influence of natural convection, where hot fluid rises and cold fluid descends more clearly.

• For Ri = 5, high-velocity regions are clearly concentrated at the top, while low velocities are distributed at the bottom and sides. The velocity gradient becomes more distinct, indicating the dominance of natural convection.

From this, we conclude that increasing the nanofluid concentration generally enhances the thermal conductivity of the fluid, promoting heat transfer. The velocity gradient and its distribution are clearly affected by both the nanofluid concentration and Ri, with the flow regime transitioning from forced convection to natural convection as Ri increases.

IV.4.3 Vertical Velocity Contours

The Figures (III.6-7-8-9) illustrate contour plots of vertical velocity within the trapezoidal cavity, showing variations due to changes in Ri and nanofluid concentration.

- For φ = 0 %

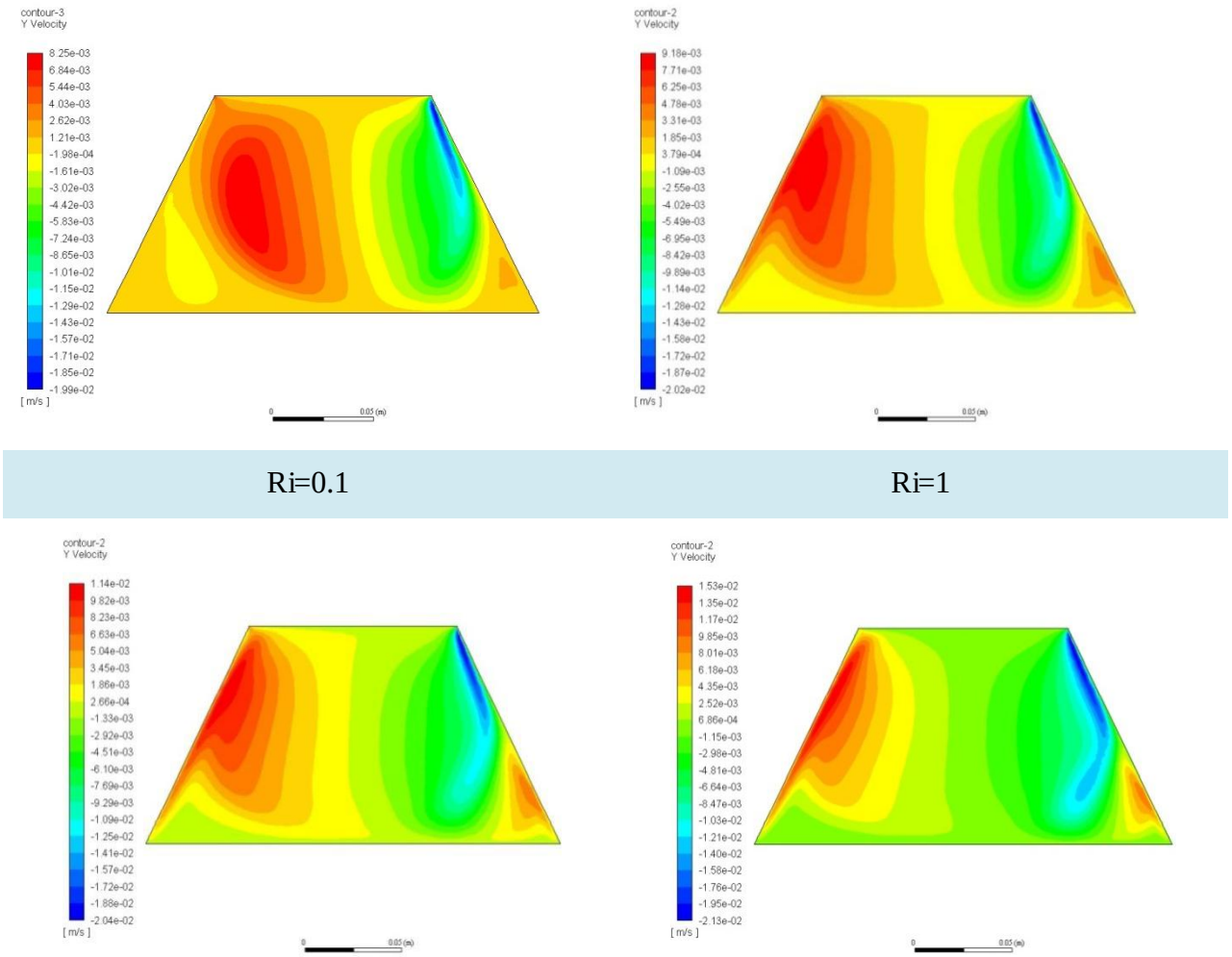

Ri=0.1	Ri=1
Ri=2	Ri=5

Figure IV.6: Vertical Velocity Contours for φ = 0 %

- For φ = 2 %

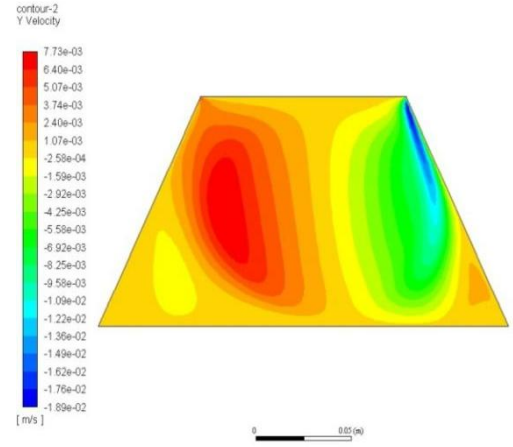

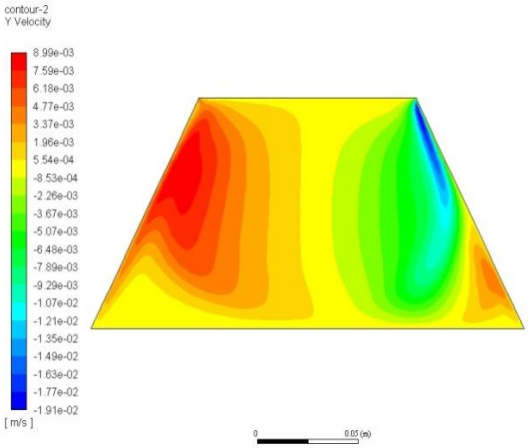

Ri=0.1 Ri=1

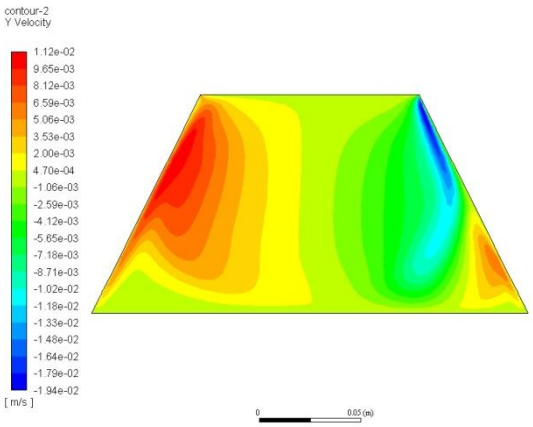

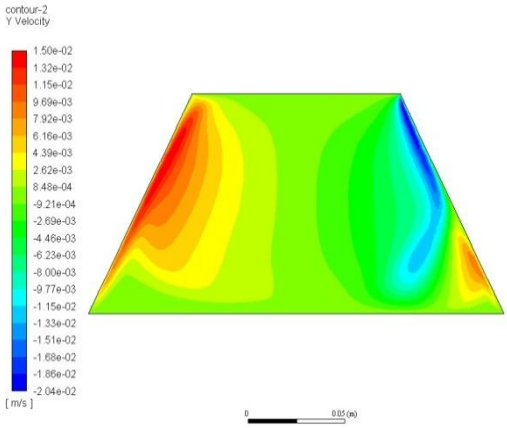

Ri=2 Ri=5

Figure IV.7: Vertical Velocity Contours for $\varphi = 2\%$

- For φ = 4 %

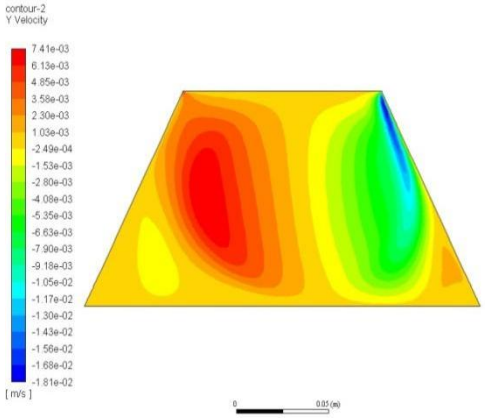

Ri=0.1

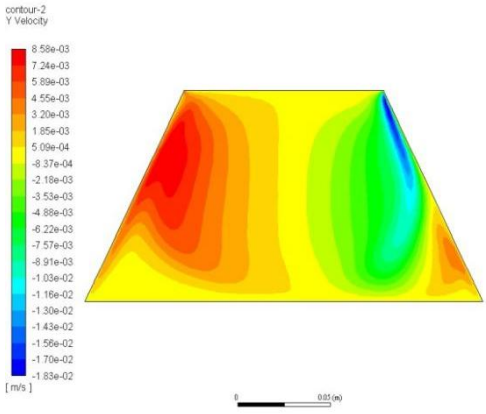

Ri=1

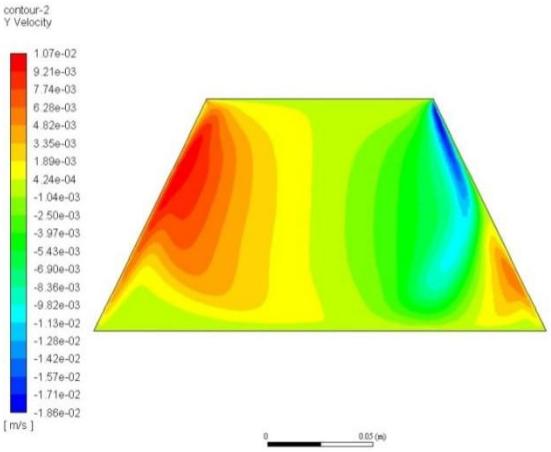

Ri=2

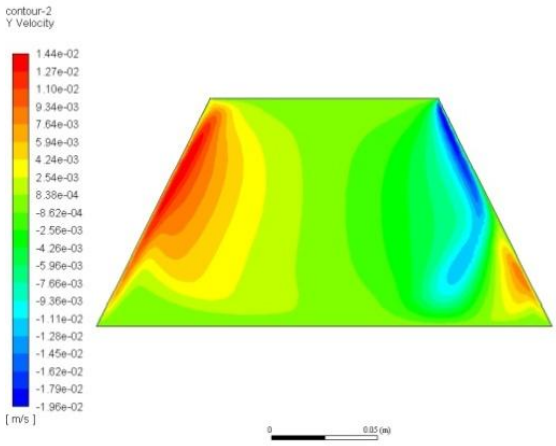

Ri=5

Figure IV.8: Vertical Velocity Contours for φ = 4 %

- For φ = 8 %

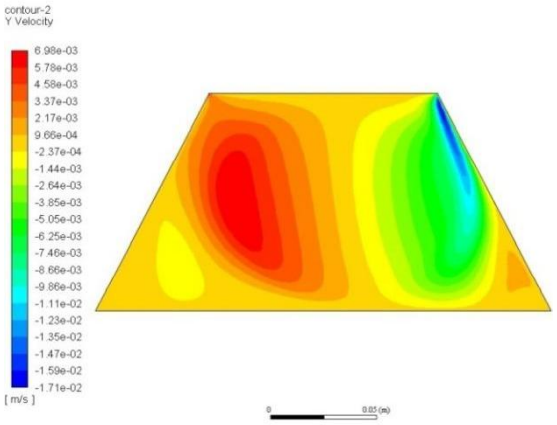

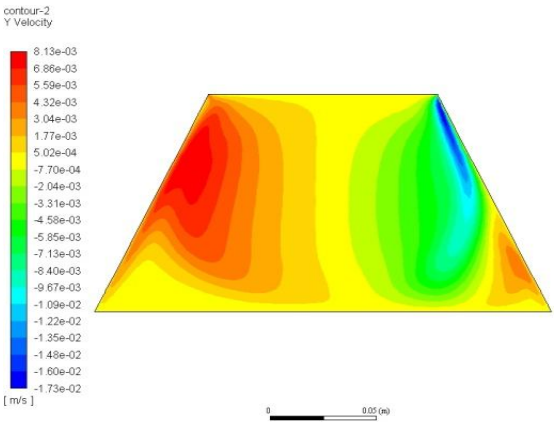

Ri=0.1 Ri=1

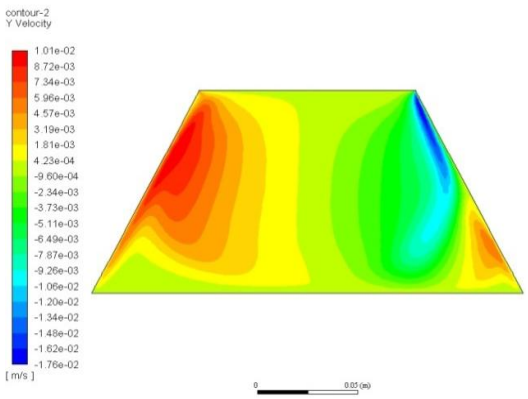

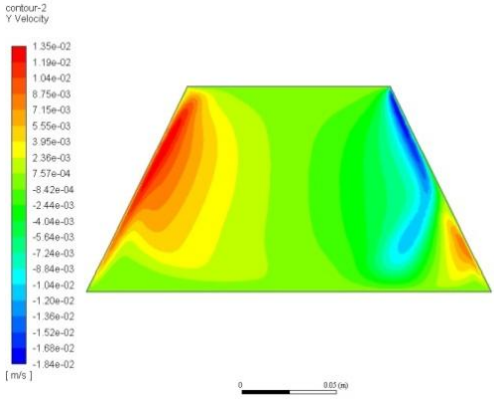

Ri=2 Ri=5

Figure IV.9: Vertical Velocity Contours for φ = 8 %

Two vortices are observed for Ri = 0.1 and 1, and three vortices for Ri = 2 and 5, where high vertical velocities occur on the left side, and negative velocities (downward flow) occur on the right.

• For Ri = 0.1, the vertical velocity distribution shows strong vortices and clear transition zones between positive and negative values. Maximum velocities are concentrated in the center, indicating forced convection dominance.

• For Ri = 1, a balance between forced and natural convection results in a more uniform velocity distribution. While regions of positive and negative velocity still exist, they are less extensive than at Ri = 0.1.

• For Ri = 2 and 5, the flow becomes more stable and less disturbed, indicating the increased role of natural convection.

This shows that variations in vertical velocity distribution reflect changes in heat transfer and mixing efficiency inside the cavity. Strong vortices and high velocities enhance thermal mixing, whereas more stable flow reduces mixing. Moreover, increasing nanofluid concentration tends to improve heat transfer.

IV.4.4 Stream Function Contours

The stream function is used in fluid mechanics to describe flows. It represents streamlines, which are the paths followed by fluid particles in a steady flow. These lines are defined by: ψ = constant, meaning that the stream function is constant along each streamline. In two dimensions, the fluid velocity components u and v can be expressed from the partial derivatives of the stream function as:

$$u = \frac{\partial \Psi}{\partial y}\ ; \quad v = -\frac{\partial \Psi}{\partial x} \qquad \text{VI.1}$$

The stream functions for different concentrations at different values of the Richardson number (Ri = 0.1, 1, 2, 5) are presented in figures IV.10, IV.11, IV.12 and IV.13. Many counter-rotating vortices are formed inside the cavity, and it is observed that high velocities are typically found in the upper region due to the movement of the top wall at velocity U_0. For □=0, five cells are formed inside the cavity. The big one occupying most of the cavity volume, with clockwise recirculation with one cell at the left side and two others at the right side. The secondary cells near the bottom wall, resulting from the intercation between natural convection generated by the heated lower wall and the forced convection resulting from the horizontal velocity of the upper wall. With the augmentation of natural convection effect, the small cells diminished progressively except the small cell in the left side of the main rotating vortex as indicated in figure IV.10. The same remarks are observed for the other volume concentrations. We concluded that increasing the Richardson number changes the vortex pattern inside the cavity. Also the presence of the hybrid nanofluid enhances heat transfer and modifies the flow distribution. This is clearly demonstrated by the change in the shape and size of the central vortex with changing Ri.

- For $\varphi = 0$ %

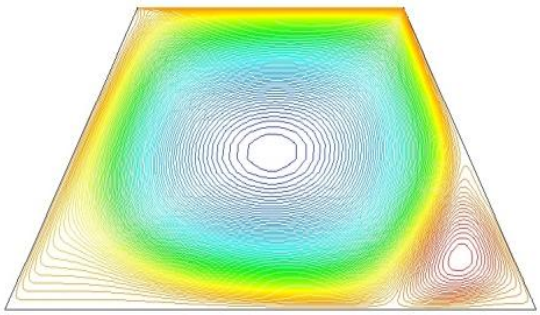

Ri=0.1

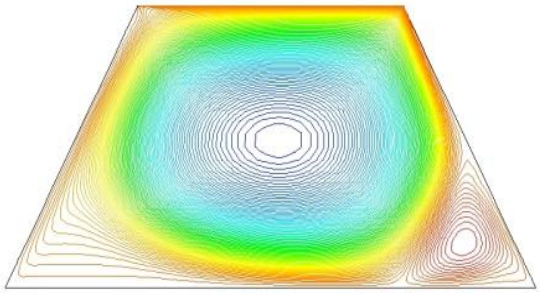

Ri=1

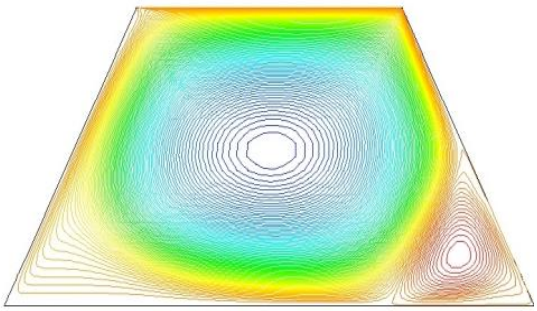

Ri=2

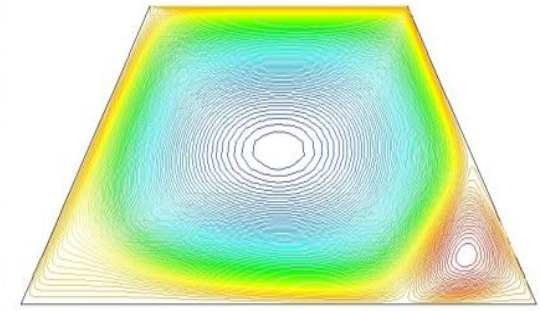

Ri=5

Figure IV.10: Stream Function Contours For φ =0 %

- For $\varphi = 2\ \%$

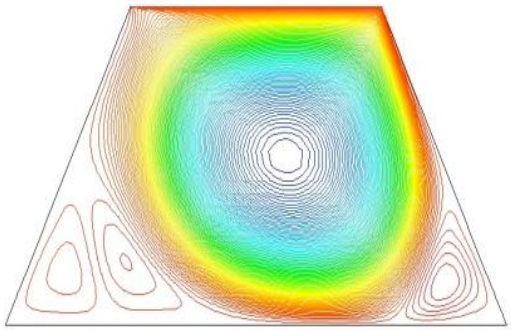

Ri=0.1

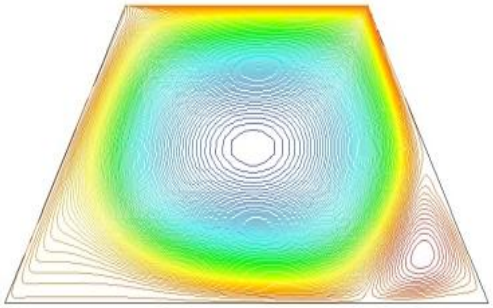

Ri=1

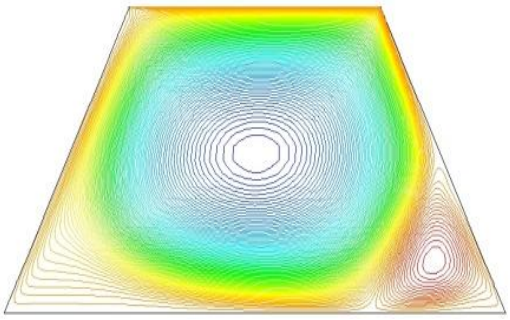

Ri=2

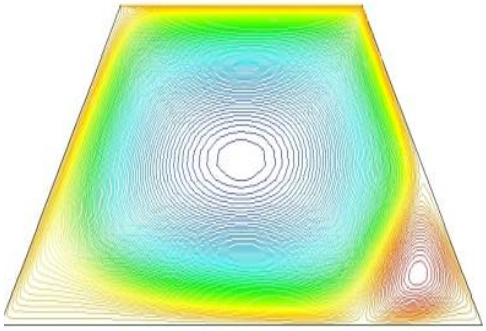

Ri=5

Figure IV.11: Stream Function Contours for φ = 2 %

- For $\varphi = 4\ \%$

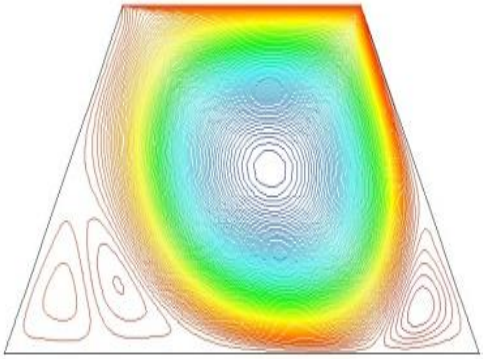

Ri=0.1

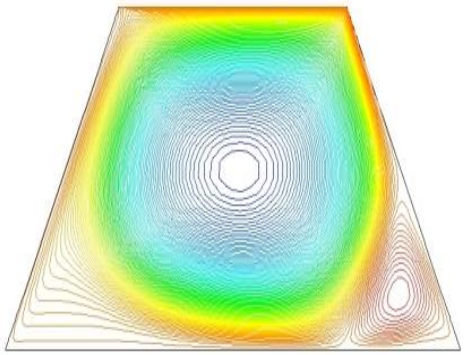

Ri=1

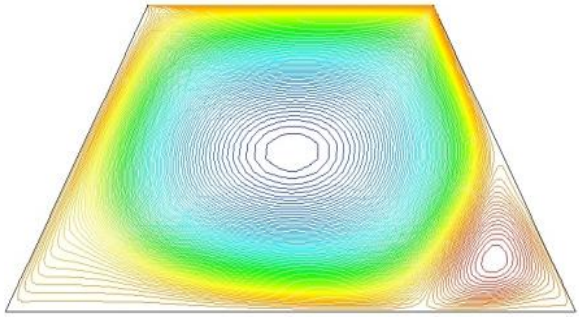

Ri=2

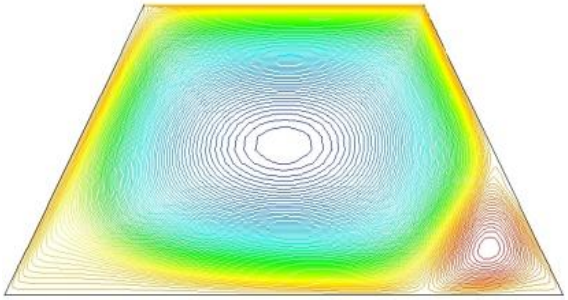

Ri=5

Figure IV.12: Stream Function Contours for φ = 4 %

- For φ = 8 %

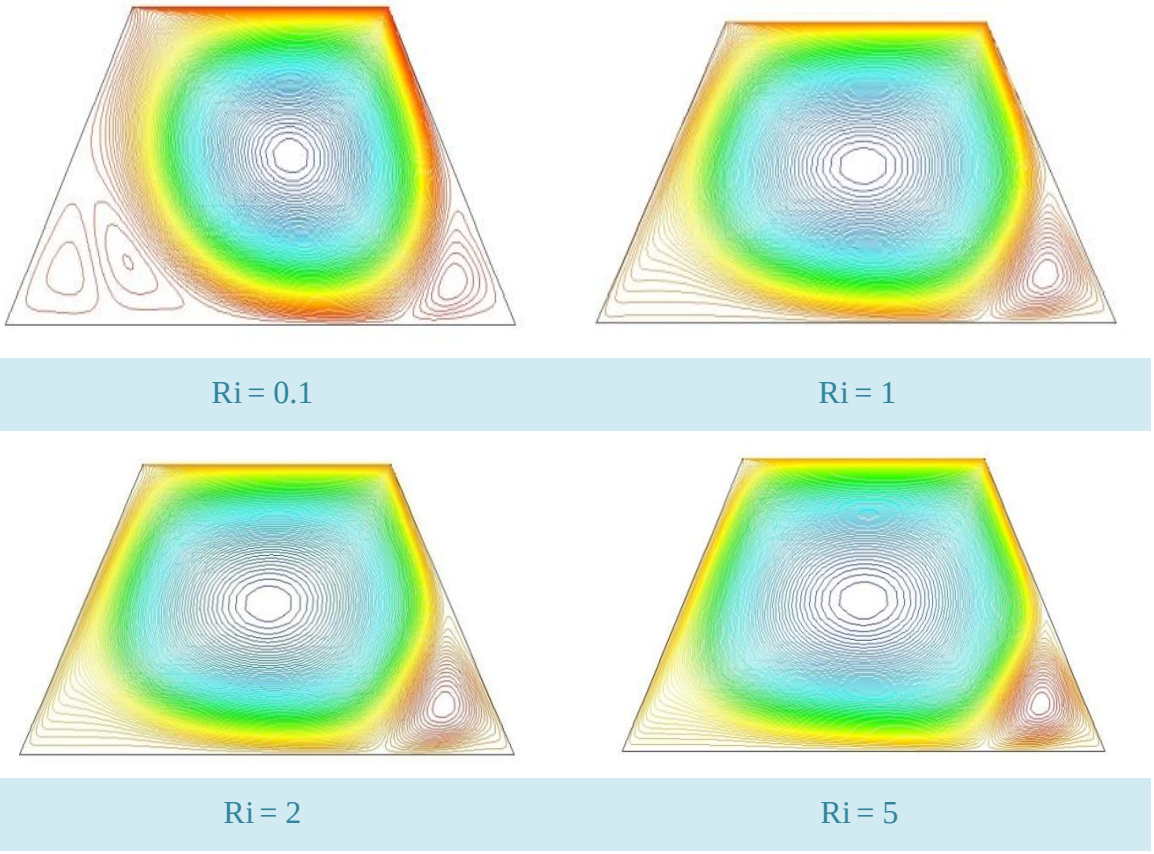

Figure IV.13: Stream Function Contours for φ = 8 %

IV.4.5 Temperature Contours

Figures (III.10-13) depict temperature contours within the trapezoidal cavity filled with hybrid nanofluid, for different Richardson numbers and nanoparticle volume concentrations.

- For φ = 0 %

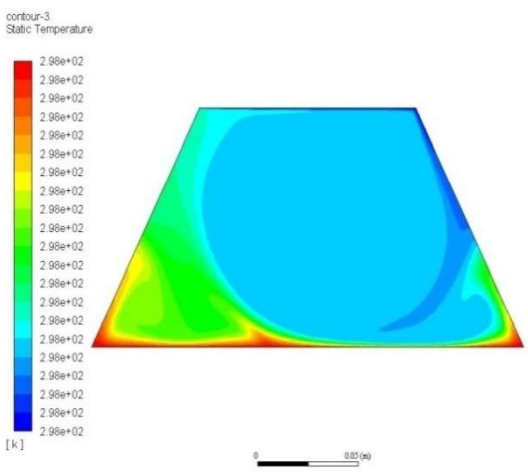

Ri= 0.1

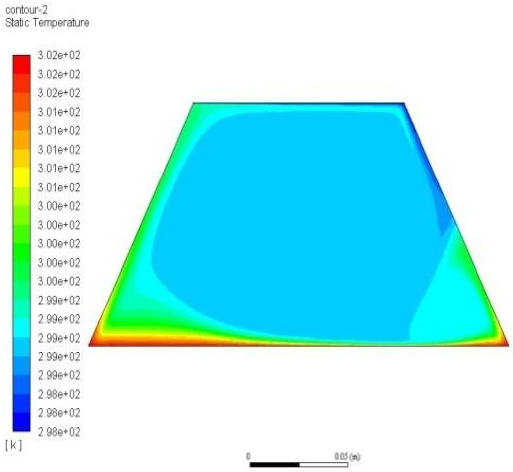

Ri= 1

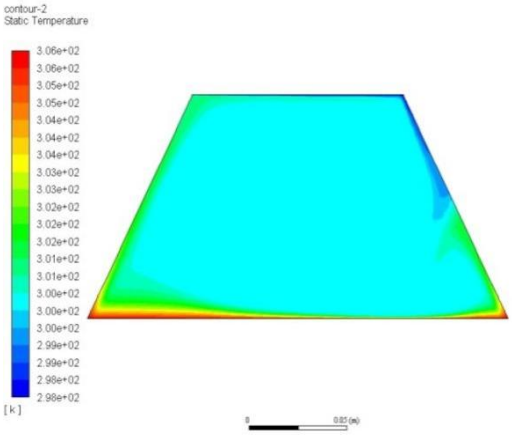

Ri= 2

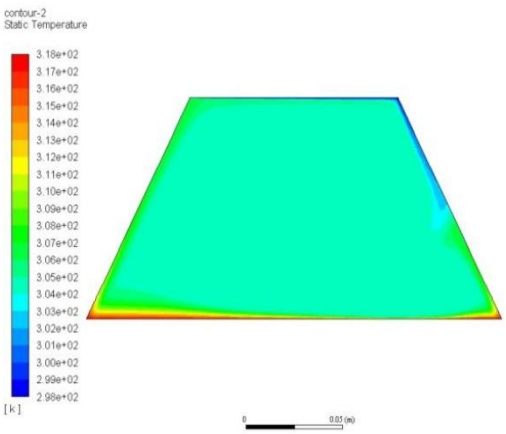

Ri= 5

Figure IV.14: Temperature Contours for φ = 0 %

- For φ =2 %

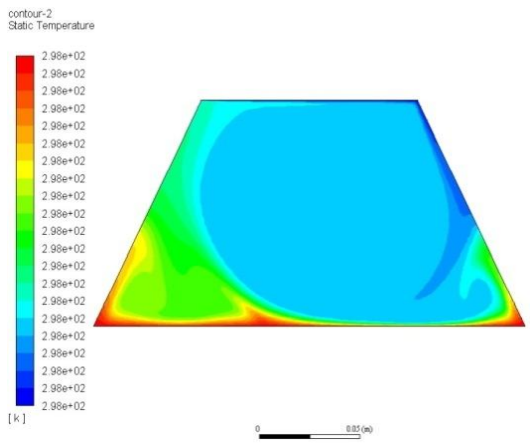

Ri=0.1

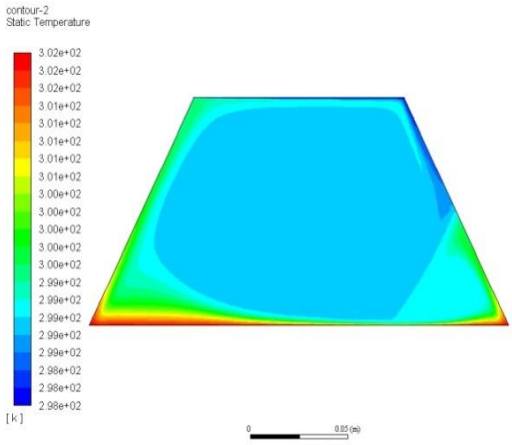

Ri=1

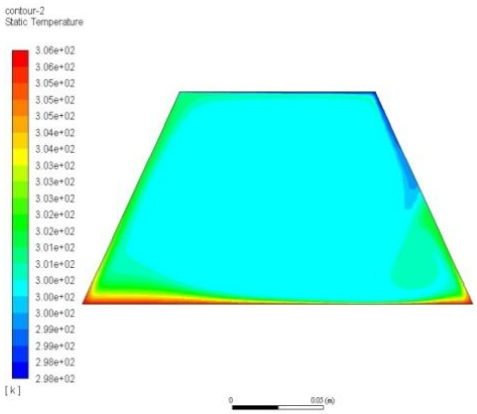

Ri=2

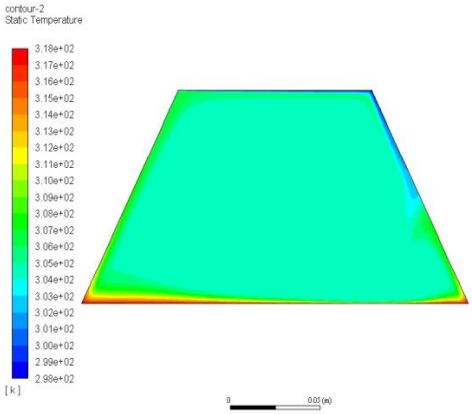

Ri=5

Figure IV.15: Temperature Contours for φ = 2 %

For φ = 4 %

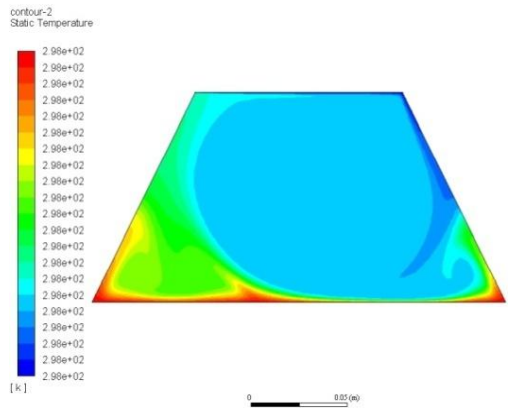

Ri=0.1

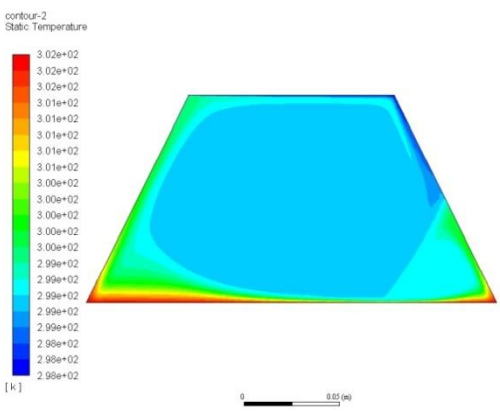

Ri=1

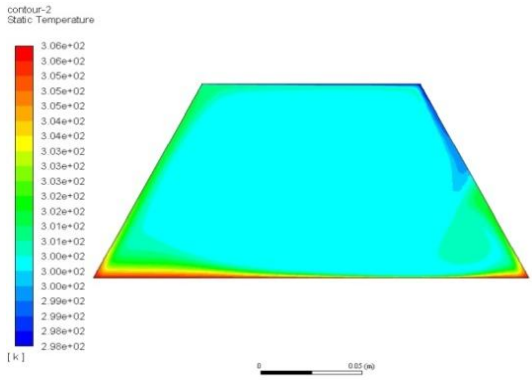

Ri=2

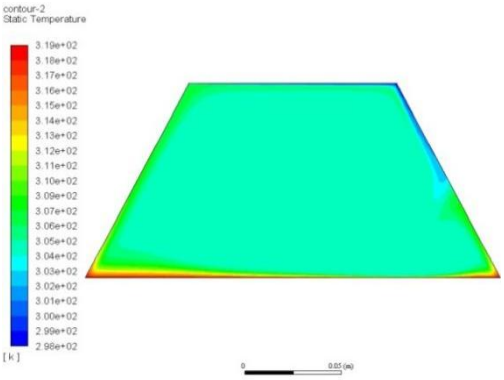

Ri=5

Figure IV.16: Temperature Contours for φ = 4 %

- For φ = 8 %

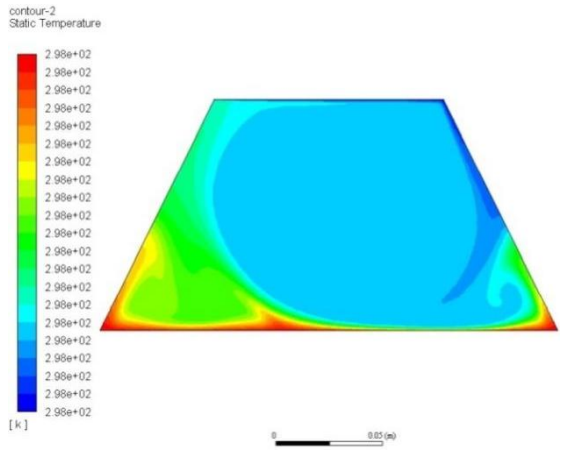

Ri= 0.1

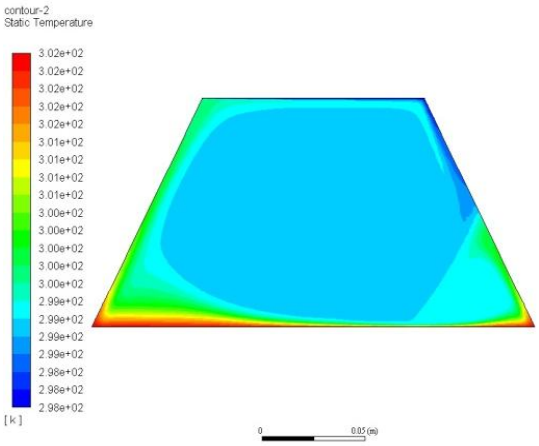

Ri= 1

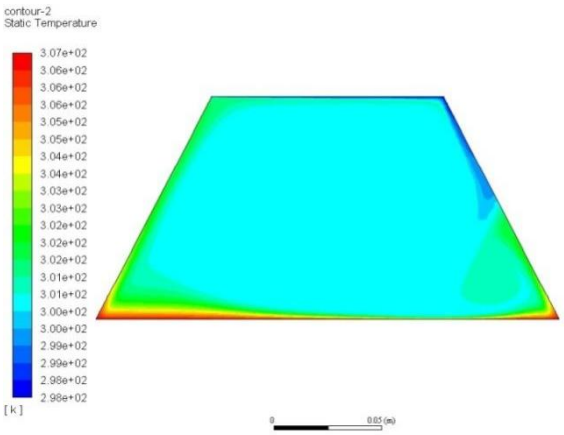

Ri= 2

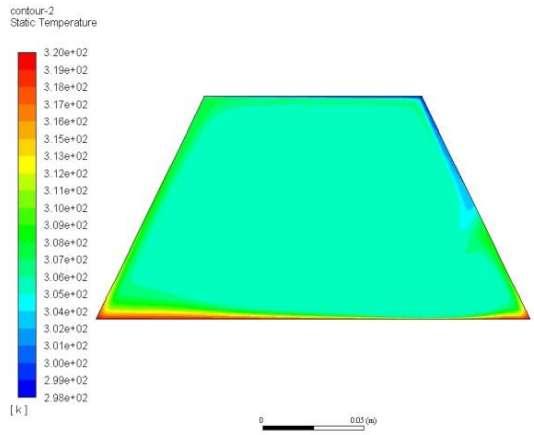

Ri= 5

Figure IV.17: Temperature Contours for φ = 8 %.

•For Ri = 0.1 and 1, two thermal cells (vortices) are formed.

• For Ri = 2 and 5, only one dominant thermal vortex is observed.

•Higher temperatures are observed on the left side, and lower temperatures on the right side.

• For Ri = 0.1, the temperature distribution is relatively uniform, indicating that heat transfer is mainly due to forced convection, with efficient mixing due to the nanofluid motion.

• For Ri = 1, a similar pattern is observed, showing a balance between forced and natural convection.

• For Ri = 2 and 5, the temperature distribution shows hot regions near the bottom wall and colder zones across the rest of the cavity, highlighting the dominance of natural convection.

Thus, we conclude:

•Increasing nanofluid concentration improves heat transfer in all cases.

•However, the type of convection (forced or natural) governs the heat distribution pattern.

•The trapezoidal shape affects the isotherm distribution due to the variation of thermal currents inside the enclosure

IV.4.6 Local Nusselt Number Variation

The local Nusselt number quantifies the ratio between convective and conductive heat transfer at a specific point on a surface. It is expressed as:

$$Nu(x) = -\frac{k_{hnf}}{k_f}\frac{\partial \theta}{\partial y} \qquad \text{VI.2}$$

The local Nusselt number variation is presented in figure IV.15 for different concentration of nanoparticles. The curves in all cases exhibit a peak near the middle of the range (around x=0.13), which represents highest heat transfer location.

Across all cases, it is observed that as the Richardson number (Ri) increases, the local Nusselt number at the peak also increases. This indicates that increasing Ri leads to enhanced heat transfer performance.

• For φ=0, increasing Ri from 0.1 to 5 results in a noticeable rise in the local Nusselt number at the peak. This indicates that natural convection is more effective in enhancing heat transfer in the absence of nanoparticles.

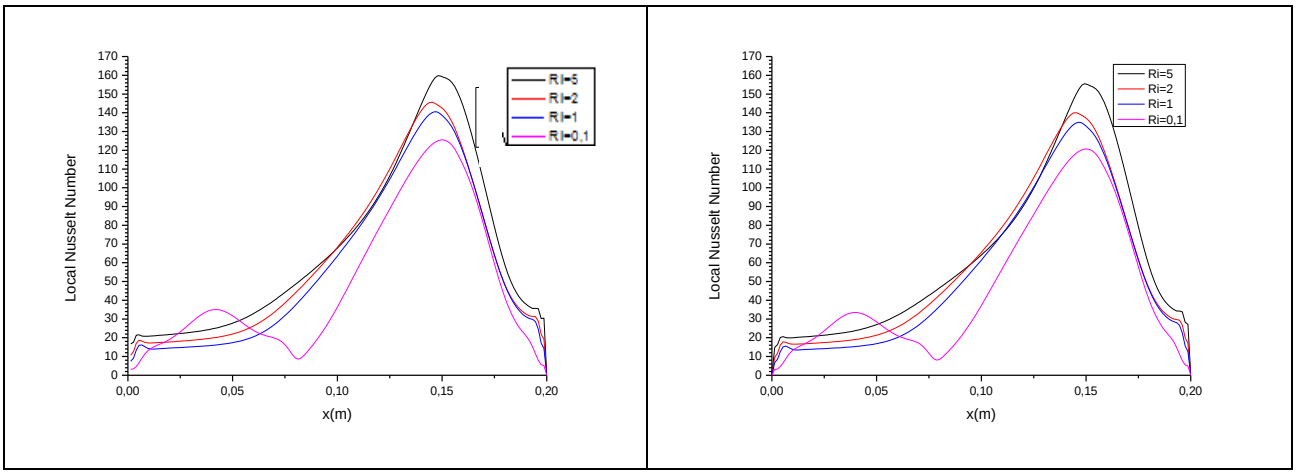

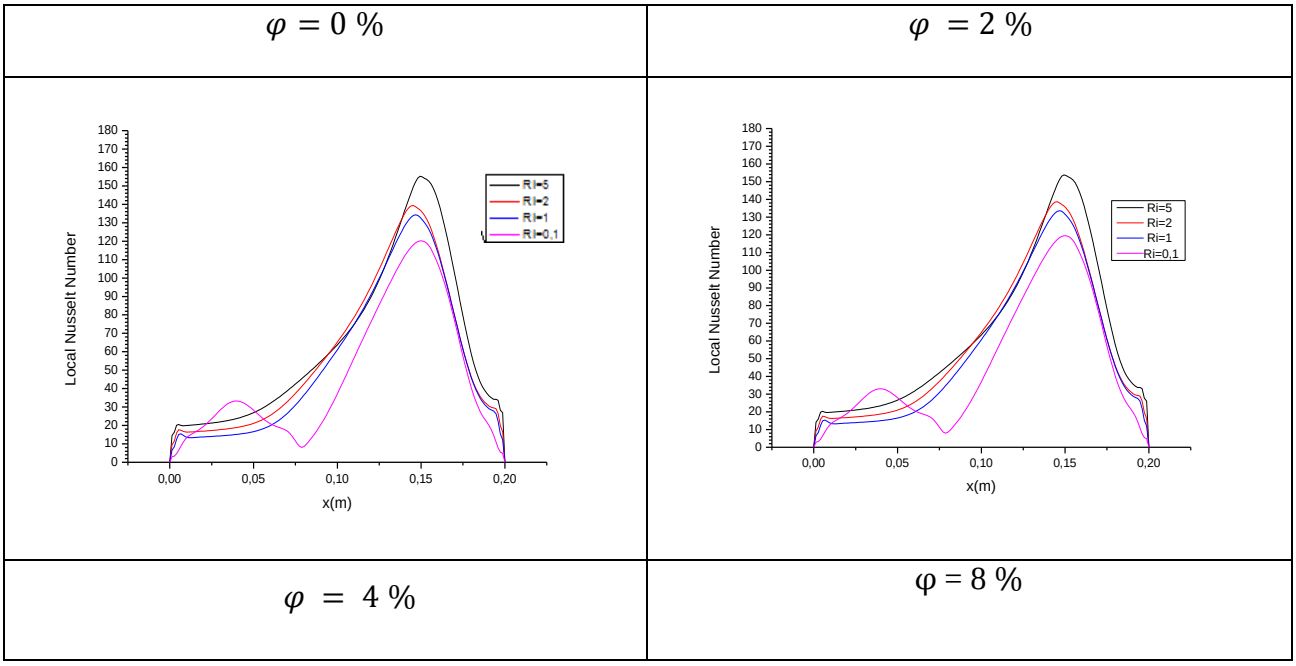

Figure IV.18: Variation of Local Nusselt Number Along The Bottom Wall

for φ=2 and 4 and 8, the curves are generally elevated, particularly at the peak, indicating improved heat transfer performance. The use of hybrid nanofluids can be increase the effective thermal conductivity, which in turn enhances the Nusselt number.

IV.4.7 The Average Nusselt Number

The average Nusselt number represents the average heat transfer coefficient across the entire surface. It is defined by:

$$Nu_{moy} = -\frac{\int_0^H Nu.dy}{H} \qquad \text{VI.3}$$

A curve showing the relationship between the Richardson number and the average Nusselt number is presented in Figure IV.14.

For Ri = 0 (forced convection), we observe that the lowest value of the Nusselt number (Nu) occurs

For φ= 4%, while the highest value is found at φ= 0%. This suggests that the presence of nanoparticles under forced convection conditions does not significantly enhance thermal performance. For Ri = 0.1 to 1, the Nusselt number increases with increasing φ, indicating that nanoparticles enhance heat transfer in this mixed convection regime. For Ri = 5 (dominant natural convection), the Nusselt number increases notably with higher ϕ, which implies that nanofluids improve thermal conductivity and enhance natural convection heat transfer. From this, we conclude that:

• Increasing the concentration of nanoparticles leads to effective results in improving heat transfer for each Richardson number, especially at high Ri (natural convection).

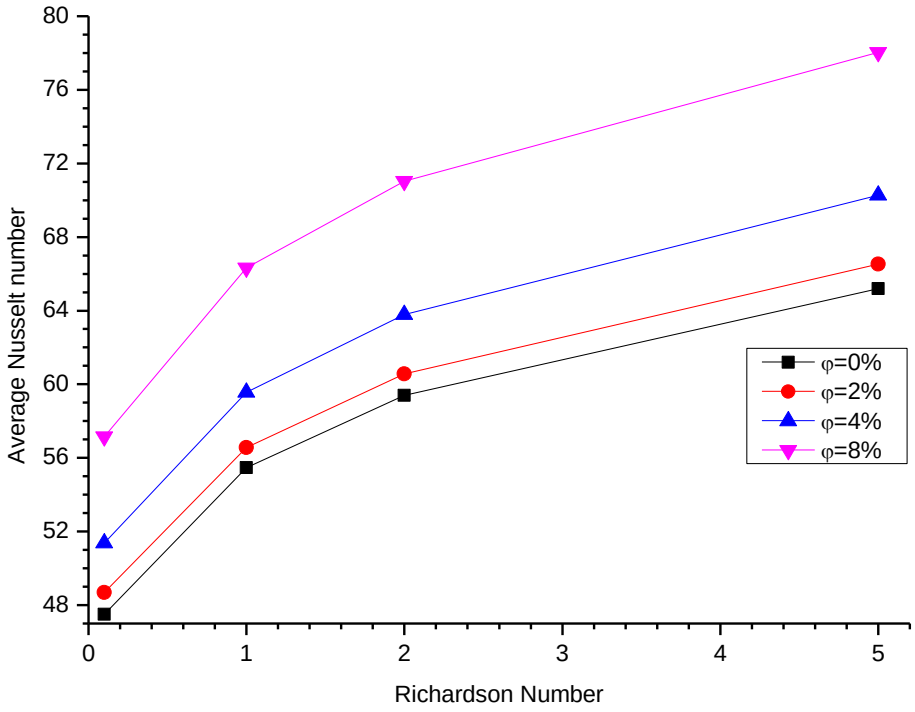

Figure IV.19: Relationship Between the Richardson Number and the Average Nusselt Number

We found that increasing the nanoparticle concentration (φ) leads to a significant enhancement in heat transfer, which becomes more pronounced at higher Richardson numbers. For instance, compared to **Ri = 0.1 at φ = 0%**, the following improvements were noted:

Table IV.5: Heat transfer improvement results

Ri **ϕ**	**ϕ = 0 %**	**ϕ = 2 %**	**ϕ = 4 %**	**ϕ = 8 %**
Ri = 0.1		2.46%	7.55%	16.91%
Ri = 1	14.37%	16.02%	20.27%	28.4%
Ri = 2	20.04%	21.59%	25.55%	33.15%
Ri = 5	27.15%	28.62%	32.42%	39.15%

The best thermal performance was recorded at φ = 8% and Ri = 5, resulting in a 39.15% enhancement representing the optimal condition in this study.

IV.5 Conclusion

In this chapter, we presented the results of a numerical study was conducted to investigate turbulent mixed convection and heat transfer inside a trapezoidal cavity filled with a hybrid nanofluid. The system is characterized by a heated lower wall, a moving cooler upper wall, and thermally insulated vertical sidewalls. The effects of the solid volume fraction and the Richardson number were studied in detail. Initially, a mesh independence study was presented; the mesh was considered acceptable if the residuals of the governing equations converged to a small value. After that, the results of each case were analyzed The Average Nusselt Number and Local Nusselt Number Variation and Temperatur Contours and Stream Function Contours and Horizontal Velocity Contours and Vertical Velocity Contours

The main conclusions obtained are as follows:

- ✓ Heat transfer is enhanced with increasing nanoparticle concentration and Richardson number.
- ✓ The combination of high nanoparticle concentration and high Richardson number yields a considerably greater enhancement in heat transfer than either factor alone.
- ✓ The most important enhancement (39.15%) for heat transfer is found for φ = 8% and Ri = 5

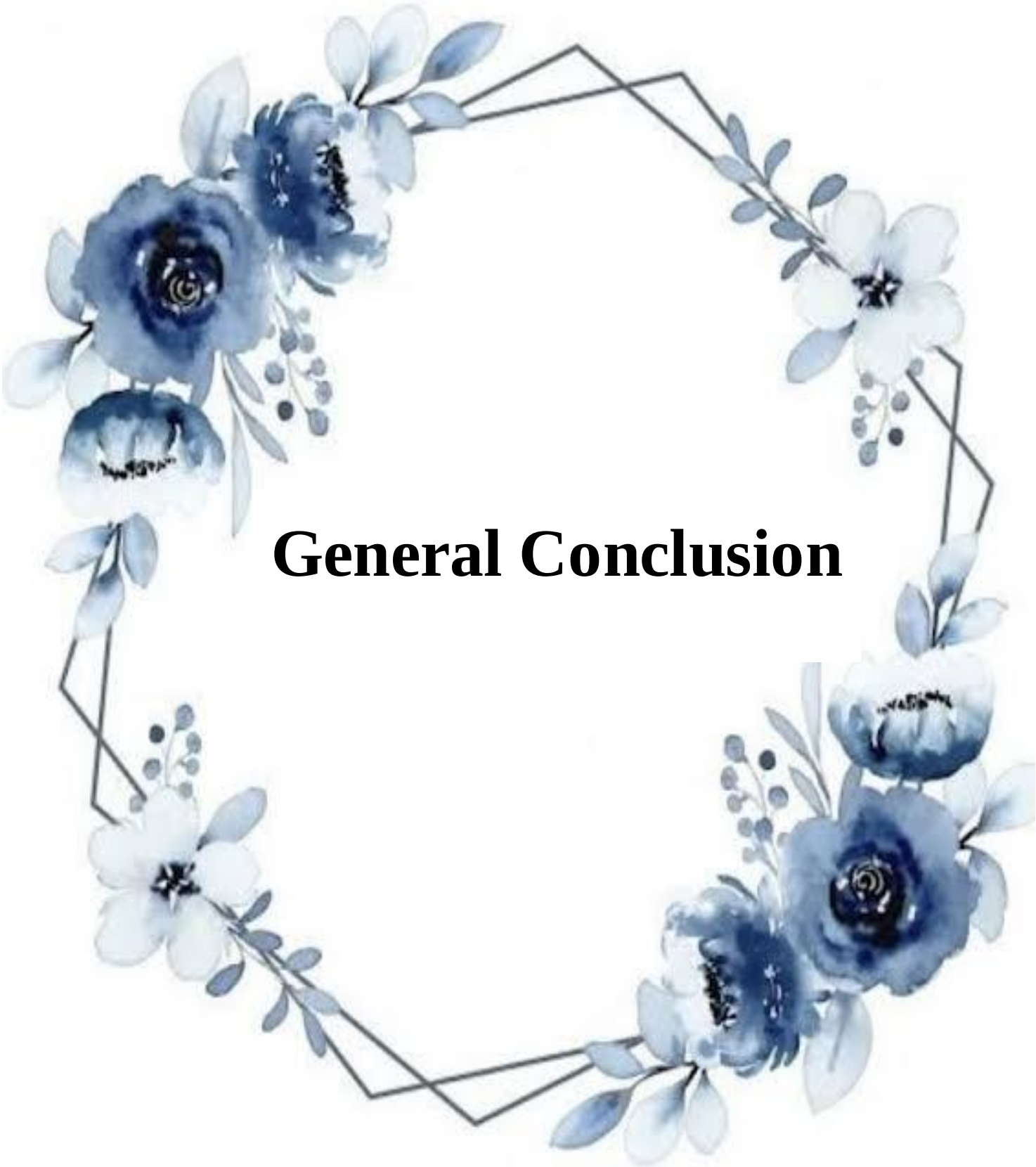

General Conclusion

General Conclusion

In this research work, a numerical study was carried out to investigate turbulent mixed convection and heat transfer within a trapezoidal cavity filled with a hybrid nanofluid. The system is characterized by a hot bottom wall, a cooler moving top lid, and thermally insulated vertical sidewalls.

The turbulent flow with heat transfer within the cavity is gouverned by the Reynolds Average Navier stokes equations (RANS) and energy equation. The mathematical model and numerical method were validated by comparing them to the results in the litterature for a steady mixed convection in a partially heated trapezoidal enclosure. To select the adequate number of nodes, a grid independent treatment is used where we found that the mesh 150x150 is sufficient. The trapezoidal enclosure is filled with a hybrid nanofluid composed of copper Cu and aluminum oxide Al_2O_3 .

The geometrical configuration is realized with Gambit software, and the set of partial differnetial equations are resolved using Ansys Fluent. A series of numerical simulations were conducted to examine the effects of hybrid nanofluid concentration and the Richardson number (Ri) as key governing parameters.

For the present study, numerical simulations are reported for a fixed Reynolds number Re=3160, and for Richardson numbers: Ri=0.1, 1, 2 and 5 and for both pure water and hybrid nanofluid at different volume fractions. The results were analyzed through horizontal and vertical velocity countours as well as temperature and stream function contours. The relationship between the average Nusselt number and the Richardson number was thoroughly investigated, and the variation of the local Nusselt number along the bottom wall was assessed under the influence of different volume fractions (φ) and Ri values. The results showed that :

- Heat transfer is enhanced with increasing nanoparticle concentration and Richardson number.
- The combination of high nanoparticle concentration and high Richardson number yields a considerably greater enhancement in heat transfer than either factor alone.
- The most important enhancement (39.15%) for heat transfer is found for φ = 8% and Ri = 5.

This is a Future Expectations :

Table IV.6: Future Expectations

Type of Improvement	Current Rate (2020–2025)	Future Expectations (by 2030 and beyond)
Thermal Conductivity	10–40% increase over the base fluid	Up to 100%
Convective Heat Transfer Coefficient	20–50% increase	50–100% increase
Cooling System Efficiency	10–30% increase	30–60% increase

[1] M. Shoaib, M. A. Raj, M. T. Sabir, K. S. Nisar et al. , "Numerical analysis of 3-D MHD hybrid nanofluid over a rotational disk in presence of thermal radiation with Joule heating and viscous dissipation effects using Lobatto III A technique," *Alexandria Engineering Journal,* vol. 60, pp. 3605-3619, 2021.

[2] I. Zeghbid, and R. Bessaih, "Etude de la Convection Mixte dans des Cavités," Constantine, Université des Frères Mentouri - Constantine Faculté des Sciences de la Technologie, Département de Génie Mécanique, pp. 8-9, 2017.

[3] F. Aissa and I. Lamouri , "Simulation numérique de la convection mixte d'un nano-fluide dans un canal Vertical.," Tiaret, Université Ibn Khaldoun de Tiaret Faculté des Sciences Appliquées Département de Génie Mécanique, pp.23-35, 2020.

[4] L. Almearas, J. Appenzeller and C. Vilain, «CHIMIE MPSI.PTSI,», france-jouve, VUIBERT PREPAS, vol. 16.17, 2013.

[5] A. Al-Sarkhi, E. Abu-Nada, B .A. Akash and J. O. Jaber, "Numerical investigation of shrouded fin array under combined free and forced convection," *International Communications in Heat and Mass Transfer,* vol. 30, pp. 435-444, 2003 .

[6] H.F Oztop and I. Dagtekin "Mixed convection in two-sided lid-driven differentially heated square cavity," *International Journal of Heat and Mass Transfer,* vol.47, pp. 1761-1769, 2004.

[7] M. Fennouche and R. Kram, "Simulation numérique en régime laminaire Simulation numérique en régime laminaire," Mila, Centre Universitaire Abdelhafid Boussouf -Mila Institut des Sciences et de Technologie, Département des Sciences et Techniques, pp.13-18, 2020.

[8] S. B. Maiga, S. J. Palm, C. T. Nguyeb, G. Roy and N. Galanis, "Heat transfer enhancement by using nanofluids in forced convection flows," *International Journal of Heat and Fluid*

Flow , vol. 26, no. 4, pp. 530-546, 2005.

[9] H. F. Oztop, "Combined convection heat transfer in a porous lid-driven enclosure due to heater with finite length," *international communication in heat and mass transfer,* vol. 33. pp. 772-779, 2006.

[10] M. Akbari, A. Behzadmehr and F. Shahraki, "Fully developed mixed convection in horizontal and inclined tubes with uniform heat flux using nanofluid," *International Journal of Heat And Fluid Flow,* vol. 29, pp. 545-556, 2008.

[11] E. Abu-Nada and A. J. Chamka, "Mixed convection flow in a lid driven square enclosure filled with a nanofluid," *European Journal of Mechanics-B/Fluids,* vol. 29, pp. 472-482, 2010.

[12] A. Benaouda, S. Mekroussi, H. Ameur and S. Kherris, "Effect of aspect ratio and non uniform temperature on mixed convection in a double lid-driven cavity," *Numerical heat Transfer Application,* vol. 83, pp. 237-247, 2022.

[13] A. H. Nezhad, A. Behzadmehr and S. Alikhani, "Periodic mixed convection of a nanofluid in a cavity with top lid sinusoidal motion," *mechanical engineering science,* vol. 203-210, pp. 2149-2160, 2011.

[14] A. A. Arani, S. M. Sebdani, M. Mohmoodi, A. Ardeshiri et al, "Numerical study of mixed convection flow in a lid-driven cavity with sinusoidal heating on sidewalls using nanofluid," *Super lattices and Microstructures,* vol. 51, pp. 893-911, 2012.

[15] R. Nasrin, M. A. Alim and A. J. Chamka, "Combined convection flow in triangular wavy chamber filled with water–CuO nanofluid: Effect of viscosity models," *International Communications in Heat and Mass Transfer,,* vol. 39, pp. 1226-1236, 2012.

[16] R. Jmai, B. B. Beya and T. Lili , "Heat transfer and fluid flow of nanofluid-filled enclosure with two partially heated side walls and different nanoparticles," *Super lattices and Microstructures* , vol. 53, pp. 130-154, 2013.

[17] M. M. Billah , M. M. Rahman and U. M. Sharif, "Heat Transfer Enhancement of Nanofluids in a Lid-Driven Triangular Enclosure having a Discrete Heater," *Procedia Engineering*, vol. 56, pp. 330-336, 2013.

[18] A. Karimipour, M. H. Esfe, M. R. Safaei, D. T. Semiromi et al., "Mixed convection of Copper-Water nanofluid in a shallow inclined lid driven cavity using lattice Boltzmann method," *physical A: statical mechanics and its Aplication*, pp. 150-168, 2014.

[19] F. Garoosi, S. Garoosi and K.Hooman , "Numerical simulation of natural convection and mixed convection of the nanofluid in a square cavity using Buongiorno model," *Powder technology*, vol. 268, pp. 279-292, 2014

[20] Z. Mehrez, A. E. Cafsi, A. Belghith and P. L. Quéré, "The entropy generation analysis in the mixed convective assisting flow of Cu–water nanofluid in an inclined open cavity," *Advanced powder Technology* , vol. 26, pp. 1442-1451, 2015

[21] H. Hadib, S. Hossen and S. Saha, "Effect of Tilt Angle on Pure Mixed Convection Flow in Trapezoidal Cavities Filled with Water-Al_2O_3 Nanofluid," *procedia engineering*, vol. 105, pp. 388-397, 2015

[22] S. Mohammad, "Etude numérique de la convection mixte dans les enceintes lors de l'écoulement d'un nanofluide" Tiaret, Université Ibn Khaldoun de Tiare faculté des Sciences Appliquées Laboratoire de Recherche des Technologies Industrielles, pp. 56 , 2023.

[23] R. Bessaih and M. Khentoul, "Etude Numérique de la Convection Mixte dans un Canal Horizontal Contenant des Ailettes," Constantine, Université des Frères Mentouri - Constantine Faculté des Sciences de la Technologie, Département de Génie Mécanique, 2016, p. 23 .

[24] A. Aghaei, H. Khorasanizadeh, G.Sheikhzadeh and M. Abbaszadeh, "Numerical study of magnetic field on mixed convection and entropy generation of nanofluid in a trapezoidal enclosure," *The Journal of Magnetism and Magnetic Materials* , vol. 403, pp. 133-145, 2016.

[25] A. Raizah, S. E. Ahmed, A. K. Hussein and M. A. Mansour, "MHD Mixed Convection in Trapezoidal Enclosures Filled with Micropolar Nanofluids," *Nanoscience and Technology: An International Journal,* vol. 9, p. 343–372, 2018.

[26] A. Al-Rashed, G.A. Sheikhzadeh, M. Afrand, A. Aghaei et al., "Effect of a porous medium on flow and mixed convection heat transfer of nanofluids with variable properties in a trapezoidal enclosure," *journal of thermal analysis and calorimetry* , vol. 139, pp.741-754, 2019.

[27] N. Muhammad, S. Nadeem and A. Issakhov, "Finite volume method for mixed convection flow of Ag–ethylene glycol nanofluid flow in a cavity having thin central heater," *physical A : Statical mecahanics and its application,* vol. 537,pp. 122-132, 2020.

[28] V. Ardalan, R. Alizadeh, A. Fattahi, N. A. Rasi et al. , "Analysis of unsteady mixed convection of Cu–water nanofuid in an oscillatory, lid-driven enclosure using lattice Boltzmann method," *Journal of Thermal Analysis and Calorimetry,* vol. 145, pp. 2045-2061, 2021.

[29] W. Shinwari, T. Hayat, Z. Abbas and S. Momani, "Numerical study for trihybrid nanomaterial flow by convectively heated curved sheet," *Case Studies in Thermal Engineering*, vol. 53, pp. 103-113, 2024.

[30] Q. R. Al-Amir, H. K.Hamzah, F. H.Ali, R.N.Al-Kaby et al., "MHD Corrugated Wall Lid-Driven Mixed Convection in a Porous-Nanofluid Staggered Enclosure," *Iranian Journal of Science and Technology, Transactions of Mechanical Engineering,* vol. 24, pp. 1133-1161, 2025

[31] K. Bouarour and M. Lebbi, "Numerical investigation of hybrid nanofluid flow in lid driven cavity with a heated obstacle", *Proceedings Of The Romanian Academy,* vol. 25, pp 119-128, 2024

[32] M. K. Triveni and R. Panua, "Numerical investigation of mixed convection in a lid-driven triangular cavity with a circular cylinder using ANN modeling," *international journal heat*

and technology , pp. 903-918, 2017.

[33] R. Sarlak, S. Yousefzadeh, O. A. Akbari, D. Toghraie, et al., "The investigation of simultaneous heat transfer of Water/Al_2o_3 nanofluid in a close enclosure by applying homogeneous magnetic field," *intenational journal of mechanical sciences, vol. 133, pp.674-688, 2017* .

[34] P. Pashaie, M. Farhadi, H. Baseri and M. Jafari, "Nusselt Number Estimation along a Wavy Wall in an Inclined Lid-driven Cavity using Adaptive Neuro-Fuzzy Inference System (ANFIS)," *intenationall journal of Engineering,* vol.*26,* pp. 383-392 , 2013.

[35] H. Li, X. Li, J. Zhan, W. Chen and W. Zong, "Study of Turbulent Kinetic Energy and Dissipation Based on Fractal Impeller," *MDPI,* vol. 15, , pp. 7772, 2023.

[36] "Physics & AI engineering simulation in the cloud," [Online]. Available: https://www.simscale.com/docs/simulation-setup/global-settings/k-epsilon/.

[37] M. Sandali, "Etude dynamique et thermique d'un capteur solaire à air à double passe avec milieu poreux," Telemcen, université abou bekr Belkaid Faculté de technologie Département de génie mécanique, pp. 93-95, 2014.

[38] "Initiation aux logiciels Gambit et Fluent," university of Batna.

[39] W. Ibrahim and M. Hirpho, " Modeling and simulation of hybrid Casson nanofluid mixed convection in a partly heated trapezoidal enclosure," *International Journal of Thermofluids vol.15,* pp. 100-166, 2022.

الجمهورية الجزائرية الديمقراطية الشعبية
People's Democratic Republic of Algeria
وزارة التعليم العالي والبحث العلمي
Ministry of Higher Education and Scientific research

University of Ghardaia
Faculty of Sciences and Technology
Department of Common Teaching in Sciences and Technology

جامعة غرداية
كلية العلوم والتكنولوجيا
قسم التعليم المشترك في العلوم والتكنولوجيا

Approval for Final Printing of a Master's Dissertation

	Name and Surname	Signature
President	Djemoui Lalmi	
Examiner 1	Redha TAHTAH	
Examiner 2	Faris AISSAOUI	
Supervisor	Bouraoui Kamel	

I, the undersigned, Mr: Djemoui Lalmi.

President of the jury for the student(s): Amel Djemaa Ouled Hadj Youcef

Field (الشعبة): Physics; **Specialization (التخصص)** : Energy Physics and Renewable Energies

Thesis Title: **Numerical Analysis of Mixed Convection in a Trapezoidal Cavity Filled with a Hybrid Nanofluid**

Hereby authorize the above-mentioned student(s) to print and submit their final manuscript to the department.

Ghardaia : ...2025...Août...02...

President of the jury

Head of the department

رئيس قسم التعليم المشترك في العلوم والتكنولوجيا
علوية فيصل

جامعة غرداية
قسم التعليم المشترك في العلوم والتكنولوجيا
كلية العلوم و التكنولوجيا